UNIVERSITY OF KWAZULU-NATAL

INYUVESI YAKWAZULU-NATALI

HIGH PRESSURE VAPOUR-LIQUID EQUILIBRIUM MEASUREMENT FOR PERFLUORINATED CHEMICALS USING A STATIC ANALYTICAL APPARATUS

Emmanuel Gande

[BSc. Eng., UKZN]

A thesis submitted in the College of Agriculture, Engineering and Science

University of KwaZulu-Natal

Durban

In fulfilment of the requirements for the degree

Master of Science in Engineering, Chemical Engineering

June 2016

Supervisors: Prof. Paramespri Naidoo, Prof. Deresh Ramjugernath, and Dr. Wayne Nelson

FINAL COPY

DECLARATION

I, Emmanuel Gande declare that:

The research reported in this dissertation/thesis, except where otherwise indicated, is my original work.

(i) This dissertation/thesis has not been submitted for any degree or examination at any other university.

(ii) This dissertation/thesis does not contain other persons' data, pictures, graphs or other information, unless specifically acknowledged as being sourced from other persons.

(iii) This dissertation/thesis does not contain other persons' writing, unless specifically acknowledged as being sourced from other researchers. Where other written sources have been quoted, then:

a) their words have been re-written but the general information attributed to them has been referenced;

b) where their exact words have been used, their writing has been placed inside quotation marks, and referenced.

(iv) Where I have reproduced a publication of which I am an author, co-author or editor, I have indicated in detail which part of the publication was actually written by myself alone and have fully referenced such publications.

(v) This dissertation/thesis does not contain text, graphics or tables copied and pasted from the Internet, unless specifically acknowledged, and the source being detailed in the dissertation/thesis and in the References sections.

Signed: _____

Date: _____

As the candidate's supervisor, I, Prof. P. Naidoo agree to the submission of this dissertation:

Prof. P. Naidoo

As the candidate's supervisor, I, Prof. D. Ramjugernath agree to the submission of this dissertation:

Prof. D. Ramjugernath

As the candidate's supervisor, I, Dr. W. Nelson agree to the submission of this dissertation:

Dr. W. Nelson

ACKNOWLEDGEMENTS

I would like to take this opportunity to acknowledge and extend my deepest gratitude to the following people and organisations for their tremendous contribution towards the compilation of this work:

- Firstly, God Almighty, to whom I am eternally grateful for making my tertiary education a reality. Philippians 4:13 (KJV) "*I can do all things through Christ which strengtheneth me*."
- I'm profoundly grateful to my supervisors, Associate Professor Paramespri Naidoo, Professor Deresh Ramjugernath and Doctor Wayne Nelson for their invaluable assistance, guidance, support and expert knowledge.
- The workshop and technical staff of the Thermodynamics Research Unit at the University of KwaZulu-Natal for their help throughout the duration of the project: Ayanda Khanyile, Sanjay Deeraj
- My colleagues for the wonderful experiences we shared in and outside the office: Thabo Magubane, Devash Rajcoomar, Philani Biyela, Piniel Bengesai, Kuveshan Padayachee, Zibusiso Lubimbi and Jesita Reddy.
- The DST/NRF South African Research Chairs (SARChI), through the Fluorochemical Expansion Initiative (FEI), for supporting this project.
- And lastly, my family for their prayers and support.

ABSTRACT

The current study contributes to the continuing research on the measurement and correlation of phase equilibrium data of binary mixtures of 1, 1, 2, 3, 3, 3-hexafluoro-1-propene (R-1216) and alkanes. Fluorinated refrigerants such as R-1216 (not in pure form) are excellent contenders within the next generation of refrigerants that can meet the requirements of Montreal and Kyoto protocols. Since these refrigerants could prove their suitability to be excellent candidates as probable replacements of refrigerants with higher global warming potentials, as such the refrigeration industry is in need of experimental data regarding R-1216 and its mixtures so as to enhance process efficiencies. R-1216 was chosen as the focus of the study because has gained eminence in research activities as it finds use as an intermediate in chemical reactions and as a monomer in the production of polymers among other applications.

Within the larger research project, investigations have been undertaken into the experimental measurement of vapour pressures and densities for pure hexafluoropropylene and the measurement of isothermal binary vapour-liquid equilibrium (VLE) data for systems involving R-1216 and alkenes (ethylene, propylene, and 1-butene). And, phase equilibrium data for mixtures involving R1216 with ethane (R-170), propane and n-butane have been measured.

This work is a continuation of the work on binary mixtures of R-1216 with alkanes. This study concerned the measurement of isothermal high-pressure binary HPVLE data for mixtures of R-1216 + [n-pentane, n-hexane and n-heptane] at temperatures ranging between 352 – 423 K, and pressures up to 3.0 MPa.

The experimental VLE data [R-1216 + n-pentane and R-1216 + n-hexane] was measured using two high pressure static apparatus established on the *static analytic* method. The low volume equilibrium cell (18 cm^3) is furnished with a movable Rapid-Online Sampler – Injector (ROLSI™) for repeatable phase sampling. The second apparatus design has a volume of 60 cm^3 and is made of stainless steel having sapphire windows. The R-1216 + n-heptane system was measured on the apparatus of the cell design of Chiyen (2010). The systems of ethylene + 1, 1, 2, 3, 3, 3-hexafluoro-1-propene binary system at 268.24 K and ethane + n-hexane binary system at 298 K were used as test systems.

The combined expanded uncertainties were approximated at 0.06 K and 0.007 MPa for the temperature and pressure respectively. The isothermal data was correlated with a thermodynamic model comprising the Peng-Robinson equation of state with the Mathias-Copeman alpha function, the non-random two-liquid (NRTL) local composition model, and the Wong-Sandler mixing rule. The binary interaction parameters (τ_{12}, τ_{21} and κ_{12}) were regressed for each individual isotherm.

Plots of the variation of the binary interaction parameters with temperature indicated that the parameters did not exhibit linearity. For parameters fitted to individual isotherms, there appeared to be discontinuities in the correlated model parameters at the critical temperature of R1216 (358.9 K), as the parameters changed sign or magnitude. Similar observations have been reported in literature and were believed to be a consequence of the variance in absorption of a gas in subcritical conditions and in supercritical conditions in a liquid.

Overall, the model results showed an absolute average deviation in the mole compositions of < 2% in all occurrences. Generally, the experimental data is fairly well correlated by the regression model used.

NOMENCLATURE

Symbols

a	Cubic equation of state parameter
a_i	Activity
a_{ij}	Temperature dependence parameter in the NRTL τ parameter
A	Helmholtz free-energy ($kJ.mol^{-1}$)
b_{ij}	Temperature dependence in the NRTL τ parameter
B_{ij}	Second virial coefficient
C_i	Mathias-Copeman parameters
f	Fugacity
F_1	GC detector response
G	Molar Gibbs free energy ($kJ.mol^{-1}$)
H	Enthalpy ($kJ.mol^{-1}$)
ΔH_v	Heat of vaporisation ($kJ.mol^{-1}$)
k_{ij}	Binary interaction parameter for the Wong Sandler mixing rule
m	Mass of substance (kg)
n	Number of moles
P	Pressure (Pa)
P^{sat}	Saturated vapour pressure (Pa)
Q	Heat duty ($kJ.mol^{-1}$)
R	Universal gas constant ($J.mol^{-1}.K$)
T	Temperature (K)
u_c	Combined standard uncertainty
u_i	Standard uncertainty
U	Internal energy ($kJ.mol^{-1}$)
U_c	Combined expanded uncertainty
V_m	Molar volume ($m^3.mol$)
x	Liquid phase mole fraction
y	Vapour phase mole fraction
Z	Compressibility factor

Greek Letters

$\alpha_i(T)$	Alpha function of the cubic equation of state
α_{ij}	Non-randomness interaction parameter in the NRTL equation
ϕ_i	Fugacity coefficient for species i
γ_i	Activity coefficient for species i
μ_i	Chemical potential for species i
ρ	Density ($kg.m^{-3}$)
τ_{ij}	Interaction parameter in the NRTL activity coefficient model
ω	Acentric factor
σ	Standard deviation
φ_i	Volume fraction

Subscripts

c	Critical property
cal	Calibration
CALC	Calibrated value of the property
corr	Correlation
EOS	Property computed using an equation of state
i	Component classification
ij	Interaction between species i and j
ref	Reference property
TRUE	True value of the property
y	Property evaluated by way of an activity coefficient model

Superscripts

E	Excess property
id	Property evaluated for an ideal gas
L	Liquid phase property
o	Property evaluated at standard state
OL	Liquid phase property evaluated at standard state

s	Property evaluated at saturation pressure
V	Vapour phase property
∞	Property evaluated at infinite pressure reference state

Overbars

^	Thermodynamic property of a component in a mixture.
–	Partial property

Abbreviations

DDB	Dortmund Data Bank
DDBSP	Dortmund Data Bank Software Package
EOS	Equation of state
GC	Gas chromatograph
HPVLE	High pressure vapour-liquid equilibrium
MC	Mathias-Copeman
NIST	National Institute of Standards and Technology
NPT	National pipe thread
NRTL	Non-Random-Two-Liquid
PR	Peng Robinson
PSRK	Predictive Soave Redlich Kwong
REFPROP	Reference Fluid Thermodynamic and Transport Properties
ROLSI	Rapid On-line Sampler Injector
SRK	Soave Redlich Kwong
SS	Stainless Steel
TCD	Thermal conductivity detector
TRU	Thermodynamics Research Unit
VLE	Vapour-liquid equilibrium
WS	Wong-Sandler

TABLE OF CONTENTS

LIST OF FIGURES

LIST OF TABLES

1

CHAPTER ONE

INTRODUCTION

This research was undertaken in the Thermodynamics Research Unit (TRU), Discipline of Chemical Engineering, at the University of KwaZulu-Natal (UKZN), under the auspices of the Nuclear Energy Corporation of South Africa (NECSA).

Pelchem, the chemical division of NECSA, embarked on the Fluorine Expansion Initiative (FEI) to encourage industry to increase the beneficiation of South Africa's fluorspar (CaF_2) reserves (Swanepoel, 2009). Although South Africa possesses the world's largest (CaF_2) reserves, much of the acid grade fluorspar is exported. It is therefore hoped to promote local beneficiation.

This study is part of the ongoing research program in the determination of the thermodynamics properties of fluorocarbons as well as their mixtures. The objective was to build an experimental property databank for the exploration of novel fluorocarbon expertise and equipment for commercial applications.

The larger research project sets out to add to the measurements of the thermodynamic data involving hexafluoropropylene (R-1216) and hexafluoropropylene oxide (HFPO). Previously, phase equilibrium data for mixtures involving hexafluoropropylene with ethane (R-170), propane and n-butane were measured (Subramoney et al., 2012, Subramoney et al., 2015). Here, the measurement of the binary VLE data of binary combinations of R-1216 with n-pentane, n-hexane and n-heptane, was undertaken.

R-1216 has gained attention in industrial as well as research activities and is used as an intermediate in chemical reactions (Krespan, 1986), as a monomer used to prepare fluoropolymers (Aravindan and Vickraman, 2007, Stolarska et al., 2007) and in the epoxidation reactions in the production of HFPO (Ikeda et al., 1990, Huang et al., 2006). Chlorofluorocarbons (CFCs) among other ozone-depleting substances (ODSs) have been established to be the primary contributors to the depletion of the ozone layer. CFCs are chemically inactive with the potential to remain in the atmosphere for lengthy periods of time. A warning was first raised in 1974 about the role of CFCs in the depletion of the ozone layer which led to the reductions in the emission of ODSs (Molina and Rowland, 1974). The drastic loss of ozone above the Antarctic has led to global efforts to minimise emissions of the ODSs, which resulted in the Montreal Protocol and its modifications to phase out production of ODSs.

Since the introduction of these protocols, there has since been much interest in the development of environmentally friendly replacements with a low Ozone Depleting Potential (ODP). Potential substitutes include hydrochlorofluorocarbons (HCFCs) and hydrofluorocarbons (HFCs) and combinations of these. An advantage is that they contain hydrogen which makes them vulnerable to hydroxyl radicals in the atmosphere (Francisco and Maricq, 1996)

The Montreal Protocol on Substances that Deplete the Ozone Layer of 1987 was signed to prohibit the consumption and production of substances with an ozone-depleting potential (ODP) (Velders et al., 2007). There has since been a vast amount of study into developing more environmentally friendly replacements with a low Ozone Depleting Potential (ODP). Potential substitutes include hydrochlorofluorocarbons (HCFCs) and hydrofluorocarbons (HFCs) and combinations of these as they contain hydrogen which makes them vulnerable to hydroxyl radicals in the atmosphere (Francisco and Maricq, 1996).

HCFCs and HFCs have been approved as potential substitutes on the premise that their chemical and physical properties were appropriate for the task (Francisco and Maricq, 1996). However, their thermo-physical properties differ from those of CFCs and hence the measurement of the properties of the pure components and binary or ternary mixtures of these.

While R-1216 is currently used as an intermediate in chemical reactions (Krespan, 1986), as a monomer used to prepare fluoropolymers (Aravindan and Vickraman, 2007, Stolarska et al., 2007) and in the epoxidation reactions production of HFPO (Ikeda et al., 1990, Huang et al., 2006), it has the potential for use in many more applications.

In this research, experimental measurements and modelling were undertaken on isothermal high-pressure vapour-liquid equilibrium (HPVLE) data were measured and presented for three binary systems:

i. pentane + 1, 1, 2, 3, 3, 3-hexafluoro-1-propene (R-1216) between 353 and 393 K at pressures up to 3.14 MPa.
ii. hexane + 1, 1, 2, 3, 3, 3-hexafluoro-1-propene (R-1216) between 343 and 371 K at pressures up to 2.85 MPa
iii. heptane + 1, 1, 2, 3, 3, 3-hexafluoro-1-propene (R-1216) between 373 and 423 K at pressures up to 3.29 MPa

This dissertation write-up is structured so that the second chapter highlights published literature VLE data of binary systems involving combinations of 1, 1, 2, 3, 3, 3-hexafluoro-1-propene (R-1216) with varying alkane chain length components. The thermodynamic models implemented in correlating the data are discussed.

The third chapter examines phase equilibrium techniques used in the measurement of HPVLE data. The focus is on the difficulties encountered in HPVLE experimentation and the equipment design features used to overcome the challenges.

The fourth chapter reviews the thermodynamic models that are suitable to use on similar systems involving binary pairs of hydrocarbons and 1, 1, 2, 3, 3, 3-hexafluoro-1-propene (R-1216 where Aspen Plus® was used to model the experimental data by way of the Peng-Robinson equation of state integrating the non-random two-liquid local composition model (NRTL) with the Wong-Sandler mixing rule, allowing the accurate depiction of the phase equilibrium.

The fifth chapter gives a background and a description of the VLE equipment used in the project. The core features of the equilibrium cell design are highlighted.

The sixth chapter presents the experimental procedure followed in conducting the accurate measurement of VLE data.

The seventh chapter presents the experimental results as well as the data regression. Binary VLE results for the two test systems as well as for the three novel systems that consist of binary pairs of 1, 1, 2, 3, 3, 3-hexafluoro-1-propene (R-1216), n-pentane/, n-hexane/, n-heptane are presented.

2

CHAPTER TWO

2. PROJECT BACKGROUND

This study is part of an ongoing research program into the determination of the thermodynamic properties of fluorocarbons as well as their mixtures. Thus far the following experimental data has been chartered: the pure component saturated vapour pressures plus densities of hexafluoropropylene (Coquelet et al., 2010); and VLE data for binary mixtures comprising perfluoroalkanes and perfluoroolefin (Coquelet et al., 2009, Subramoney et al., 2012, Subramoney et al., 2013a, Subramoney et al., 2013b, Subramoney et al., 2015). In this work, *P-x-y* data for the systems R-1216 + [n-pentane, n-hexane and n-heptane] has been measured.

This research is an extension of the work of (Subramoney et al., 2012, Subramoney et al., 2015), which set out to attain a series of binary isothermal VLE data for mixtures of perfluoroalkenes with a homologous series of alkanes.

Subramoney et al. (2015) revealed that a small change in the alkane length could have a striking effect on the phase behaviour. For example, no azeotropic behaviour was observed for the ethane (R170) + 1,1,2,3,3,3-hexafluoro-1-propene binary system whereas, the propane + R-1216 system exhibited a maximum pressure azeotrope and the R-1216 + n-butane system exhibited near-azeotropic behaviour. These results revealed unexpected phase behaviour changes across the alkane homologous series because, as they belong to the same family of alkanes, more similar phase behaviour was expected. The pattern of these results show why isothermal experimental VLE data are invaluable in the elucidation of the behaviour of mixtures. This in turn allows for the fitting of the thermodynamic model's interaction

parameters, and expedites the design of separation process units, which are equilibrium stage based.

2.1 Published Thermodynamic Data

A brief background will be given to the work that has been published in the fluorocarbon research field. It should be noted that the experimental isothermal binary VLE for all published systems considered herein were correlated using a model which consisted of the Peng-Robinson equation of state comprising the Mathias-Copeman α function, Wong-Sandler mixing rule, and the non-random two-liquid (NRTL) local composition activity model. The collective model is called the PR-MC-WS-NRTL model. For all binary systems documented herein the model was found to correlate to the data well, as the absolute average deviation in the mole compositions was < 2% for all systems.

The critical properties of R-1216 as measured by Coquelet et al (Coquelet et al., 2010), compared to the values listed by the National Institute of Standards and Technology (NIST) are shown in Table 2-1. The measurements were conducted at temperatures in the 253.26 – 358.76 K range. From this examination, it was established that $T_c = (358.8 \pm 0.1)\ K$ and $P_c = (3.129 \pm 0.001)$ MPa.

Aspen Plus® reports that $T_c = 363$ K (predicted using the Marrero-Morejón and Pardillo-Fontdevila (1999) method) and $P_c = 3.419$ MPa (predicted using the Ambrose-Walton method (Poling et al.)). An adjustment had to be made for this in Aspen Plus® as this greatly affects the outcome of the simulation. A deviation of 4.1 K and 0.283 MPa is observed for temperature and pressure respectively between the data as measured by Coquelet et al. (2010) and that listed by Aspen Plus®.

Table 2- 1: Comparison of the Pure-Component properties and Mathias-Copeman parameters as measured by Coquelet et al. (2010) with data reported in Aspen Plus®

Coquelet et al. (2010)							
Critical properties				Mathias-Copeman parameters			
T_c/K	P_c/MPa	$\rho_c/kg.m^{-3}$	ω	Z_c	C_1	C_2	C_3
358.9	3.136	579.03	0.3529	0.27226	0.8926	-0.5100	3.1585

Aspen Plus® (NIST)			
Critical properties			
T_c/K	P_c/MPa	$\rho_c/kg.m^{-3}$	ω
363.0	3.419	567.39	0.3199

Isothermal binary VLE data at five temperatures in the range 293.93 K – 322.89 K and pressures up to 4.6 MPa for the binary system of ethane (R-170) + 1, 1, 2, 3, 3, 3-heaxafluoro-1-propene (R-1216) was measured by Subramoney et al. (2012), and is presented in Figure 2-1. The data was measured using the "static analytic" method, and making use of electromagnetic capillary samplers which permits repeatable phase sampling. Neither azeotropic behaviour nor liquid-liquid immiscibility was exhibited over the range of the researched temperatures.

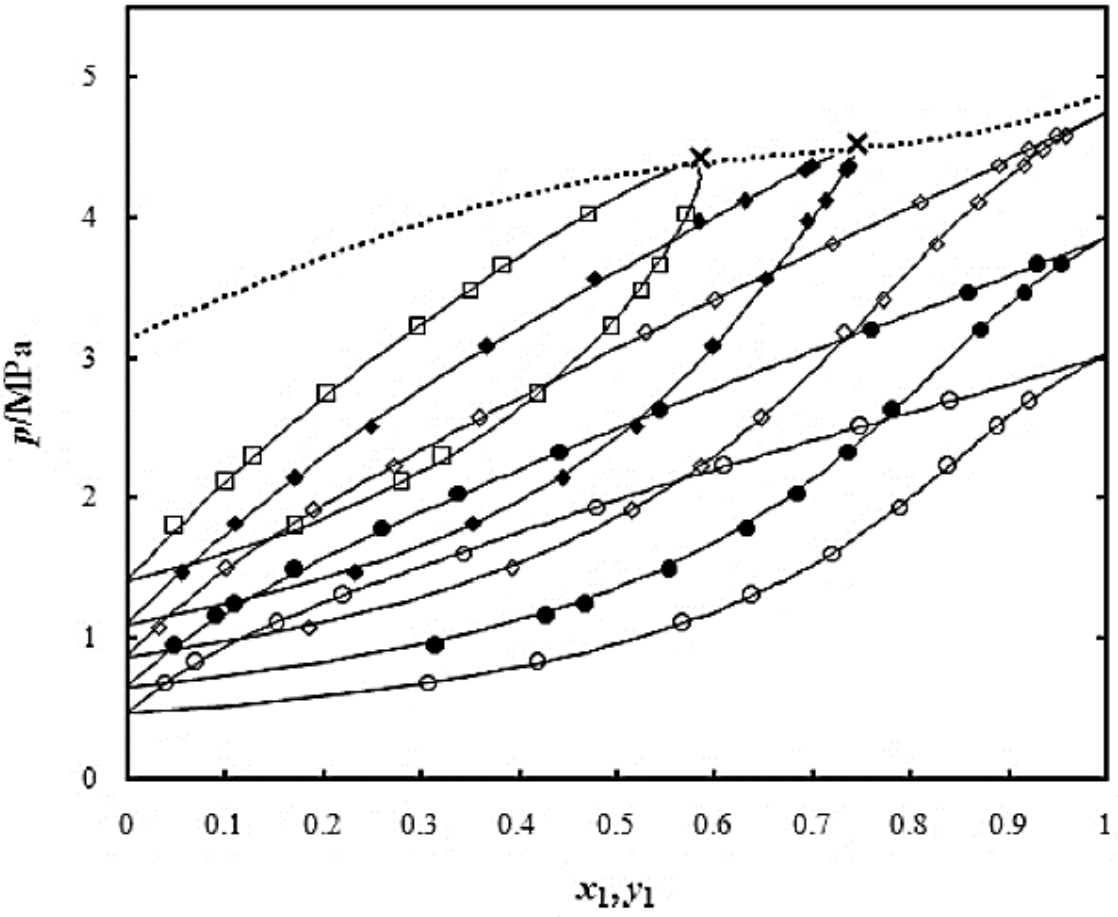

Figure 2- 1: Isothermal VLE data for the binary system of ethane + R-1216 (2) at 282.93 K (○), 293.96 K (●), 303.94 K (◊), 312.90 K (♦) and 322.89 K (□) extracted from (Subramoney et al., 2012).

Isothermal binary VLE data for the propane + 1, 1, 2, 3, 3, 3-heaxafluoro-1-propene (R-1216) was measured by Subramoney et al. (2015) at three temperatures in the range 312.90 K to 342.92 K and pressures up to 3.0 MPa, and is presented in Figure 2-2. As remarked by Subramoney et al. (2015), a small change in the alkane chain length can have a striking consequence on the phase behaviour. The system exhibited a pressure-maximum azeotrope for the investigated temperature range.

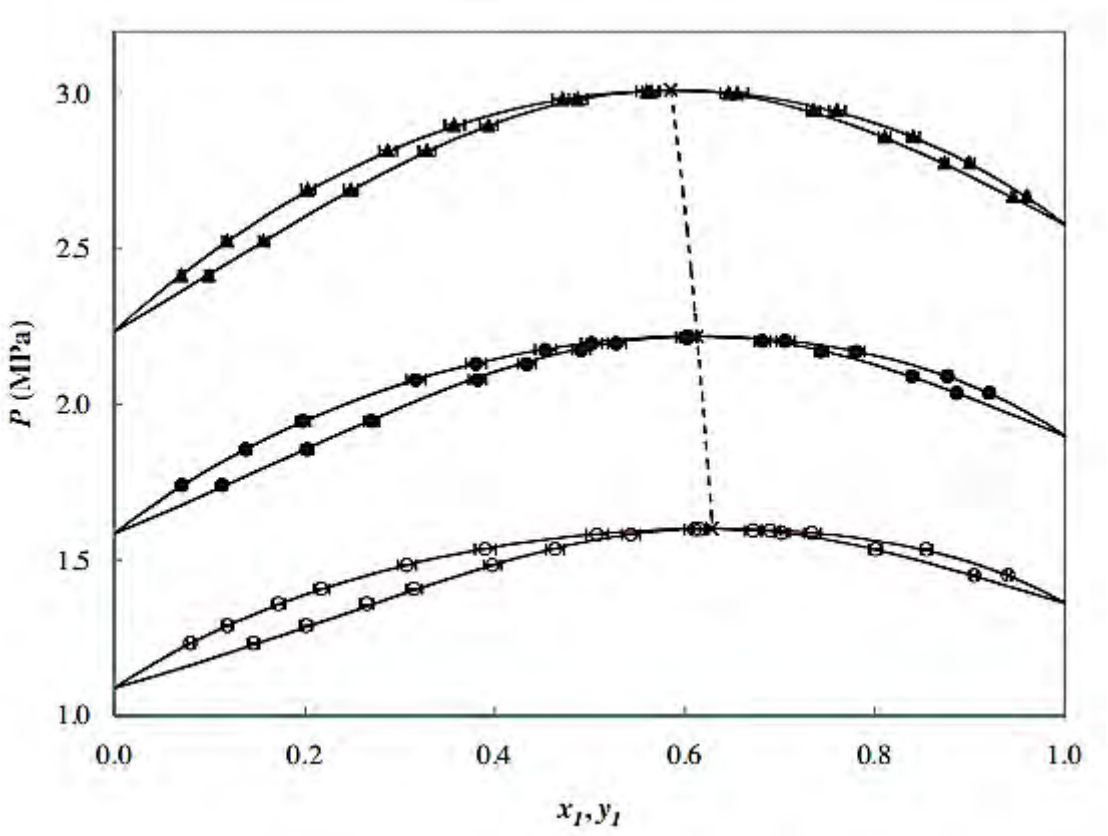

Figure 2- 2: Isothermal VLE data for the binary system of propane (1) + R1216 (2) at 312.90 K (○), 327.88 K (●) and 342.92 K (▲) extracted from Subramoney et al. (2015)**.**

Isothermal binary VLE data for the 1, 1, 2, 3, 3, 3-heaxafluoro-1-propene (R-1216) + n-butane was measured by (Subramoney et al., 2015) at three isotherms (312.90 , 327.88 and 342.88 K) and pressures up to 2.2 MPa, and is presented in Figure 2-3. The measured system presented near azeotropic behaviour at high 1, 1, 2, 3, 3, 3-heaxafluoro-1-propene concentrations; no azeotrope was established experimentally.

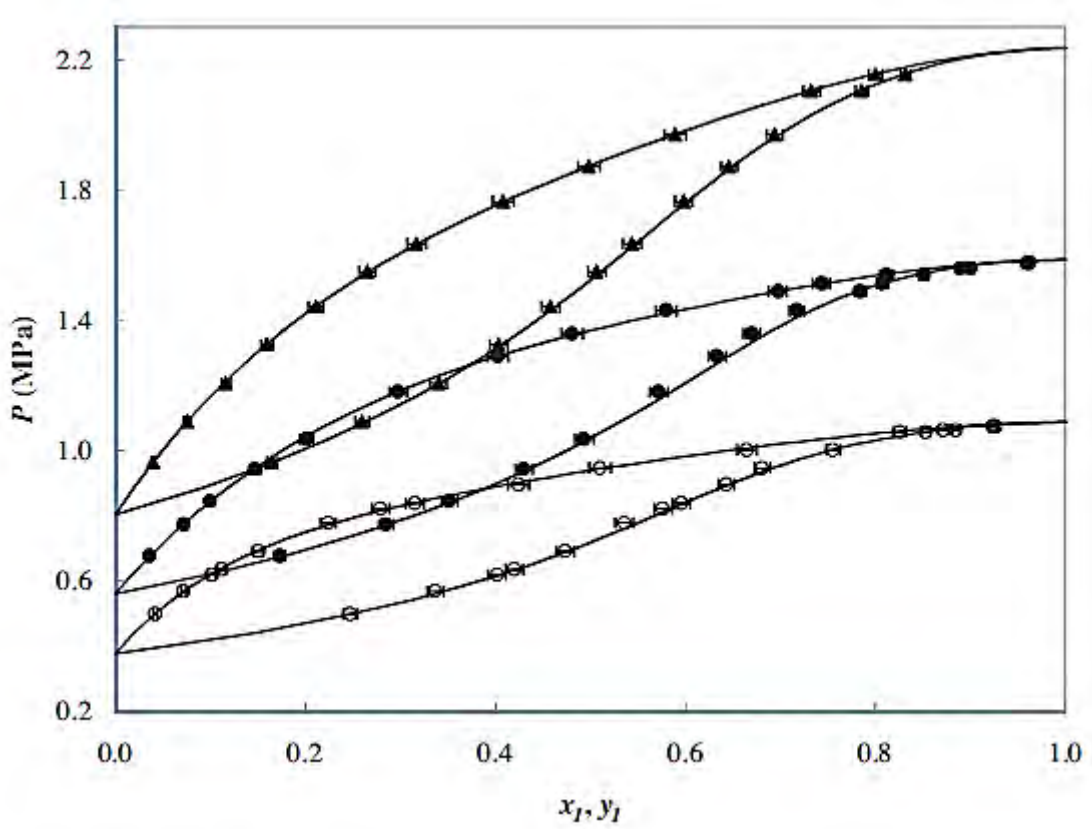

Figure 2- 3: Isothermal VLE data for the binary system of R-1216 (1) + n-butane (2) at 312.90 K (○), 327.88 K (●) and 342.88 K (▲) extracted from Subramoney et al. (2015).

Binary VLE data measurements were also conducted on mixtures of R1216 with alkenes. This presented an interesting review on the phase behaviour of the mixture across the alkene homologous series. Isothermal binary VLE data for the 1, 1, 2, 3, 3, 3-heaxafluoro-1-propene (R-1216) + ethylene was measured by Subramoney et al. (2013a) between 258 and 308 K at pressures up to 4.56 MPa, and is presented in Figure 2-4.

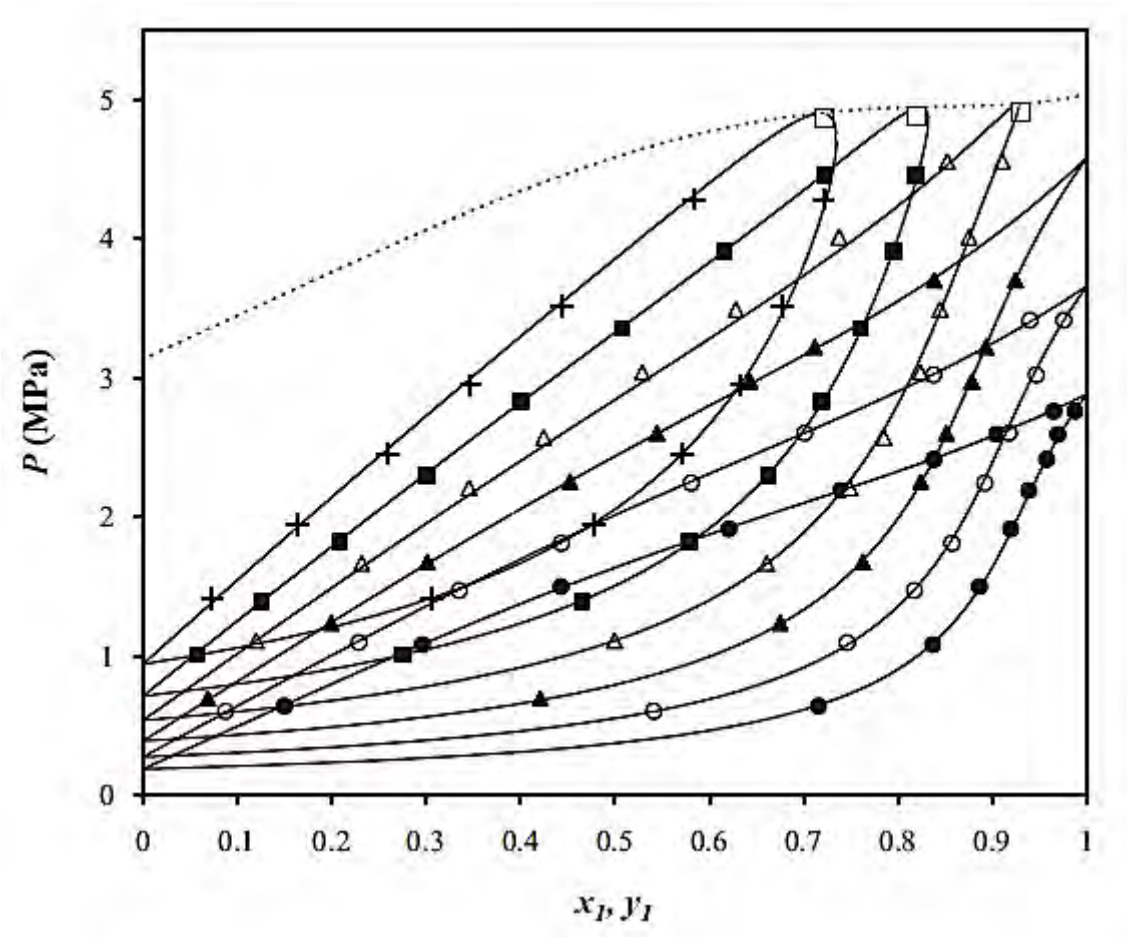

Figure 2- 4: Isothermal VLE data for the binary system of ethylene (1) + R-1216 (2) at 312.90 K (○), 327.88 K (●) and 342.88 K (▲) extracted from Subramoney et al. (2013a)

Isothermal binary VLE data for the 1, 1, 2, 3, 3, 3-heaxafluoro-1-propene (R-1216) + propylene was measured by Coquelet et al. (2009) between 263.17 and 353.14 K at pressures up to 4.0 MPa, and is presented in Figure 2-5. It was noticeable that the azeotrope vanished for temperatures below the critical temperature of propylene.

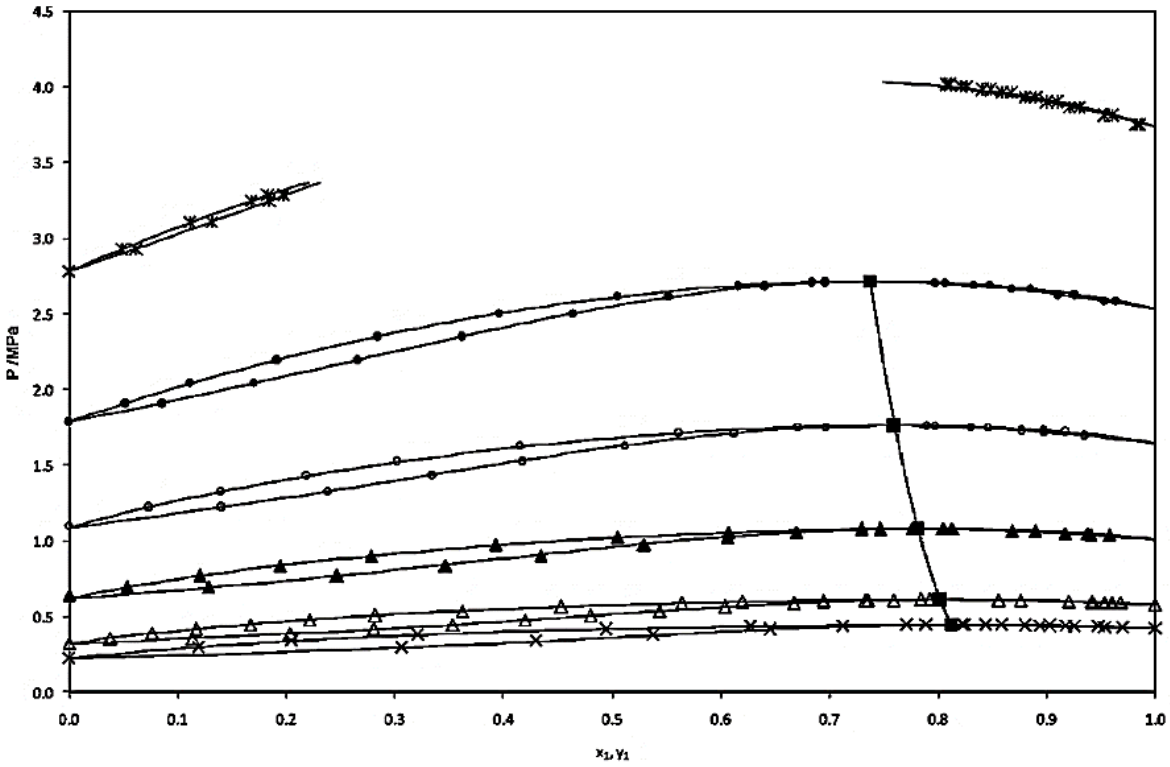

Figure 2- 5: Isothermal VLE data for the binary system of propylene (1) + R-1216 (2) measured by Coquelet et al. (2009): ×, 263.17 K; Δ, 273.16 K; ▲, 293.12 K; ○, 313.11 K; ●, 333.11 K; ◊, 353.14 K. Extracted from Coquelet et al. (2009).

Isothermal binary VLE data for the 1, 1, 2, 3, 3, 3-heaxafluoro-1-propene (R-1216) + 1-butene was measured by Subramoney et al. (2013b) between 313.05 and 343.10 K at pressures up to 2.3 MPa, and is presented in Figure 2-6. Near azeotropic behaviour was noted at elevated R-1216 compositions, more so for the 313.05 K isotherm.

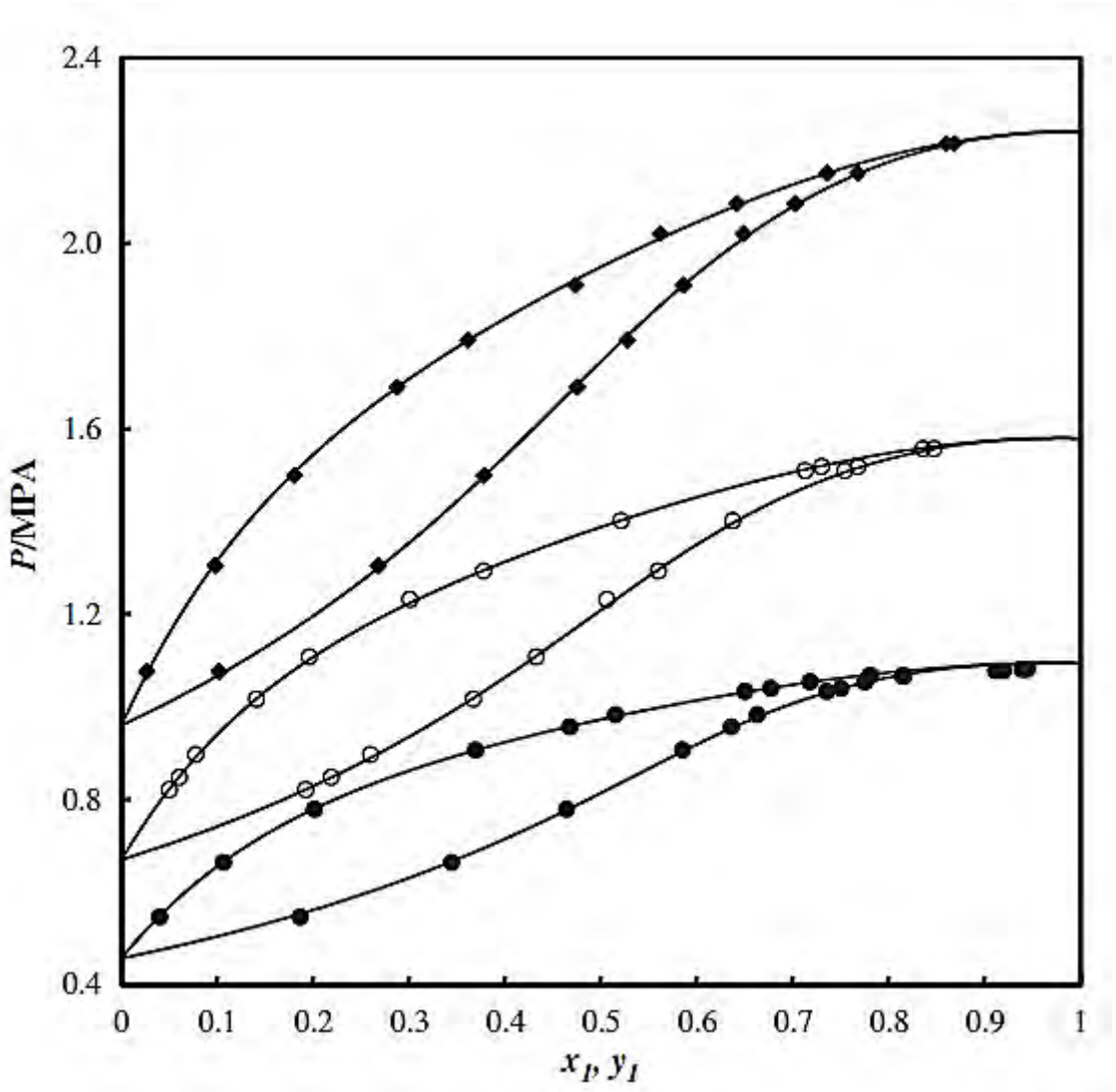

Figure 2- 6: Isothermal VLE data for the binary system of R-1216 + 1-butene measured by Subramoney et al. (2013b): ●, 313.05 K; ○, 327.81 K; ♦, 343.10 K. Extracted from Subramoney et al. (2013a).

3

CHAPTER THREE

3. LITERATURE REVIEW OF HIGH-PRESSURE VAPOUR-LIQUID EQUILIBRIUM EXPERIMENTAL METHODS

Vapour-liquid equilibrium (VLE) data finds use in separation processes in the petrochemical and chemical industry where distillation technology is most commonly used. While simulation packages offer a wider variety of prospects for process synthesis, design and optimisation, the merit of the results acquired when using these packages depends on the excellence of the models and the model parameters employed.

In some instances, calculations employing a group contribution method may suffice. These are based on the predictions of phase equilibrium thermodynamics' theories, which offer a framework that permit interpolation and extrapolation of minimal experimental data. A limitation of the group contribution method is that the activity coefficients can only be computed when the interaction parameters exist else the prediction itself could be inaccurate. This then leads to measurement of experimental data.

In other instances, a precise knowledge of the liquid and vapour phase equilibrium data of the components under study is indispensable. Here, accurate experimental data together with a good description of the thermodynamic models employed are required. The required vapour-liquid equilibrium experimental data must then be obtained in order to inform the thermodynamic model. Various types of apparatus are deployed to accurately measure the VLE data by means of static or dynamic equipment. The static method can further be

subdivided into either the analytical or synthetic method. Each experimental layout has its distinctive merits, preferences, as well as its specific range of applicability.

This chapter describes the experimental method appropriate for this work together with its merits and demerits. The chapter begins with a classification of the types of experimental methods employed in measuring VLE data. This is followed by a review of the method suited to this study making reference to literature from the *Thermodynamics Research Unit (TRU)*. Lastly, the preference for the measurement of isothermal data over isobaric, given its convenience, is motivated.

3.1 Classification of Experimental Equipment

The challenges attendant on the task of the accurate measurement of high pressure vapour-liquid equilibrium (HPVLE) has generated much effort and innovation. The diversity in the approaches taken by researchers attest to the complexity attendant in ascertaining the most accurate and dependable method (Raal and Mühlbauer, 1994a). HPVLE equipment can be classified based on a number of factors such as:

- the nature of the equilibrium data required;
- the operating conditions (temperature and pressure);
- the properties of the components under investigation (thermal stability, corrosive properties, volatility, explosive tendencies).

Deiters and Schneider (1986) in their review of mixture thermodynamics make reference to *density* and *field* variables. *Field* variables are variables having the same value in coexisting phases (e.g. temperature and pressure), whereas *density* variables are normally different (e.g. molar volumes and molar fractions). Numerous techniques have been developed over the years for the meticulous measurement of *field variables*, rendering the experimental determination of pressure and temperature much easier. Deiters and Schneider (1986) in their review of HPVLE experimental methods based their classification of experimental methods according to the techniques utilised in the experimental determination of *density variables*. The techniques used to determine the mole fractions are the *synthetic* and *analytical* method.

The *synthetic* method entails the preparation of a mixture using known amounts (composition) of each component and charged into a pressure vessel. A homogenous phase of the vessel's contents is formed by adjusting the pressure and temperature. The phase compositions are

computed from the amounts that were charged into the pressure vessel at the beginning. For the duration of the experiment, either the temperature or pressure are adjusted until the observance of the realisation of a new phase. The conditions of temperature and pressure at which this phase partitioning commences and the compositions describe a point on the phase envelope. *P-x* and *P-y* diagrams can be obtained from results of this form through cross plotting (Deiters and Schneider, 1986).

In contrast to the *synthetic* method, for the *analytic* method the amounts of the mixture charged into the equilibrium cell do not necessarily have to be known. The temperature and pressure are adjusted coupled with stirring of the mixture to stimulate interaction between the phases until phase equilibrium is reached. At equilibrium, the temperature and pressure are invariable and the stirring is discontinued to allow the phases to separate. Samples are then withdrawn from the liquid and vapour phase to analyse the compositions of each component. The main challenge with the *analytical* method is in avoiding the disturbance of equilibrium in the course of sampling (Raal and Mühlbauer, 1998). Recent developments overcome this by making use of a Rapid On-Line Sampler-Injector (ROLSI™) with which the withdrawn sample size can be adjusted from several hundredths to several milligrams (Guilbot et al., 2000). The experimental results obtained from the *analytical* method are either isobaric (*T-x-y*) or isothermal (*P-x-y*) phase diagrams.

The unique features of the *synthetic* and *analytic* method can be unified to give a classification identified as the *combined* method. It follows that the typical results from experiments of this nature are sets of three types of phase diagrams viz. isotherm (*P-x-y*), isobar (*T-x-y*), and isopleths (*P-T*) phase diagrams.

Raal and Mühlbauer (1994a) base their classification of experimental methods on whether one or both phases are circulated through the equilibrium chamber. Where phase circulation occurs, the method is categorised as a *dynamic* or *flow* method. The opposite is categorised as the *static* method. A further subdivision of the static method exists. The line of demarcation is drawn depending on whether the phases undergo sampling or not. In the instance where sampling takes place it is termed the *static analytical method*, else it is termed the s*tatic non-analytic method.* For the dynamic category, further subdivision is determined by the circulating phase:

vapour, liquid or existence of both. Only *P-x-y* or *T-x-y* data can be produced from dynamic methods.

The latest review articles concerning HPVLE experimentation are Dohrn et al. (2010) covering the period 2000 to 2004, Fonseca et al. (2011) covering the period 2005 to 2008, Dohrn et al. (2012) covering the period 2009 to 2011.

Figure 3-1 shows the classification of high-pressure vapour-liquid experimental equipment and the subdivisions thereof. The figure has been adapted from Raal and Mühlbauer (1998).

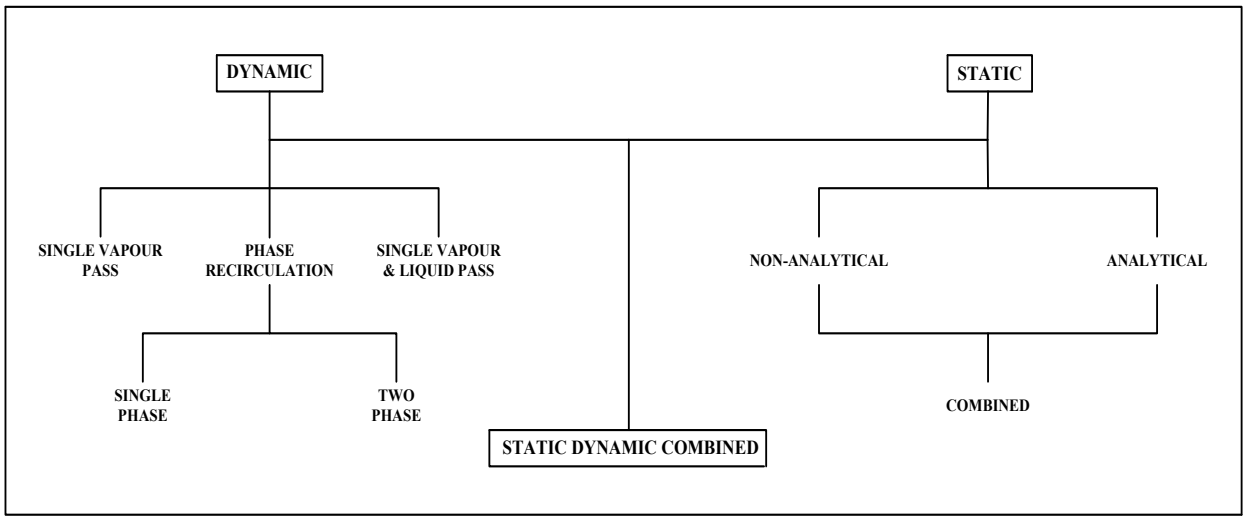

Figure 3 - 1: Classification of High-Pressure Vapour-Liquid Experimental Equipment (Raal and Mühlbauer, 1998)

3.2 Principal Features of HPVLE Experimental Equipment

The salient features of a characteristic HPVLE experimental apparatus comprise the following (Raal and Mühlbauer, 1998):

i. An equilibrium cell in which the two phases exist in equilibrium.
ii. An isothermal environment in which the equilibrium cell immersed. A thermo-regulated environment can be made use of using an ethylene glycol/water mixture, water bath (Ohgaki and Katayama, 1975a, Kaminishi et al., 1989) or oil bath (Legret et al., 1980, Schotte, 1980).

iii. A mixing technique to accelerate the attainment of equilibrium.
    a. Static cells of make use of internal stirrers (Klink et al., 1975, Figuiere et al., 1980, Guillevic et al., 1983).
    b. Dynamic methods employ internal stirring and recirculation of the phases (Freitag and Robinson, 1986, Blanc and Setier, 1988, Inomata et al., 1989).

iv. Instruments to measure the temperature and pressure.

v. For the synthetic apparatus, a technique to adjust the temperature and pressure of the cell by varying the volume to influence the separation of the phases.

vi. For the analytic apparatus, devices to analyse the samples

3.3 Difficulties in HPVLE Experimentation

The information below has been summarised from Mühlbauer and Raal (1995) and Naidoo (2004)

3.3.1 Determining the Attainment of Equilibrium

Equilibrium denotes a static condition, implying the non-existence of change. It further means the lack of any propensity toward change in the macroscopic properties of the material of the system under consideration with respect to time (Smith et al., 2005). The type of method and the system investigated are the pivot on which the equilibration time rests. In the dynamic apparatus, the method of internal mixing is recirculation which ensures greater contact of the phases (Naidoo, 2004). It may take a few minutes for equilibrium to be attained with the dynamic apparatus. In the static apparatus, the time taken for the attainment of equilibrium is much longer although recent developments with improvements in the mixing techniques have overcome this. The attainment of equilibrium is accelerated by greater rates of stirring. Mechanical stirring results in fluid friction, and as a result, dissipating heat energy generated to the surroundings (Raal and Mühlbauer, 1994a). Strictly speaking, a true equilibrium condition is never attained as a result of the temperature gradient created together with the retarding resistances.

Pressure, temperature, vapour and liquid composition, and in certain instances stability of refractive index (Besserer and Robinson, 1971), are used to ascertain whether equilibrium has been attained. The criterion suggested for use by Fredenslund et al. (1973) is a change in pressure of less than 0.05 % in half an hour.

3.3.2 Degassing of the Liquid Components at the Commencement of Experimentation

The presence of volatile impurities elevates the vapour pressures and hence gives an inaccurate representation of the VLE data. It is therefore pertinent to remove the impurities by way of degassing.

3.3.3 Measurement of Temperature and Pressure

Preferably high quality measuring devices that have temperature-compensation over wide ranges are desired. The most common temperature sensors are platinum resistance thermometers (Pt-100Ω). Quartz thermometers are used as standards against which primary temperature measuring devices can be calibrated as a result of their high sensitivity to temperature deviations.

3.3.4 Evading the Disturbance of Equilibrium in the course of sampling

The mechanism for sampling of each of the phases involves a change in the equilibrium cell volume. Upon sampling, the upset to the equilibrium condition is accompanied by a large change in the equilibrium cell volume. In essence, the change in volume is directly proportional to the disruption to the equilibrium condition. Hence, the change in the pressure of the equilibrium cell can be used to quantitatively analyse the volume change.

There are two volume changes linked with sampling in both the dynamic and static method which distract the equilibrium state. These are:

i. The change in the volume of the equilibrium cell associated with the size of the sample withdrawn for analysis.
ii. The change in the volume of the equilibrium cells associated with the sampling method employed.

The requisite size of the sample is principally influenced by the analytical device's requirements. It is desirable that the volume change in the equilibrium cell elicited by the analytic device be minimal. Besserer and Robinson (1971) and Wagner and Wichterle (1987) documented pressure changes of 0.1 and 0.01 bar respectively as a result of their sampling methods using GC sampling valves (6 port valve).

Baba-Ahmed et al. (1999) and Guilbot et al. (2000) made use of a ROLSI ™ (Rapid On-Line Sampler-Injector) for sample withdrawal and conveying it to the gas carrier lines connected to it and the GC and thus completing a sample loop. The ROLSI™ is capable of allowing measurements over large ranges of temperature (0 to770 K) and pressure (0 to1000 bar), for corrosive components together with samples ranging from 1 μg to some mg (Richon, 2003).The Thermodynamics Research Unit (TRU) at the University of KwaZulu-Natal also employs the use of the ROLSI™ (Rapid On-Line Sampler-Injector) on the HPVLE apparatus. Published data from the research unit includes work by Narasigadu (2011), Tshibangu et al. (2013) and Nelson et al. (2015a). The researchers used an equilibrium cell design of Narasigadu (2011) that has a sapphire tube that is sealed between two SS 316L metal flanges. The equilibrium cell has a maximum capacity of approximately 18 cm^3 and enables the measurement of phase equilibrium data for small volumes. The novelty in the design is the incorporation of a movable metallic rod that has similar dimensions to that of the capillary of the ROLSI™ and compensates for any volume disturbances during sampling. The solid rod approaches the direction of the ROLSI™ capillary. This works as a volume compensation mechanism to negate any disturbance to the volume upon moving the ROLSI™ capillary as it enters or exits liquid phase. Other researchers use two capillary samplers (Rivollet et al., 2004, Valtz et al., 2005), one for sampling in the liquid and the other in the vapour phase.

3.3.5 Accurate analysis of the withdrawn sample

Gas chromatography (GC) and spectroscopy are the two principal methods used for analysis. Analysis of the phases at equilibrium can be conducted on withdrawn samples or in situ. Sample withdrawal presents challenges in that the withdrawn sample should not alter the equilibrium condition and the samples have to be representative of the equilibrium condition. Withdrawn samples transferred to the GC via gas carrier lines are an inaccurate representation of the equilibrium phases if they are not homogenised. As such, the gas carrier lines are heat traced with Nichrome® wire whose temperature is set to be at least 10 to 15 K above the temperature of the equilibrium cell to prevent condensation of the samples.

Gas Chromatography

The most common method for phase analysis is gas chromatography, particularly for multicomponent mixtures. Besserer and Robinson (1971) and Kalra et al. (1978) have reported refractive index measurements done simultaneously with gas chromatography.

However, the drawback of this approach is that the high pressure high temperature equilibrium condition is appreciably different from that of the input to the GC (Raal and Mühlbauer, 1994a).

The two principal types of detectors for gas chromatography analysis are:

- Thermal conductivity detector (TCD) which can be used in the detection of both hydrocarbons and non-hydrocarbons.
- Flame ionisation detector (FID) which can be used in the detection of organics only. Nonetheless, its sensitivity is more than that of the TCD.

The primary limitation of phase analysis using gas chromatography is that the high pressure equilibrium state from which the sample for analysis is withdrawn is comparatively different from the state upon being admitted into the chromatograph. An observation made by Deiters and Schneider (1986) is that the quantitative establishment of the compositions normally does not pose any problems. As a result of the problems presented by the preparation and handling of the sample, this procedure is therefore of paramount importance as it is the pivot upon which the accurate phase analysis rests (Naidoo, 2004). Another problem presented occurs in the accurate GC calibration of the detectors for gas and gas-liquid mixtures in the absence of dependable commercial standards (Raal and Mühlbauer, 1994a).

Spectroscopic Method

Rigas et al. (1958), Street and Sonntag (1964), and Yonker et al. (1984) report the use of mass spectroscopy. In-situ phase composition analysis is accomplished by means of photometric methods or spectroscopy. According to Beer's law, absorbance is commensurate with concentration (proportionality between amount of substance per unit volume and absorbance). The use of infrared spectra is reported by Swaid (1984); where the absorption bands are usually well detached, to ascertain phase concentrations.

Nevertheless, there are challenges encountered in the use of visual, infrared and ultraviolet spectroscopy or Raman scattering method (Mühlbauer and Raal, 1995):

i. The extensive calibration techniques necessary compared with those needed for gas chromatography.

ii. The use of visual or ultraviolet spectroscopy is mainly limited to aromatic or coloured compounds.

iii. In the use of infrared spectroscopy, there is a strong like-hood of the overlapping of absorption bands of various compounds.

3.3.6 Attaining Isothermal Conditions

Attaining truly isothermal conditions is pivotal to the accurate experimentation of HPVLE. Raal and Mühlbauer (1994a) have reported that from observation the existence of temperature gradients in the equilibrium cell of the apparatus will result in substantial error. Even small vertical gradients in the equilibrium cell have a detrimental effect. The following recommendations have been proposed:

a) It is proposed that conductive paths to or from the cell, in the form of, fittings, sampling devices or attachments must be evaded (Raal and Mühlbauer, 1994a). The attachments and fittings should be immersed inside the invariable temperature bath together with the equilibrium chamber to subdue the problem. Direct radiative energy exchange between the bath heaters and the chamber must be evaded to guarantee the absence of local hot spots.

b) A number of temperature sensors are positioned in the walls of the equilibrium cell to test the homogeneousness of the temperature. At high temperatures, there may be the existence of thermal gradients inside the equilibrium cell as a result of heat escaping from the fluid surface. Thermal gradients are detrimental as they lessen the quality of the measurement and change the vapour composition by promoting the condensation of the vapour-liquid equilibrium mixture onto the tip of the capillary while sampling in the vapour phase (Nelson et al., 2015a). Rogers and Prausnitz (1970), Figuiere et al. (1980), Legret et al. (1980) and Konrad et al. (1983) among other authors have reported having measured cell temperature or bath profiles.

c) Use of materials with large heat capacities, such as water and silicon oil, that require a large amount of heat to be added to effect a change of temperature for a unit mass and are excellent at retaining heat.

d) For uniform temperature baths, the regulated environment encasing the equilibrium cell and is to be adiabatic. Duraback, copper, polyurethane foam and Fibrefrax are employed in lining the inside of the baths to avert confined thermal disturbances (Naidoo, 2004). Mühlbauer (1990) reports having used fibreglass mineral wool as

insulation material. Naidoo et al. (2008) in their design of a new high-pressure apparatus housed the equilibrium cell in rectangular shaped air-bath which was insulated with Fibrefrax Duraback whose interior was lined with copper to foster temperature uniformity.

Recent designs make use of an air bath, bath containing a fluid or the apparatus can be placed in an oven (Guilbot et al., 2000).

3.4 The Static Analytical Method for High Pressure Vapour-Liquid Equilibrium Experimentation

3.4.1 Description of the Static Analytical Method

Figure 3-2 below illustrates the features of a typical static apparatus.

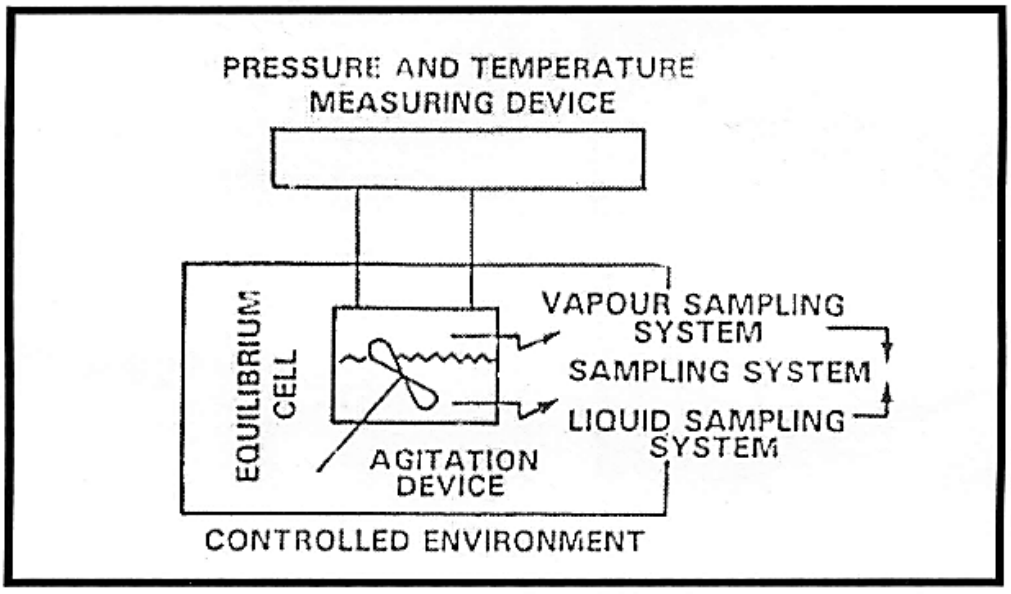

Figure 3- 2: Typical features of the static analytical method [extracted from Raal and Mühlbauer (1994b)].

For the static method for measuring vapour/liquid equilibrium data, it is essential that the liquids which make up the system be thoroughly degassed. The components being investigated are injected into the equilibrium cell. The liquid component is injected into the equilibrium cell by flushing with the volatile component or employing a pump. The volatile component is dispensed directly from the cylinder in which it is stored whereas high boiling more volatile

components such as butane and propane should be heated and pumped in by a compressor type device (Mühlbauer, 1990). The agitation of the equilibrium cell contents is then undertaken so as to stimulate contact between the phases and therefore hasten the attainment of equilibrium. Upon attainment of equilibrium, the pressure and temperature are noted and liquid and/or vapour samples are withdrawn from the equilibrium cell. Their compositions are then analysed. It is important to regulate the temperature and pressure of the equilibrium cell so as to produce the desired VLE isobaric or isothermal phase diagrams.

3.4.2 Problems associated with the static analytical method

i. The equilibration time can be lengthy (Malanowski, 1982). This necessitates the inclusion of some sort of mixing device or mechanism in the equipment design and in so doing complicating the equilibrium cell design.
ii. A need arises to compensate for the drop in pressure as a result of sampling (Dohrn et al., 2012).
iii. The liquid component needs to be thoroughly degassed as discussed in Section 3.3.2.
iv. A withdrawal device is necessary when sampling phases. In addition, the preparation of the sample for analysis is essential as well, as discussed comprehensively in Sections 3.3.5.
v. At high temperatures, there may be the existence of thermal gradients inside the equilibrium cell as a result of heat escaping from the fluid surface. Thermal gradients are detrimental as they lessen the quality of the measurement and change the vapour composition by promoting the condensation of the vapour-liquid equilibrium mixture onto the tip of the capillary while sampling in the vapour phase.

3.5 Review of Recent Equipment Development

For a review of the static analytic apparatus, the reader is referred to Mühlbauer and Raal (1995), Dohrn and Brunner (1995), Christov and Dohrn (2002), Dohrn et al. (2010), Fonseca et al. (2011), and Dohrn et al. (2012). A summary of the main and interesting equipment designs developed and published in the literature are provided in these articles. Furthermore, designs after 2012, have been a modification of previous equipment designs. Weir and De Loos (2005) provide a detailed discussion of equipment developments for high pressure phase equilibrium studies. The summary below highlights the features of the experimental devices

housed in the TRU. This discussion was based just on these equipment designs and modifications, as it summaries the general features of the equilibrium design and interesting modifications up until the equipment used in this study.

The HPVLE Apparatus of Naidoo (2004)

The equilibrium cell design of Naidoo (2004) was a modification of the apparatus of Kissun (2001). The equipment was initially designed and commissioned by Ramjugernath (2000). The cell was fabricated using SS 316L with a diameter of 12 cm and a height of 20 cm. The cell has an internal volume of 200 cm^3 and is equipped with a stirrer. The cell design includes a piston which can be used to vary the volume by altering the displacement of the piston. The equipment had an operating limit of 448 K and 175 bars for the temperature and pressure respectively. The unit incorporated jet-mixers to vaporise and homogenise samples in the liquid phase in preparation for being conveyed to the GC. Samples from the jet-mixers were sent to the GC using the 8-port vales. Isothermal conditions were maintained using an air bath which is equipped with a temperature controller. The temperature was measured using 4 Pt-100 resistors located in the air bath and another 4 Pt-100 resistors located in the cell body. On the other hand, 3 Sensotec pressure transducers were used to measure pressure.

The modifications by Kissun (2001) included the incorporation of a refrigeration unit to permit measurements to be undertaken at temperatures as low as 250 K. The liquid-phase jet-mixer was redesigned to enable its operation at low temperatures so as to overcome the instabilities in the temperature profile within the air bath that were created by the elevated operating temperatures of the previous jet-mixer. The modifications undertaken included a resizing of the liquid jet-mixer. This was to overcome the inaccuracies which were as a result of the previous jet-mixer as its mixing profile showed a non-uniform pattern especially for heavy liquids. The novelty in the equilibrium cell design of Naidoo was the stepper motor circuit which allows the accurate quantification of the piston displacement; this is essential in P-V-T measurements in varying the volume. The equipment was also set up for the data acquisition of the temperature (cell, jet-mixers and air bath) and cell pressure.

The HPVLE Apparatus of Chiyen (2010)

The equilibrium cell design of Chiyen was a modification to the static HPVLE apparatus of Naidoo (2004). The changes implemented were necessitated by the need to improve the sample analysis technique. Previously, sample withdrawal was undertaken using two GC 8-port valves where the fluid was conveyed to the sample loop and flushed to the GC using the carrier gas. The challenge encountered was the inclination of the more volatile chemical to flash prudentially and as such jet-mixers were incorporated into the cell design. This sampling technique presented errors and was lengthy. The modifications undertaken comprised the incorporation of the ROLSI™ (Rapid-Online-Sampler-Injector) device and removal of the jet-mixers. The piston chamber located at the top of the equilibrium cell was removed so as to mount the ROLSI™. Also, a redesign of the air-bath to improve the temperature profile was undertaken. The ROLSI™ allows for the withdrawal of very small sample volumes and as a result the equilibrium remains undisturbed. Repeatable sample amounts can be withdrawn with the use of the ROLSI™. Samples sizes can be several hundredth to several milligrams (Guilbot et al., 2000)

The HPVLE Apparatus of Narasigadu (2011)

A unique feature of the equilibrium cell design of Narasigadu (2011) is the sapphire tube that is sealed between two metal flanges. The equilibrium cell has a maximum capacity of approximately 18 cm^3 and enables the measurement of phase equilibrium data for small volumes. The sampling of phases is achieved using the ROLSI™ and ensures that the equilibrium is not disturbed during sampling. The small equilibrium cell volume enables equilibrium to be attained in a comparatively shorter time. The novelty in the design is the incorporation of a movable metallic rod that has similar dimensions to that of the capillary of the ROLSI™ and compensates for any volume disturbances during sampling. Narasigadu (2011) demonstrated that the apparatus performed very well and produced reproducible and accurate results over a temperature range of 253 to 473 kPa and pressures up to 1600 kPa. The measurements undertaken included VLE, VLLE and LLE data. As a result of the temperature gradients at high temperatures, a heater cartridge was included and inserted into a cavity bored in a metallic block and placed on the top flange and was able to decrease the temperature gradient to less than 0.2 K. The temperature sensors were housed in the flanges.

The HPVLE Apparatus of Nelson (2012)

Nelson (2012) reproduced the equilibrium cell design of (Narasigadu, 2011) as it was suitable of the measurement of HPVLE data for the hazardous compounds. His study involved the measurements of isothermal VLE data for silanes. Due to the toxicity of the chemicals under investigation; to fully mitigate the risks during experimentation, the apparatus was located in a glovebox to ensure that any probable chemical leak may not spread to the entire laboratory. The glove-box was purged with nitrogen whereas the workspace was equipped with an extraction unit as well as a gas-filtering system. The equipment of Nelson (2012) incorporated a thermal press which uses the thrust of the piston to compress and load the vapour and liquid components into the equilibrium cell by way of inducing a pressure gradient. The pressure gradient between the thermal press and the equilibrium cell was attained by gently applying heat to the thermal press. The convenience of this in his work was that the hazardous chemicals which he was working with could be safely stored prior to loading. The thermal press design does not have O-rings and is therefore leak-tight. As a consequence of the restriction that the glove-box places in being able to be in direct contact with the equipment, electronic (solenoid) valves were used. The working range of the valves is a pressure range from vacuum to 85 bar and temperatures between 278 K and 378 K.

4

CHAPTER FOUR

4. REVIEW OF THE THEORETICAL PRINCIPLES IN THERMODYNAMICS FOR HIGH PRESSURE VAPOUR-LIQUID EQUILIBRIUM

Accurate high pressure thermodynamic data for fluorocarbons such as 1,1,2,3,3,3-hexafluoro-1-propene is required for a better understanding of their behaviour and utilisation in process design and synthesis. Thermodynamic modelling and interpretation of experimental HPVLE data allows the interpolation and extrapolation of data to conditions where data has not been measured.

4.1 Vapour-Liquid Equilibrium Modelling

A review of the theoretical principles in thermodynamics for HPVLE is presented herein. The modelling and interpretation of isothermal HPVLE data can be achieved using two methods. The first method is termed the *combined method* or $(\gamma - \phi)$ which essentially is a logical development of the low-pressure correlation methods. The combined method uses the fugacity and activity coefficients to describe the vapour and liquid non-idealities respectively. The method allows excellent representation of phase behaviour for complex systems in the low to moderate pressure ranges (0 – 500 kPa). The difficulties encountered in describing the high pressure region were overcome by the development of the *direct method* or $(\phi - \phi)$. The direct method was used in the regression and modelling of all data in this work. As such, the method is described in detail herein.

The Direct Method

For the direct method, the vapour and liquid phase non-idealities are described by fugacity coefficients (ϕ) by employing EoSs:

$$\hat{f}_i^V = y_i\hat{\phi}_i^V = \hat{f}_i^L = x_i\hat{\phi}_i^L \tag{4-1}$$

The equilibrium condition is described by:

$$y_i\hat{\phi}_i^V = x_i\hat{\phi}_i^L \tag{4-2}$$

Consequently, the equilibrium ratio K is given by:

$$K_i = \frac{y_i}{x_i} = \frac{\hat{\phi}_i^L}{\hat{\phi}_i^V} \tag{4-3}$$

For the liquid phase,

$$ln\hat{\phi}_i^L = \left(\frac{1}{RT}\right)\int_{V^L}^{\infty}\left[\left(\frac{\partial P}{\partial n_i}\right)_{(T,V,n_j)} - \frac{RT}{V^L}\right]dV - ln\left[\frac{PV^L}{n_T RT}\right] \tag{4-4}$$

and for the vapour phase,

$$ln\hat{\phi}_i^V = \left(\frac{1}{RT}\right)\int_{V^V}^{\infty}\left[\left(\frac{\partial P}{\partial n_i}\right)_{(T,V,n_j)} - \frac{RT}{V^V}\right]dV - ln\left[\frac{PV^V}{n_T RT}\right] \tag{4-5}$$

The effect of composition, pressure and temperature on the vapour and liquid fugacity can be determined by the effect of these variables on the fugacity coefficient.

$$\hat{\phi}_i^V = \phi(T, P, y_i, \ldots\ldots\ldots, y_N) \tag{4-6}$$

$$\hat{\phi}_i^L = \phi(T, P, x_i, \ldots\ldots\ldots, x_N) \quad (4\text{-}7)$$

The vapour and liquid phase fugacity coefficients are evaluated using an appropriate EoS describing the phase behaviour through the exact thermodynamic model. Figure 4-1 displays the computational flow diagram for the regression isothermal binary VLE data. The input to the iteration as computed by a program are the temperature condition, *T* and the compositions $\{x_i\}$ as well as the parameters for the calculation of the saturated pressure $\{P_i^{sat}\}$, activity coefficients for species $\{\gamma_i\}$, and fugacity coefficient for species $\{\phi_i\}$. Initial estimates of the mixing rule are set as well as the tolerance for the pressure iterations. The pure component saturated vapour pressure $\{P_i^{sat}\}$ is calculated from the Antoine equation, whereas $\{\gamma_i\}$ values are computed from the activity coefficient correlation. The pressure *P* and vapour composition are computed from the equation shown on the schematic. The next pressure value is determined by an iterative procedure using methods such as the Newton-Raphson Method (NRM). The iteration procedure continues until the change in *P* from one iteration to another is less than the tolerance, consequently converging to some final value of vapour composition and pressure.

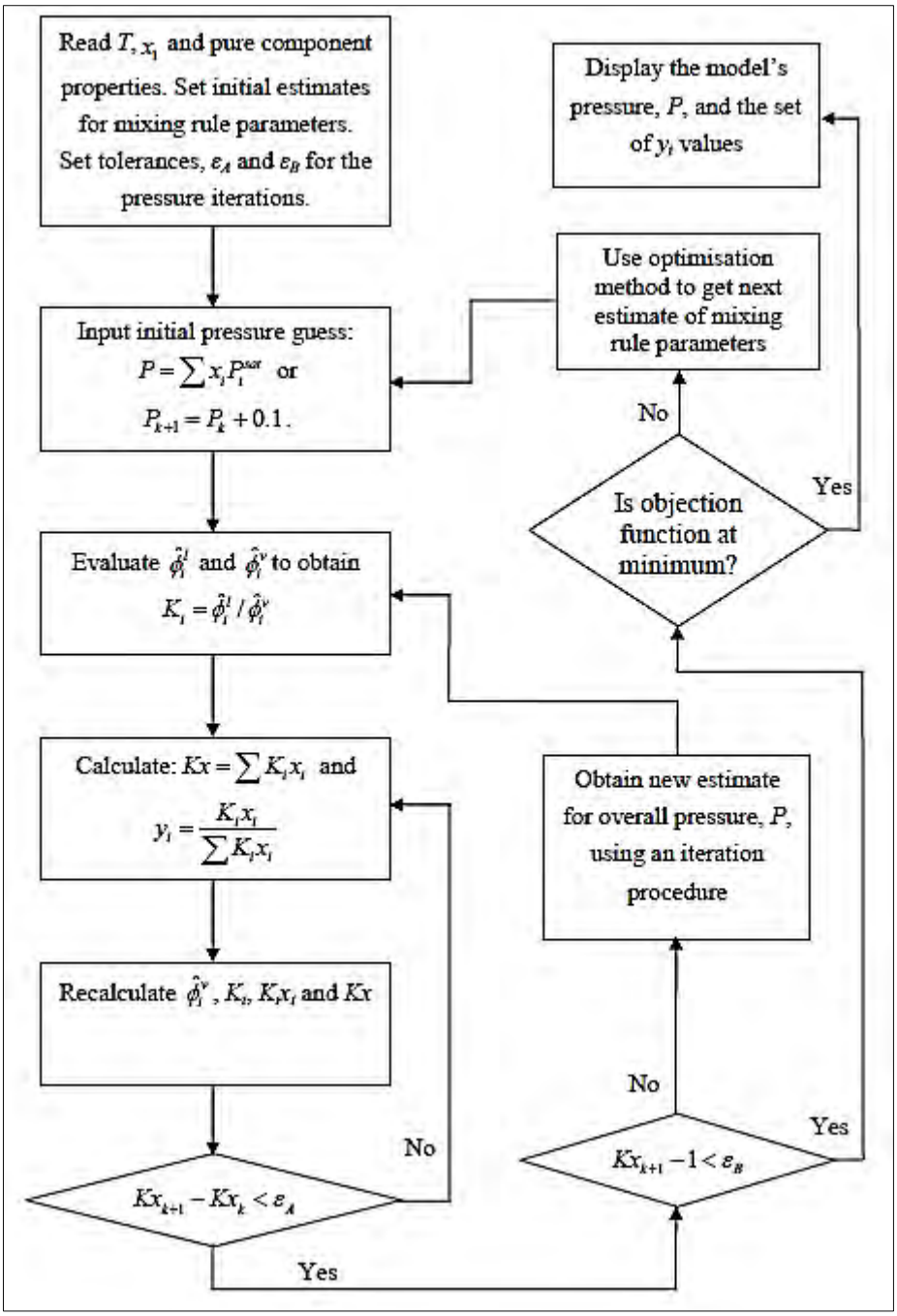

Figure 4-1: Schematic diagram of the isothermal vapour-liquid equilibrium bubble-pressure calculation procedure for the direct method to attain parameters for the mixing rules used (Smith et al., 2005). Extracted from Narasigadu (2011).

Previously before the advent of simulation packages such as CHEMCAD and Aspen Plus®; a number of challenges were encountered with regard to the use of the direct method. Previous texts (Westhaus and Sass, 2004, Luyben, 2013) indicate that a number of challenges were encountered before the development of simulation packages and help files. These are highlighted below together with recent developments:

1. The selection of the most appropriate EoS to adequately describe both the vapour and liquid phase non-idealities. The EoS must be adaptable enough to fully describe a pure substance's P-V-T behaviour for the liquid and vapour phase within the bounds of the pressure and temperature under investigation. Recently, with the use of thermodynamic modelling and regression on simulation packages, the data can be interpolated and extrapolated to determine the phase behaviour at conditions where experimental data has not been measured.
2. The selection of an appropriate mixing rule to correctly describe the mixture properties. Mixing rules are to a certain extent empirical and have a tendency to be system specific. A large array of mixing rules is available to select from within simulation packages at present.
3. Previously there were difficulties with locating the appropriate roots for both the liquid- and vapour molar densities when higher than third order equations of state are employed (Raal et al., 1980).

Much of these challenges encountered in modelling using the direct method have been overcome through the use of simulation packages for data regression. A vast number of equations of states, mixing rules and Gibbs energy models are available embedded in simulation packages. Also available are predictive models methods and simulation methods based on statistical mechanics and potential energies. The COSMO-RS (Real Solvation) model, whose foundation is in quantum chemistry can be applied in predictions of binary vapour-liquid equilibria (activity coefficient of a component within a mixture) and has been shown to have high predictive power (Spuhl and Arlt, 2004, Grob and Hasse, 2005). Also, the molecular based Perturbed-Chain Statistical Associating Fluid Theory (PC-SAFT) equation of state which makes use of a pressure explicit mathematical function (Privat et al., 2010) can be used.

4.2 Thermodynamic Models

This work made use of the direct method to regress the VLE data, by means of the PR EoS integrating the Mathias-Copeman (MC) alpha function and making use of the Wong-Sandler mixing rules in conjunction with the NRTL activity coefficient model. The models are examined below. The thermodynamic model implemented has been previously used for binary

systems of R-1216 + alkanes and gave a good representation of the correlated data, where the absolute average deviation in the mole compositions of < 2% for all systems investigated. The reader is referred to (Subramoney et al., 2012) and Subramoney et al. (2015)

The different thermodynamic models are examined below.

Peng-Robinson (Peng and Robinson, 1976)

The Peng-Robinson equation of state is a modification of the Soave-Redlich-Kwong (SRK) equation as proposed by Peng and Robinson (1976) through the development of a new two-constant EoS whose attractive pressure term of the semi-empirical van der Waals equation is modified. The Peng-Robinson equation addresses the shortcomings of the SRK equation such as its lack of success in generating satisfactory density value for the liquid although the computed vapour densities are generally adequate. The proposed equation is of the form

$$P = \frac{RT}{V-b} - \frac{a(T)}{V(V+b)+b(V-b)} \tag{4-8}$$

Equation (4 - 8) can be rewritten as

$$Z^3 - (1-B)Z^2 + (A - 3B^2 - 2B)Z - (AB - B^2 - B^3) = 0 \tag{4-9}$$

where

$$A = \frac{aP}{R^2T^2} \tag{4-10}$$

$$B = \frac{bP}{RT} \tag{4-11}$$

$$Z = \frac{PV}{RT} \tag{4-12}$$

Applying Eq. (4 - 9) at the critical-point gives

$$a(T_c) = 0.45724\frac{R^2T_c^2}{P_c} \tag{4-13}$$

$$b(T_c) = 0.07780\frac{RT_c}{P_c} \tag{4-14}$$

$$Z_c = 0.307 \tag{4-15}$$

At temperatures with the exception of the critical, let

$$a(T) = a(T_c) \cdot \alpha(T_r, \omega) \tag{4-16}$$

$$b(T) = b(T_c) \tag{4-17}$$

where $\alpha(T_r, \omega)$ is a dimensionless function of the acentric factor and reduced temperature. At the critical temperature the function equals unity.
The relationship between α and T_r may be linearized by the ensuing equation

$$\alpha^{0.5} = 1 + \kappa(1 - T_r^{0.5}) \tag{4-18}$$

In Eq. (4 - 18) κ is a constant that is typical of each substance. The constants are related to the acentric factor in the following manner

$$\kappa = 0.37464 + 1.54226\omega - 0.26992\omega^2 \tag{4-19}$$

Employing the thermodynamic relationship for a pure component

$$ln\frac{f}{P} = \int_0^P \left(\frac{V}{RT} - \frac{1}{P}\right) dP \tag{4-20}$$

$$ln\frac{f}{P} = Z - 1 - ln(Z - B) - \frac{A}{2\sqrt{2}B} ln\left(\frac{Z+2.414B}{Z-0.414B}\right) \tag{4-21}$$

The mixture parameters in Eq. (4 - 9) and (4-25) are defined by

$$a = \sum_i \sum_j x_i \, x_j \, a_{ij} \tag{4-22}$$

$$b = \sum_i x_i \, b_i \tag{4-23}$$

where

$$a_{ij} = \left(1 - \delta_{ij}\right) a_i^{0.5} a_j^{0.5} \quad (4\text{-}24)$$

For a binary mixture with components i and j in a mixture, the fugacity coefficient is given by

$$ln\frac{f_j}{x_j P} = \frac{b_j}{b}(Z-1) - ln(Z-B) - \frac{A}{2\sqrt{2}B} \times \left(\frac{2\sum_i x_i a_{ij}}{a} - \frac{b_j}{b}\right) ln\left(\frac{Z+2.414B}{Z-0.414B}\right) \quad (4\text{-}25)$$

The Peng-Robinson and the Soave-Redlich-Kwong equations of state find extensive use in industry. Their attractiveness stems from their need of not much input information (only the acentric parameters as well as the critical properties), little computational time and the generation of excellent phase equilibrium predictions for hydrocarbon systems (Peng and Robinson, 1976). The Peng-Robinson equation performs as competently as or better than the Soave-Redlich-Kwong and displays its greatest advantages in liquid phase density prediction (Peng and Robinson, 1976, Han et al., 1988). The Peng-Robinson property method is appropriate for non-polar or mildly polar mixtures. Examples include hydrocarbons and light gases. It is also suitable in the high temperature and high pressure region. The α parameter in the Peng-Robinson equation of state is a temperature function and it improves the correlation for the pure component vapour pressure.

Mathias-Copeman (MC) Alpha Function (Mathias and Copeman, 1983)

In this work, the Mathias-Copeman alpha function (Mathias and Copeman, 1983) was employed in conjunction with the Peng-Robinson EoS, as a result of its particular development to enhance the description of polar component vapour pressures. The Mathias-Copeman alpha function is expressed as follows:

$$\alpha_i(T) = \left[1 + C_{1,i}\left(1 - \sqrt{T_{R,i}}\right) + C_{2,i}\left(1 - \sqrt{T_{R,i}}\right)^2 + C_{3,i}\left(1 - \sqrt{T_{R,i}}\right)^3\right]^2 \quad (4\text{-}26)$$

In Eq. (4 - 26) $C_{1,i}$, $C_{2,i}$ and $C_{3,i}$ are the Mathias-Copeman parameters. The vapour pressure of component i is used to regress the parameters, where T_R designates the reduced temperature for component i.

The Mathias-Copeman alpha function is an extension of the Peng-Robinson alpha function and it offers a more accurate fit for the vapour pressure for polar compounds (Subramoney et al., 2013b). It is for this reason that the MC alpha function is used. Literature data has shown the

Mathias-Copeman alpha function to be adequate in fitting vapour pressure data for fluorocarbons and hydrocarbons. Subramoney et al. (2012) and Nelson et al. (2015b) used the Mathias-Copeman expression to correct the α function for a more accurate representation of the vapour pressure.

Wong-Sandler (WS) Mixing Rules (Wong and Sandler, 1992)

The Wong and Sandler (1992) mixing rules allow extrapolation of data over vast ranges of conditions of temperature and pressure. The WS mixing rules make use of a relationship between the excess Helmholtz energy A^E and equation of state. The WS mixing rules were used above other mixing rules such as the second-order Modified Huron Vidal (2MHV) mixing rules as the Huron-Vidal mixing rules use a relationship between the equation of state properties and the excess Gibbs energy. While the Huron-Vidal mixing rule has been used for some complex mixtures with success, it does not satisfy the second virial coefficient boundary condition (Wong et al., 1992). The WS mixing rule satisfies the second virial coefficient and is capable of demanding that the EoS predict the same A^E at infinite pressure (A^E_∞). The advantages of the integration of the A^E instead of G^E at infinite pressure consist of, primarily, the requirement that V^E be zero is not necessary, and furthermore, A^E is basically pressure independent whereas G^E, which is a function of pressure, when computed at low pressure from an EoS does not necessarily guarantee that it will be similar to that from an activity coefficient model.

In these equations, A^E_∞ the excess Helmholtz free-energy at infinite pressure is used to obtain the molar excess Gibbs free energy as a function of the composition and temperature only by making the assumption that $A^E_\infty(T,P,x_i) \approx A^E_0(T,P,x_i) \approx G^E_0(T,P,x_i) = g^E$ (Orbey and Sandler, 1998).

For the Wong-Sandler mixing rule the mixing terms are computed from

$$b_m = \frac{RT\sum_i^N\sum_i^N x_i x_j\left(b_{ij}-\frac{a_{ij}}{RT}\right)}{RT-\left[\sum_i x_i\frac{a_i}{b_j}-\frac{A^E_\infty(T,P,x_i)}{\Omega}\right]} \tag{4-27}$$

with

$$\left(b - \frac{a}{RT}\right)_{ij} = \frac{1}{2}\left[b_i - b_j\right] - \frac{\sqrt{a_i a_j}}{RT}\left(1 - k_{ij}\right) \quad (4\text{-}28)$$

and

$$a_m = b_m\left[\frac{\sum_i^N x_i a_i}{b_i} + \frac{A_\infty^E(T,P,x_i)}{\Omega}\right] \quad (4\text{-}29)$$

For the Peng-Robinson EoS $\Omega = \frac{1}{\sqrt{2}} ln\left(\sqrt{2} - 1\right) \approx -0.62323$

In Eq. (4-28), κ_{ij} is the binary interaction mixing parameter. For the R-1216 + alkane systems measured and regressed in literature, Subramoney et al. (2012) obtained a κ_{12} value of 0.345 in the Ethane (R170) + 1,1,2,3,3,3-Hexafluoro-1-propene (R-1216) binary system, and Subramoney et al. (2015) obtained values less than 0.2 for all isotherms regressed individually for binary mixtures of 1,1,2,3,3,3-hexafluoro-1-propene (R-1216) with either propane or n-butane.

Non-Random Two-Liquid (NRTL) Equation (Renon and Prausnitz, 1968)

Renon and Prausnitz (1968) implemented the concept of *local composition* in their development of the NRTL (Non-Random-Two-Liquid) equation. In contrast to Wilson's equation, this equation is suitable for partially miscible and wholly miscible systems (Prausnitz et al., 1998). The parameter α gives an indication of the non-randomness of the mixture; a value of zero for α_{12} means the mixture is entirely random.

The NRTL equation for the excess Gibbs energy is given by:

$$\frac{G^E}{RT} = x_i x_j \left(\frac{\tau_{ji} G_{ji}}{x_i + x_j G_{ji}} + \frac{\tau_{ij} G_{ij}}{x_j + x_i G_{ij}}\right) \quad (4\text{-}30)$$

and the activity coefficient for the components 1 and 2 of a binary mixture is given by:

$$ln\gamma_i = x_j^2\left[\tau_{ji}\left(\frac{G_{ji}}{x_i + x_j G_{ji}}\right)^2 + \frac{\tau_{ij} G_{ij}}{\left(x_j + x_i G_{ij}\right)^2}\right] \quad (4\text{-}31)$$

where

$$G_{ij} = exp\left(-\alpha_{ij}\tau_{ij}\right) \quad (4\text{-}32)$$

where x_i and x_j are the liquid mole fractions of the respective components. The non-randomness parameter, α_{ij} is an adjustable parameter or can be set to 0.3.

The binary interaction parameters τ_{ij} and τ_{ji} are defined in Aspen Properties® as a function of temperature,

$$\tau_{ij} = a_{ij} + {}^{b_{ij}}/_{T} + c_{ij} lnT + f_{ij} T \qquad (4\text{-}33)$$

In Eq. (4 - 33) a_{ij}, b_{ij}, c_{ij} and f_{ij} are asymmetrical and are the reason for the model's dependence on temperature,

$$\alpha_{ij} = c_{ij} + d_{ij}(T - 273.15) \qquad (4\text{-}34)$$

where T is recorded in Kelvin. In this study a value of zero is assigned to d_{ij}, whereas c_{ij} is not regarded as an adjustable parameter, and for this reason is set at 0.3.

The recommended c_{ij} values for different types of mixtures are as follows (Henley et al., 2011): 0.2, saturated hydrocarbons with polar non-associated liquids and systems that exhibit liquid-liquid immiscibility; 0.3, non-polar substances or non-polar with polar non-associated liquids and those that have small deviations from ideality; 0.47, strongly self-associated substances with non-polar substances. Subramoney et al. (2015) studied binary mixtures of similar components in their work (R-1216 + hydrocarbons) and assumed the non-randomness parameter α_{ij} to be temperature independent and set it at 0.3. Their experimental data were well represented by the model. Furthermore, Walas (2013) endorses that α_{ij}(non-randomness factor) is characteristically fixed at 0.3 in reference to non-aqueous mixtures.

4.3 Data Regression using Aspen Plus®

The regression of the measured VLE data was undertaken on Aspen Plus® by making use of built-in thermodynamic property models. The Property Methods function in Aspen Plus® packages the methods and models used to calculate thermodynamic properties. A unique combination of methods and models used for calculating a property is called a route. A property method is selected from existing property methods in Aspen Plus® or a custom-made property method can be created by modifying an existing property method.

According to (Nelson, 2012), it is generally preferred and expedient for one parameter set; that is, either a scalar or rather a temperature-dependent parameter set to characterise the experimentally determined phase equilibrium of all isotherms of a unique binary mixture. The parameters are fitted simultaneously to all experimentally determined isotherms of the measured VLE data. Where the parameters of a particular model integrate temperature dependence, it is inherent that the parameters must make use of the temperature dependence specified in Aspen Plus®. Therefore, it constitutes a good practice to fit the parameters concurrently to all experimentally determined isotherms of the VLE data.

The PRWS Property Method is based on the Peng-Robinson-Wong-Sandler equation of state model, which is an extension of the Peng-Robinson equation of state. The Wong-Sandler mixing rules make a prediction of the binary interaction parameters at any pressure. The PRWS property method is appropriate for use for mixtures of polar and non-polar compounds, in conjunction with light gases. The property method can be used up to high pressures and temperatures. Several alpha functions can be incorporated in the Peng-Robinson-Wong-Sandler equation of state model for a more accurate description of the pure component behaviour. For the PRWS Property Method, the default setting in Aspen Plus® is the Schwartzentruber-Renon-Watanasiri α function (Schwartzentruber et al., 1990), the Wong-Sandler mixing rules and the UNIFAC model for liquid phase activity coefficient. In using the UNIFAC model, the PRWS property method is predictive for any interaction that can be predicted by UNIFAC at low pressure. The Peng-Robinson alpha function was modified to include the Mathias-Copeman alpha function which is an extension of the Peng-Robinson alpha function which provides a more accurate fit for the vapour pressure (Aspentech, 2010). The Aspen Plus® default liquid phase activity phase activity coefficient model (UNIFAC) was replaced with the NRTL model.

The pure component properties were compared with the NIST (National Institute of Standards and Technology) ThermoData Engine. The NIST ThermoData Engine in Aspen Plus® allows access to experimental data and permits the evaluation of a property. The VLE data was regressed using the Britt-Luecke algorithm (Britt and Luecke, 1973) which is a rigorous maximum likelihood method. The least squares objective function was implemented, where the independent variables are assumed to be error free whereas errors in the dependent

parameters are minimised by adjusting one or more parameters. For isothermal data, the ordinary least squares objective function minimises errors in both the vapour compositions as well as pressure between the experimental and computed data. In contrast, the Maximum Likelihood objective considers errors in all variables. The Deming method, which gives an approximate solution, was made use of in initialisation. The Regression Results Deviation Dialog Box in Aspen Plus® summarizes deviations such as the average absolute deviation (AAD) and absolute average deviation (AARD) for the variable selected on the Residual Property sheet. The Bias is manually calculated separately for each variable. A high AARD value is suggestive of either a systematic or substantial random variance between the experimental data and the correlating thermodynamic model. A large positive or negative value for the Bias is indicative of systematic differences between the experimental data and the model used. An accurate representation of the experimental data by a correlating model is shown when the Bias is near zero.

Statistical analyses find use in the determination of the general measure of excellence of standard of the fit of experimental data against the implemented thermodynamic model. The statistical estimators implemented in this work for any property $\bar{\theta}$ are:
The average absolute deviation (AAD) is:

$$AAD(\bar{\theta}) = \frac{1}{N_p}\sum\left|\bar{\theta}_{EXP} - \bar{\theta}_{CALC}\right| \tag{4-35}$$

In Eq. (4-35) $\bar{\theta}_{EXP}$ and $\bar{\theta}_{CALC}$ are representative of the experimental and computed values of a property $\bar{\theta}$, whereas N_p is the number of data- points. The absolute average deviation (AARD) and the Bias are expressed as follows:

$$AARD(\bar{\theta}) = \frac{1}{N_p}\sum\frac{\left|\bar{\theta}_{EXP} - \bar{\theta}_{CALC}\right|}{\bar{\theta}_{EXP}} \tag{4-36}$$

$$Bias(\bar{\theta}) = \frac{1}{N_p}\sum\frac{\bar{\theta}_{EXP} - \bar{\theta}_{CALC}}{\bar{\theta}_{EXP}} \tag{4-37}$$

A high AARD value is suggestive of either a systematic or substantial random variance between the experimental data and the correlating thermodynamic model. A large positive or

negative value for the Bias is indicative of systematic differences between the experimental data and the implemented model. An accurate representation of the experimental data by a correlating model is shown when the Bias is near zero.

5

CHAPTER FIVE

5. EQUIPMENT DESCRIPTION

The Thermodynamics Research Unit (TRU) in the Discipline of Chemical Engineering at the University of KwaZulu-Natal has over the years gained prominence as a centre of excellence in chemical thermodynamics in the measurement of phase equilibrium studies. The TRU has successfully undertook the design, assembly and commissioning of experimental apparatus which are based on either the static or dynamic methods (Muhlbauer and Raal, 1991, Mühlbauer and Raal, 1995, Ramjugernath, 2000, Naidoo, 2004, Chiyen, 2010, Nelson, 2012, Narasigadu et al., 2013)

Two experimental apparatuses were used in this study for the measurement of isothermal VLE data. The first apparatus was designed by Ramjugernath (2000) and was modified by Kissun (2001), Naidoo (2004), and Chiyen (2010). A detailed review of the modifications and the reasons for the modifications implemented is found in §3.5. The switch from one apparatus to the other was necessitated by the problems encountered with the first equipment. It was observed that at higher pressure for one of the systems measured herein the O-rings were being corroded and would have entailed dismantling the cell and consequently would mean a lengthy period in the workshop undergoing repairs; and since the other unit was free, it was best to use that one especially for hexafluoropropylene which is expensive and hence the small equilibrium cell volume reduces the volume of chemicals used. The second apparatus was designed and commissioned by Narasigadu (2011). The apparatus enables the reliable measurement of phase equilibria data for small vapour and liquid volumes (maximum capacity of 18 cm^3). The equipment incorporates the ROLSI™ sampling device, however, the novelty in the design is the technique used to accomplish sampling of each phase. The technique entails

the use of an advancing metallic rod, of the same diameter as the ROLSI™ capillary, which compensates for volume changes in the duration of sampling (Nelson, 2012). The ensuing sections of the chapter give a comprehensive description of both equilibrium cell designs.

5.1 Equilibrium Cell Designs

Apparatus 1

The principal feature of the experimental apparatus is the equilibrium cell. The cell was fabricated using SS 316L billet with dimensions of 60 mm and 100 mm for the diameter and height respectively. The cell consists of a cylindrical cavity possessing two sapphire windows. The cylindrical cavity has a diameter of 30 mm and is 85 mm is length; thus presenting an internal equilibrium cell volume of 60 cm^3.The sapphire windows enable the observation of the liquid level, viewing of the investigated sample and to observe the positioning of the capillary of the ROLSI™ as it being raised and lowered to sample the vapour and liquid phases respectively. The cell can be operated at pressures up to as high as 20 MPa.

The sapphire viewing windows are 33 mm in diameter and a thickness of 15 mm and offer a viewing diameter of 20 mm on either side of the equilibrium cell. In order to hold the windows in one fixed position and evade any potential friction between the SS 316L metal casing and the glass, a firmly pressed gasket material was made use of to make a close-fitting surrounding as shown in Photograph 5-1. O-rings were employed as the sealing medium of the space separating the sapphire windows and gasket material. They are also used in sealing the space between the equilibrium cell body and the sapphire. The windows on either side of the cell were secured by way of five 8 mm bolts fabricated from using mild steel.

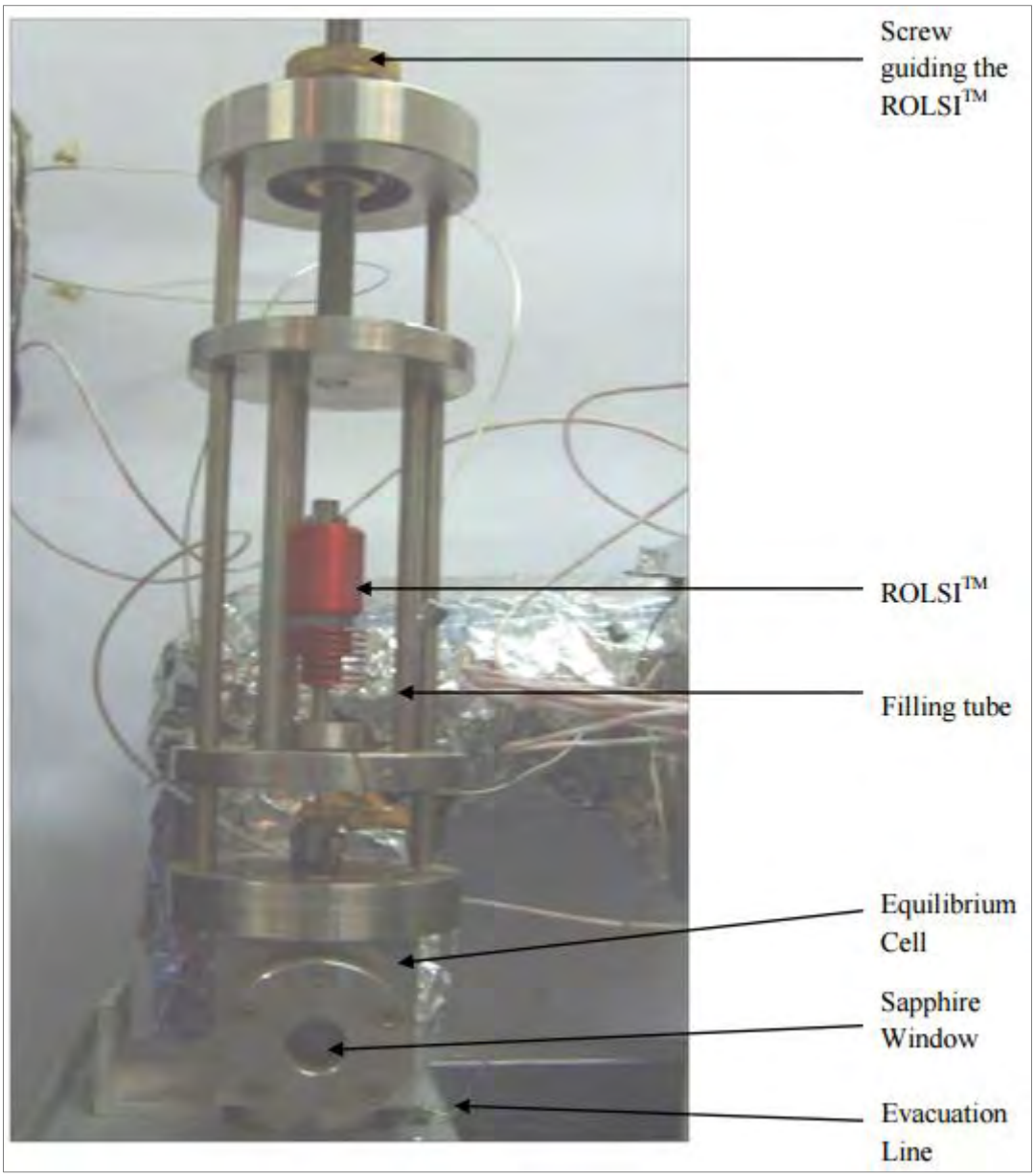

Picture 5- 1: The equilibrium cell [extracted from Chiyen (2010)]

A thumbscrew O-ring compression system was fitted onto the top flange of the equilibrium cell across which the ROLSI™ capillary passed as it is raised and lowered to sample the vapour and liquid phases respectively. The space between the underside of the top of the thumbscrew and the cell is sealed by use of Viton® O-rings. A SS 316L flange was used to support the ROLSI™. The movement of the ROLSI™ in sampling the different phases is achieved by way of a differential screw mechanism for making small adjustments of its positioning as shown in Photograph 5-1. The movement of the ROLSI™ between phases was aided by two 10 mm SS 316L tie-rods which are 210 mm in length and are fastened to the equilibrium cell using three flange blinds.

The top surface of the flange of the equilibrium cell body was bored with two 3 mm diameter holes which span right into the cell cavity. One of the holes was connected to the pressure transducer, whereas the other was sealed by way of an NPT fitting and could be used to connect to a standard pressure transducer when calibrating the pressure transducer to be used. Two other holes were drilled on either side of the cell body. The one on the top right of the cell (see Photograph 5-1) served as the entrance for the gas loading or evacuation and the lower hole was for the drainage of any residual liquid where standard drainage was ineffective and residual contents remained in the cell.

The phases in equilibrium were sampled by way of the ROLSI™ through the capillary tip which is carefully adjusted to position it in the phase of interest. GC gas carrier lines that are connected to the seat of the ROLSI™ on either side convey the sample to the GC. The GC lines were heat-traced.

The equilibrium cell is equipped with a magnetic stirrer within its interior. The stirrer rotates in accordance to the set speed of the rotor motor for the agitation of the equilibrium cell contents to hasten the attainment of equilibrium. Although the equipment has been used extensively in the Thermodynamics Research Unit and much of its design has remained unchanged; in the present work the mixing system was overhauled. The changes incorporated included inserting a Teflon fitting in the space between the gold-plated magnet and the metal base to prevent friction and therefore enhance the efficiency of the mixing. Figure 5-2 shows the magnetic stirrer. The mixing mechanism is comprised of two magnets. One magnet is connected to the roller motor chain at the bottom of the cell whereas the second is positioned inside the cell. The rotation of the rotor motor rotated the bottom magnet which activated the motion of the top magnet via dipole interactions. The speed of the roller motor in essence determined the speed of the mixing blades immediately above the top magnet. Variation of the rotor speed affects how quickly the equilibrium can be attained.

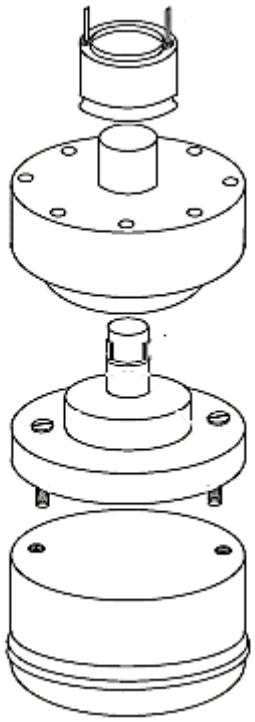

Figure 5- 2: Magnetic Stirrer [extracted from Bengesai (2016)]

To enable the accurate measurement of the temperature within the equilibrium cell; two Pt-100 temperature sensors were inserted into holes drilled at the back end of the cell. One probe was inserted at the bottom and the other at the top as shown in Figure 5-1. The motive behind the positioning of the probes is to enable the establishment of the existence of a temperature gradient which should be kept minimal. The pressure transducer was used for the measurement of the pressure and was held in a thermo-regulated block. Figure 5-1 shows the schematic of the equilibrium cell design of Tshibangu et al. (2013) similar to the one used in this work but the only differences being that the equilibrium cell used in this work did not have a variable volume press and the unique mixing unit described above.

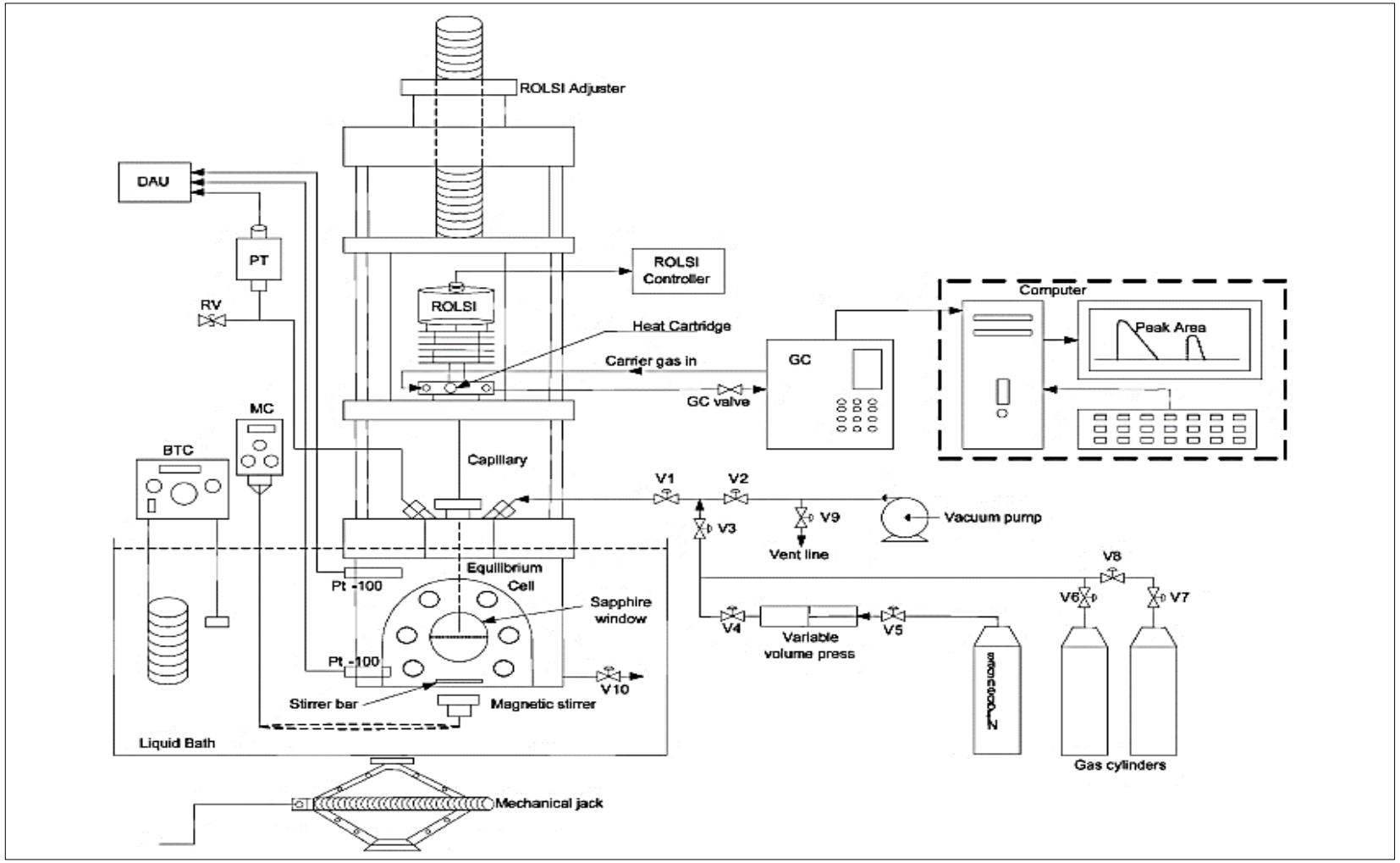

Figure 5- 1: Schematic diagram of the experimental equipment. BTC: bath temperature controller; DAU: data acquisition unit; GC: gas chromatograph; MC: mechanical circulator; PT: pressure transducer; RV: relief valve; V: valve. Extracted from Tshibangu et al. (2013)]

Apparatus 2

The second equipment was the equilibrium cell design of Narasigadu (2011). The sapphire tube has an outer diameter of 35.60 mm, internal diameter of 17.80 mm and a height of 70.00 mm. This results in a maximum cell capacity of approximately 18 cm^3 and enables the measurement of phase equilibrium data for small volumes.

The transparent sapphire tube is sealed between two SS 316 metal flanges; each with a 110 mm diameter and a thickness of 15 mm (Nelson, 2012). The equilibrium cell was sealed by making use of two O-rings positioned at each end of the equilibrium cell against the sapphire tube. The choice of O-rings used depends on the chemical behaviour of the components used during experiments. This work made use of Viton® O-rings as they are compatible with the alkanes and R-1216 used in this study.

The top flange has a 6 mm diameter hole bored on its side that tapers into a 3 mm diameter hole and serves as the equilibrium cell feed entry. Another end of the top flange is also bored with a hole of the same diameter and also tapers. This hole is connected to a 1/8″ pipe which is connected to the pressure transducer for the measurement of pressure. Another hole of 6 mm dimeter is bored to hold the heater cartridge. The third hole accommodates one of the two Pt-100s. Also found on the top flange is a hole which is 16 mm in diameter with M16 threads on it and making a pitch of 2 mm to enable the insertion of the capillary of the sampling device. .

The bottom flange also has a 6 mm diameter hole bored on its side that tapers into a 3 mm diameter hole at the equilibrium cell entry. This hole serves as the drain together with the 1/8″ pipe connected to it. The second hole of same dimensions houses the second temperature probe and has a depth of 30 mm.

Photograph 5-2 shows a dismantled image of the equilibrium cell. The equilibrium cell also features a ROLSI™ for the withdrawal of samples at equilibrium. The novelty in the design is the incorporation of a movable metallic rod that has similar dimensions to that of the capillary of the ROLSI™ and compensates for any volume disturbances during sampling.

Photograph 5- 2: Dismantled image of the equilibrium cell; [left] overhead view of the equilibrium cell; [right] view from the base of the sapphire tube. Extracted from Nelson (2012).

Equilibrium is attained through the agitation of the liquid phase of the mixture as a result of the rotation of a polytetrafluoroethylene coated magnetic stirrer bead. The stirrer's rotation was stimulated by an external stirring assembly that is made up of a horseshoe magnet connected by chain to a motor. The magnetic stirrer's rotation is as a result of the induced magnetic field. Figure 5-2 shows a schematic of the experimental apparatus of Narasigadu (2011). In contrast, the equipment used in this work did not have a GC 6-port valve as it was removed and the sample sent directly to the GC. The unit also did not have a compression device. The reader is referred to Narasigadu (2011) and Nelson (2012) for further details on the equipment.

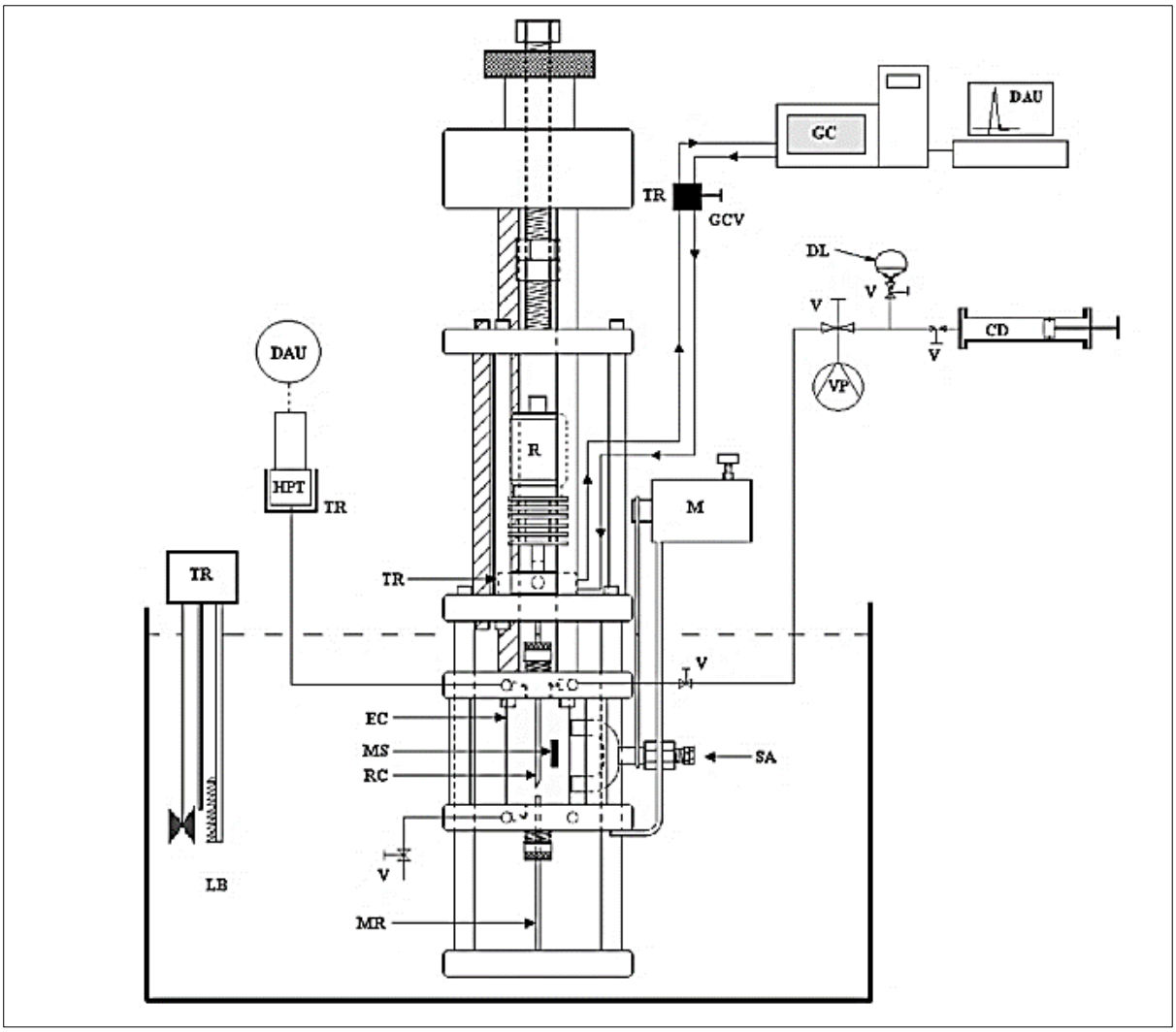

Figure 5- 2: Schematic of the experimental apparatus. CD – compression device; DAU – data acquisition unit; DL – degassed liquid; EC – equilibrium cell; GC – gas chromatograph; GCV – 6-port GC valve; HPT – high pressure transmitter; LB – liquid bath; M – motor; MR – metallic rod; MS – magnetic stirrer; R – movable ROLSI™; RC – ROLSI™ capillary; SA – stirring assembly; TR – thermal regulator; V – valve; VP –vacuum pump. Extracted from Narasigadu et al. (2013).

5.2 Equilibrium Cell Temperature and Pressure Measurement

On both equipment, the equilibrium temperature is measured through the use of two Pt-100s. These were 316 SS Class A 100 Ω platinum probes, and positioned within the cell body as explained earlier. The Pt-100s are positioned in the wells bored at the bottom and top flanges that hold the sapphire tube. The ends of the temperature probes make contact with the metal

flange just short of the equilibrium cell and give a representation of the equilibrium cell's temperature. Such positioning of the probes enable the monitoring of temperature gradients. For both equipment, a WIKA model P10 precision high-pressure transducer (maximum 250 bars) with an accuracy of 0.05 percent of the range as stated by the manufacturer was employed in the measurement of the pressure within the equilibrium cell. The pressure transducer is connected to the equilibrium cell by way of a 1/16" SS 316 line. A portion of the pressure transducer line extends beyond the level of the thermo-regulated fluid in the bath. This section of the line is heat-traced and maintained at a slightly higher temperature than the equilibrium cell to prevent the occurrence of any potential condensation of the components. The temperature of the pressure transducer line was maintained by way of heating by heat-tracing using firmly wrapped insulating Nichrome® wire that has an ACDC 1kVA voltage regulator as its source of heat. The temperature of the pressure transducer line is determined by making use of a 316 SS Class A 100 Ω platinum probe that has a 3mm diameter and is 20mm in length. The temperature of the probe is regulated using a Shinko® ACS – 13A controller. Potential heat sinks or losses were obviated by way of insulation.

As a result of the probable sensitivity of the of the pressure transducer signal to fluctuations in the temperature of its immediate surroundings, it is of paramount importance to regulate the device's temperature. As such, the pressure transducer is held in a thermo-regulated aluminium block. The output of the temperature probes as well as the pressure transducers was logged using a data acquisition unit (Agilent model 34970A) which measures the temperature and pressure within the cell respectively. The output from the data acquisition unit is then relayed to a desktop computer in which the installed software package allows the temperature and pressure to be measured and recorded in real-time computing.

5.3 Equilibrium Cell Temperature Regulation

A constant temperature within the equilibrium is achieved by immersing the cell into a temperature controlled bath fluid contained in a steel bath. The space between the interior and exterior sheets of the steel bath is lined with Fiberfrax® to serve as insulation. For both equipment, a steel bath with a volume of approximately 25 litres was used. The larger steel bath volume minimises variations in temperature and offers firmer control of the temperature such that there is insignificant temperature fluctuations. However, the large bath volume means that longer times are required for the attainment of temperature homogeneity of the thermal

fluid under consideration. The bath is surrounded by an iron framework which supports and guides the bath as it is being elevated or lowered. The other duty of the framework is to hold the equilibrium housing in a fixed position. A mechanical jack mounted underneath the bath is used to move the bath up and down within the iron framework so as to immerse the equilibrium cell within the isothermal environment/bath fluid.

The bath's fluid temperature is controlled by a Grant® precision stirred thermostatic circulator controller (Model: TFX200) which has the ability of regulating the fluid temperature to within ± 0.01 K of the set-point and has temperature range of 223.15 K to 473.15 K. The speed of the pump's circulation can be adjusted in a manner corresponding to how quickly an even temperature distribution is desired to be attained. The bath fluid used depends on the range of temperatures over which measurements are to be undertaken. For high temperatures, silicon oil (SI 044) was used as a result of its ability to maintain constantly high thermo-physical stability. It has a working temperature range of 343.15 to 423.15 K. Beyond 423.15 K thermal decomposition of silicon oil can occur. A mixture of equal volumes of ethylene-glycol and water was used for experiments conducted over a temperature range between 243.15 and 353.15 K. Freezing will occur if the temperature of the mixture is below the lower limit of the mixture whereas the mixture will vaporise at temperatures above the upper limit. For measurements conducted below room temperature, a chiller unit was used/cold finger was inserted into the thermo-regulated bath.

There is a propensity for heat to be lost from the bath fluid surface at elevated temperatures. This in turn results in unwanted thermal gradients as they are highly detrimental to the quality of the results generated. This could also result in the equilibrium mixture forming droplets onto the tip of the capillary when sampling in the vapour phase. The accumulation of droplets leads to an inaccurate representation of the equilibrium composition in the vapour phase. It was observed by Nelson (2012) that the temperature gradient existed especially when working at temperatures above 343.15 K. Therefore, an ACDC voltage regulator powered 100 W heating cartridge was inserted into a 6 mm cavity bored into the top flange. Nelson (2012) incorporated this into his design. The top flange temperature was determined by way of a Pt-100 temperature probe. In the event of the existence of a temperature gradient, a controlled heat input is applied to the top flange to eliminate the temperature gradient. The heating cartridge and the

temperature probe are attached to a controller and enable an experimentalist to have an indication of how much the heat input should be adjusted.

5.4 Sample Withdrawal and Analysis

Samples from either the liquid or vapour phase in the equilibrium cell are withdrawn using the ROLSI™ (Rapid On-Line Sampler Injector) and conveyed to a SHIMADZU gas chromatograph (Model: GC-2014). The experimental design of the ROLSI™ makes use of a capillary with a micro-stem tip; thus, it minimises the cross-sectional area at the tip of the capillary. This prevents differential vaporisation and makes certain that the majority of the pressure drop takes place at the end of the capillary near the chromatographic circuit (Fonseca et al., 2011). Differential vaporisation is detrimental as it can result to scattering results. The ROLSI™ is an excellent device permitting the withdrawal of micro-samples of varying adjustable sizes which may be in the range of several hundredths to several milligrams. The withdrawal of such small sample sizes prevents disruption of the thermodynamic equilibrium (Baba-Ahmed et al., 1999). After sample withdrawal, the samples are flushed by the carrier gas to the GC through the GC transfer lines. The transfer lines are heat-traced to prevent condensation within them.

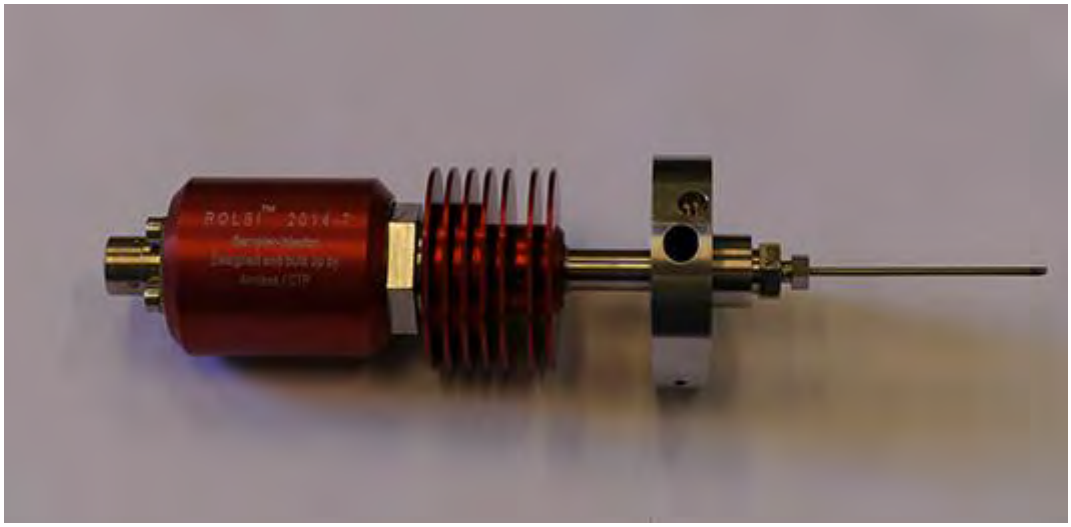

Photograph 5- 1: Rapid On-Line Sampler Injector (ROLSI™).

The constituents of the ROLSI™ are an electromagnet on one and a metallic base on another. The metallic base is coupled with a polymer seat at its end. A spring is situated in the space between the electromagnet and the metallic base. The seat makes a seal against the base of the

capillary. The downward force exerted onto the spring of the ROLSI™ is sufficient to ensure that the gap between the base of the capillary and the seat is closed. The pressure force is sufficiently large enough to withstand elevated equilibrium cell pressures of up to 600 bars as a result of the very small capillary internal diameter. The carrier gas (helium) is in continuous flow and follows a course that forms a circulation loop as it flows from end to end of the ROLSI™ sampler and through the gas chromatograph. The withdrawal of samples from the equilibrium cell is attained by breaking the seal. When the electromagnet of the ROLSI™ is activated, the force exerted on the seat directs it towards the magnet and ruptures the seal of the gas, allowing the gas to issue from the cell and be conveyed by carrier gas to the gas chromatograph. The electromagnet was deactivated by switching off which returns the seat to its former position and closes the gap between the base of the capillary and the polymer tipped seat, thereby shutting the equilibrium cell.

The temperature of the heating block of the ROLSI™, where the gas chromatograph carrier gas lines are situated, is controlled. The raised temperature of the heating block ensures that the withdrawn sample is in the gas phase, implying that it is completely vaporised. Where excess heat is generated, it is eliminated by the cooling fins positioned midway of the ROLSI™ body. The design, construction and functionality of the ROLSI™ puts a restriction on the minimum pressure at which sample withdrawal is possible. As such, the pressure in the equilibrium cell should be essentially higher than that of the carrier gas loop, as a positive pressure gradient will direct the sample to the gas chromatograph upon activation of the ROLSI™.

The ROLSI™ sampler was used in both equipment designs. As mentioned earlier, Apparatus 1 (60 cm^3) contained the ROLSI™ sampler mounted on the top flange and this was used to sample both phases. The ROLSI™ was moved by adjusting the screw as shown in Photograph 5 – 1. The position of the capillary tip was observed through the transparent sapphire windows. In Apparatus 2 (18 cm^3), the ROLSI™ was also moved by adjusting the screw. Hence to avoid disturbance to the volume, which would have resulted in change in the equilibrium condition, a moving volume compensating mechanism was incorporated as described above.

5.5 Composition Measurement

Samples withdrawn from either the vapour or the liquid phase of the equilibrium cell via the ROLSI™ were analysed using gas chromatographic methods. The gas chromatography detector has the ability to ascertain both the identity as well as the composition of the eluting components present within the carrier gas stream.

There are two types of gas chromatography detectors that find common use; which are the Thermal Conductivity Detector (TCD) and the Flame Ionisation Detector (FID). The response of the FID is based on the conducting potential of the ions or electrons generated upon combustion of the organic compounds in the flame. The FID is the most commonly used detector in gas chromatographic analysis. In contrast, the response on the TCD is dependent upon the thermal conductivity difference resultant between the eluted components and the carrier gas.

In this work, analysis of the phases in equilibrium was performed using a SHIMADZU (TCD) (model GC-2014). The GC is connected to a desktop computer by way of data acquisition software called GC Solution Version 2.42.00. The column employed was a Porapak Q packed column. The column length is 4m with an inner diameter of 3.2 mm and the material of construction is stainless steel. The GC was calibrated for all different binary combinations of systems which were investigated.

5.6 Safety, Health and Environmental Aspects of the Equipment and its Operation

Both equipment were housed in a double door enclosure; the entire setup is shown in Photograph 5-2 (Apparatus 2). The enclosure serves to contain all chemicals that could have been emitted due to sudden leaks on the equilibrium cell. An overhead extraction unit ensured that any chemical released was removed from the working space. This prevented the contamination of the entire laboratory. Discharged chemicals from the equilibrium cell were contained and stored until a time that they can be safely disposed of. Electrical wires were secured safely and away from fluids to eliminate electrical hazards. The equipment was leak tested before measurements in preparation for probable hazards such as sudden explosion. A vent line is also available to release gas into the extraction unit if need arises.

Photograph 5 - 1: Overview of the apparatus housing**.**

6

CHAPTER SIX

6. EXPERIMENTAL PROCEDURE

This chapter describes the experimental procedures to ensure that the equilibrium measurements are performed accurately. The facets enumerated in this chapter are as follows; preparation of the equilibrium cell for experimentation followed by an outline of calibration procedure of the pressure transducer and the temperature transducers. The detector calibration method by way of the direct injection method is also detailed. Lastly, the procedure for the measurement of vapour-liquid equilibrium data; that is, preparation, degassing, saturated vapour pressure and isothermal VLE data measurement.

The guiding principles for the preparation of the apparatus and the general description of the essential features of the operating techniques for the sampling as well as analysis of the vapour and liquid phases are discussed below.

6.1 Preparation of Equipment for Experimentation

6.1.1 Preparation of the equilibrium cell

Before commencement of measurements, the temperature of the bath was elevated, coupled with the evacuation of the cell. The heat of the bath fluid is essentially transferred to the equilibrium cell and this ensures that any solvents or residues present within the equilibrium cell are vaporised and ensures their removal. Hereafter the cell was cleaned in succession by loading and purging nitrogen. This procedure ensures the removal of any residual trace quantities of impurities in the equilibrium cell.

To attain accurate experimental data the apparatus has to be free of leaks. The detection of leaks in the equilibrium cell is undertaken by pressurising the equilibrium cell up to a pressure (90 bar) sufficiently higher than the anticipated maximum operating pressure. The equilibrium cell is maintained at a constant temperature of 313.15 K as it is submerged in a thermo-regulated water bath. An isothermal environment for the equilibrium cell makes it easy to ascertain that any pressure fluctuation as observed on the data acquisition unit is solely as a result of a leak. Alternately, the equilibrium cell alone can be checked for leaks by submerging it in a water bath, and the leaks can be observed by the occurrence of bubbles in the bath fluid. The equilibrium cell is meticulously examined to detect the slightest indication of bubbles. Soapy water was employed as the principal fluid in leak detection. The same technique was embarked on for the lines carrying the equilibrium sample to the gas chromatograph. On the condition that the pressure drop was within a clearly defined tolerance taking into account the effects of temperature together with the fittings' leak rates; the equilibrium cell was then regarded suitable to be used in experimentation.

The gas carrier lines connected on either side of the ROLSI™ and conveying samples to the gas chromatograph were heated to 380.15 K. Once the temperature of 380.15 K was reached, the carrier gas flow across the circulation loop was increased. This was maintained for at least half an hour. This procedure was undertaken so as to flush out any light volatile impurities within the carrier gas lines and the carrier gas was then used to flush the sampling lines and was sent to the gas chromatograph for analysis. In the case where trace amounts are picked up by the GC, then the entire procedure was repeated. In the event that no trace of components other than the carrier gas was identified then the apparatus was qualified as being ready for conducting measurements on.

6.1.2 Pressure and Temperature Calibration

Pressure Calibration

The most essential experimental variables are the equilibrium temperature and pressure as well as composition. The pressure transducer was calibrated against a reference or standard 0-250 bar gauge *WIKA CPT 6000* pressure transducer that has a specified accuracy of 0.025% which was itself calibrated precisely at ambient conditions by *WIKA* Instruments. The *WIKA CPT*

6000 is specified to possess a maximum internal uncertainty of 0.02 kPa and has no further error in pressure at ambient conditions in the range of 273 to 323 K.

The reference or standard pressure transducer was connected to the liquid outlet port of the equilibrium cell, and the equilibrium cell was pressurised using nitrogen. The P10 pressure transducer was housed in a thermo-regulated block and was maintained at 313.15 K was to be calibrated within its individual thermo-regulated block. The isothermal liquid bath housing the equilibrium cell as well as the P10 pressure transducer temperature were controlled during the calibration procedure to maintain isothermal conditions. The cell pressure as such was raised and reduced cumulatively over the complete working range of the transducer. At every steadied pressure, the pressure reading of the P10 transducer was logged using a data acquisition unit and averaged. The reference pressure transducer reading was recorded manually. It is imperative that the reference transducer be zeroed by taking into account the atmospheric pressure before commencement of the calibration. The gathered data was fitted to a first order linear equation.

Temperature Calibration

The equipment makes use of two Pt-100 probes which were calibrated against a reference *WIKA* CTB 9100 temperature probe. The standard probe was calibrated by *WIKA Instruments*, and is specified to exhibit an internal uncertainty of 0.03 K. All three temperature probes were aligned and immersed in the thermo-regulated silicon oil liquid bath. The thermo-regulated bath's temperature was increased additively, and afterwards decreased across the required operating temperature range. This procedure was repeated. Alteration of the bath temperature in this fashion allowed the detection of the indication of the presence of hysteresis within the probes. At every steadied temperature, the temperature readings of both probes were logged on a data acquisition unit over a 5 minute interval. The measured temperature value of the reference temperature probe was read from the display of the unit, and as such recorded manually. It was imperative to take an average of all recorded data values since the reference probe and Pt-100 probe instantaneous values differ. An average value gives a better representation of the temperature response.

A least squares regression was used to fit the collected data to both a first order and second polynomial. When a sensor of the Pt-100 probe detects a temperature elevation, then it follows that the resistance also increases. Hence, it follows that it is expected that the response of the Pt-100 should exhibit a linear trend. As such, the computed values when fitting either a first order or second-order polynomial have to be alike. A large difference between the computed values using either of the polynomials implies that the Pt-100 probe is damaged. It is expedient that the calibrations be checked before moving over to undertake measurements of a new system as it is possible that there can be a gradual shift in the recorded temperature value of the Pt-100s over time.

Positioning of the Liquid-Level

The equilibrium cell is filled with the liquid component up to a height that is mid-way of the cell window level. Such a liquid level leaves a volume of space between the tip of the ROLSI™ capillary to enable vapour sampling at elevated pressure and is large enough to guarantee an adequate liquid-level for low-pressure measurement. For the duration of the component loading process, the rise in the liquid-level can be viewed through the sapphire viewing windows.

6.2 GC Detector Calibration via the Direct Injection Method

The direct injection method is applicable to calibration of both gas + liquid and gas + gas binary systems. Injected into the GC by way of microliter syringes are known volumes of each pure component. The response of the GC's detector is then logged with wide-ranging injected volumes of the respective components. In the case of the gaseous component, the injected volume, pressure and temperature are noted, and the number of moles is computed via an EoS. For the liquid component, the number of moles is computed via a density correlation using the temperature, molar mass and volume of the injected liquid.

The degree of accuracy of the detector calibration using the direct method is affected by the following factors (Nelson, 2012): (1) the exactness within which the pressure and temperature can be determined and (2) the measure of the accuracy and statistical variability to which the volume of either the liquid or gas can be injected. The temperature and pressure recorded at the exit nozzle of the gas cylinder are assumed to be characteristic of the conditions of the contents of the syringe. Still, it is highly probable that the conditions of the injected gas can differ considerably from these highlighted conditions; comprising: (a) cooling effects as a

result of gas expansion; (b) minor positive pressures present within the filled syringe; (c) heating effects owing to conduction of heat to the syringe. The accuracy of the GC detector calibration is mostly affected by the measure of the closeness to desired value of the volume on the syringe as well as the closeness of repeated volumes injected. As such, the execution of the volume injections and the syringe itself (syringe sealing, fabrication errors etc.) have a bearing on the accuracy of the delivered volume. The closeness of repeated injected volumes is affected by: (i) the physical properties of the delivered gas such as boiling point and volatility; (ii) the uniformity in undertaking the injection procedure; (iii) the plunger's set-point in comparison to the graduation markings on the syringe's body (solely dependent on the assessment of the operator).

6.3 Equilibrium Measurements

6.3.1 Preparation

The equilibrium cell was primed for vapour pressure and VLE measurements by cleaning as well as testing for leaks. As a result of the low capacity of the equilibrium cell, leaks must be circumvented. Accordingly, thorough sealing of the equilibrium cell was of paramount importance. Therefore, prior to commencement of every equilibrium measurement the equilibrium cell and sampling lines were tested for leaks by charging it with nitrogen gas and all potential sources of leaks were coated with Snoop®. The identified leaks were overcome by either tightening leaking compression fittings, O-ring or NPT seals; or eventually changing of the compression fitting ferrules, O-rings or the application of PTFE thread tape (in the case of NPT threads) respectively.

The functionality of the ROLSI™ capillary was frequently tested; Snoop® coat was applied over the thumbscrew seals. The tip of the capillary was moved from the top to the lowest opposition of the cell, and afterwards moved in the opposite direction. In the event of the existence of a leak, the thumbscrews were lightly tightened. Care must be taken not to over-tighten the thumbscrews so as to prevent the wearing off of the O-rings which subsequently contaminates the equilibrium cell with fragments from the worn O-rings. The equilibrium cell was charged with nitrogen gas and immersed into the thermo-regulated fluid and the temperature controller was switched on and set to a fixed temperature of 313.15 K. An increase in temperature surges the speed of molecules and as a consequence increases the pressure

exerted. The opposite is true. As such, fixing the temperature ensures that any pressure drop is solely as a result of the presence of leaks and not the variable temperature of the cell's ambient temperature. The equilibrium cell's pressure was observed over a 5 hour period under conditions of temperature homogeneity to detect the occurrence of any decline in pressure. If a pressure drop was observed, Snoop® was applied to all potential sources of leaks with careful examination to identify the leak point.

The cell was washed numerous times at 343 K using n-hexane before charging new components into the equilibrium cell. n-Hexane is ideal because of its compatibility with Viton®. Any O-ring debris brought about by their attrition when tightening threads are also eliminated during the washing procedure. After washing the equilibrium cell, a vacuum was drawn overnight at about 343 K to remove any residual solvent. The lengthy time taken in drawing the vacuum is as a consequence of the small surface area presented by the O-rings.

6.3.2 Degassing

Usually, a small percentage of residual gases are found in the liquid components. Gaseous components may also contain light impurities that evaporate easily. The presence of impurities can have detrimental effects on the quality of the results attained. This presents considerable errors in the pressure of the binary mixture. A measurement of the pure component vapour pressures and an analysis of the constituents of the pure component by chromatography are the two techniques employed in the determination of the existence of impurities. Where impurities are present, degassing techniques must be used to eliminate such volatile impurities.

For gaseous components, the degassing procedure entailed vapour withdrawal at intervals by the application of heat so that the light volatile components are vaporised and thereafter purging them. This follows the principle that the impurities are lighter than the gases and would be the first to escape upon purging. Whereas for liquids within the equilibrium cell, degassing was undertaken by way of a vacuum pump by suction and the gas bubbles produced drawn. It constitutes good practice that for liquids with fairly high vapour pressures, the temperature of the thermal fluid in which the equilibrium cell is immersed is lowered until a pressure below or equal to 2 bars is realised. This avoids the potential damage to the vacuum pump upon purging in a burst.

6.3.3 Saturated Vapour Pressure

The purpose of measuring the pure-component vapour pressure is to validate the equipment calibrations undertaken (temperature and pressure). The measurement of vapour pressures is very much sensitive to the purity of the chemical component, as such, it is a necessity that the chemicals be both thoroughly degassed as well as of appropriate purity.

A vacuum was drawn on the cell and every leading line, and the degassed component was delivered into the equilibrium cell. The equilibrium cell was filled to full capacity, and the mixture of the components was degassed. The component was externally degassed by drawing a vacuum by injecting a needle into the vial containing the liquid. Samples of the component were injected into the GC using a syringe to confirm that the impurities have been removed by observing only one peak on the GC trace. Whereas the agitation of the liquid phase is unnecessary in the measurement of pure component saturated vapour pressure; for mass transfer and distribution of the phases, it is essential to have good stirring. Stirring is continued until the attainment of equilibrium. The attainment of phase equilibrium was assumed to be the point when the temperature and pressure readings became essentially invariable to within the temperature probe's and pressure transducer's precision. The cell's temperature and pressure were then recorded and averaged over at least a 5 minute interval. An increase in the temperature of the bath fluid within which the equilibrium cell will increase the force exerted by the molecules on the surface of the equilibrium cell. This in consequence increases the pressure within the cell. This principle was used in generating the saturated vapour curve by cumulatively altering the temperature by a defined magnitude and measuring the corresponding pressure. It constitutes good practice to be vigilant and intermittently examine the cell contents through analytical and visual methods. This ensures the identification of any possible chemical decomposition that can occur or the discharge of dissolved chemicals from the O-rings respectively.

6.3.4 Vapour-Liquid Equilibrium Measurement

Once the vapour pressure measurements were deemed satisfactory with good comparison to literature, the second component was loaded via the respective cylinder. The mixture was stirred vigorously under conditions of temperature homogeneity. The attainment of equilibrium

was assumed when the temperature and pressure steadied to within the respective instrument's accuracy (time taken depends on the system under investigation).

The mixing of the components in the liquid phase was stopped five minutes before sampling commenced to enable the gas and liquid phases to separate (Fonseca et al., 2011). Sampling was always undertaken with the vapour phase first, thereafter the liquid phase. This was done so as to avoid having residual liquid samples entrained on the stem of the capillary of the ROLSI™ which will lead to an inaccurate representation of composition of the equilibrium phases. Samples are withdrawn and analysed until at least 10 data points with a standard error (standard deviation as a fraction of the mean) below 1 percent. However greater standard errors are anticipated in the dilute regions (Nelson, 2012).

It constitutes good practice to periodically monitor the top thumbscrew for leaks for the duration of the experimentation as the ROLSI™ capillary moves across the phases during sampling. The points on the phase envelope were traversed by either (a) degassing of the chemical mixture to decrease the system pressure or (b) incrementally introducing the lighter component to raise the system pressure (c) measuring different isotherms with one mixture to lessen the amount of chemicals used. Three isotherms which represented good separation of the components were measured in this work for each binary system. Also, 10 to 15 data points were measured for each. Such a number of points allows the experimentalist to discard some points upon regressing which have a high marginal error and still remain with enough points that are representative of the VLE data.

It is of paramount importance to note the following experimental checks (Nelson, 2012):

a. As a result of the small volume of the equilibrium cell, all the more so the pressure stability of the cell will be influenced by minute gas leaks and as such misrepresent phase compositions at equilibrium.
b. The linearity of gas detector calibration was further examined. This was done by withdrawing different sample sizes in both phases at equilibrium by adjusting the time for which the ROLSI™ was open. It is of paramount importance that the sample areas fall within the calibration bounds. Where non-linearity is observed (change in composition at equilibrium) upon employing a first order polynomial it may then imply that there is an inaccuracy in the calibration (supposing that the ROLSI™ and the GC

function properly). This practice can be expedient in establishing whether it is possible to extrapolate a linear gas chromatograph calibration; in view of the fact that samples drawn beyond the calibration span still yield invariable compositions (similar to that are within the calibration span) it follows that there will not be an increase in the uncertainty of the composition analysis as a result of extrapolating to a small degree.

7

CHAPTER SEVEN

7. RESULTS AND DISCUSSION

The experimental study was mainly established on the measurement of isothermal *P-x-y* data for binary mixtures of R-1216 with alkanes. This chapter presents the experimental results as well as the data regression. Also discussed is the temperature and pressure calibration as well as the chemical purity and GC calibration as all these entities affect the accuracy of the experimental results. Isothermal *P-x-y* data was measured for three novel systems using the experimental apparatus established on the static synthetic method. Two binary test systems [ethylene + R-1216 and ethane + n-hexane] were measured to verify the experimental method, that is, the accuracy and the reproducibility.

7.1 Pressure and Temperature Calibration Results

Pressure calibration

The pressure transducer was held in the thermo-regulated aluminium block which was at a temperature of 313.15 K so at to prevent set point changes by keeping the pressure transducer body temperature constant. A high pressure (0 – 250 barg) transducer was available for calibration since all the phase equilibrium measurements we undertaken at high pressures. The P-10 pressure transducer was calibrated in the range 0 to 7.0 MPa. The maximum absolute error for the pressure transducer was 0.0014 MPa. The maximum absolute error is the error ensuing from the difference between the true pressure and the computed pressure of the measuring pressure transducer using a first order polynomial. Figure 7-1 shows the results of the high-pressure transducer calibration and is characterised by a linear relationship between the standard and the measuring transducer. The deviation of the measured pressure from the actual pressure using a first-order polynomial is illustrated by Figure 7-2. The resultant pressure

range, regressed calibration polynomial and the maximum absolute error brought by the calibration relationship are stated in Table 7-1. The expanded uncertainty in the measurement of the pressure is approximated to be within ± 0.007 MPa.

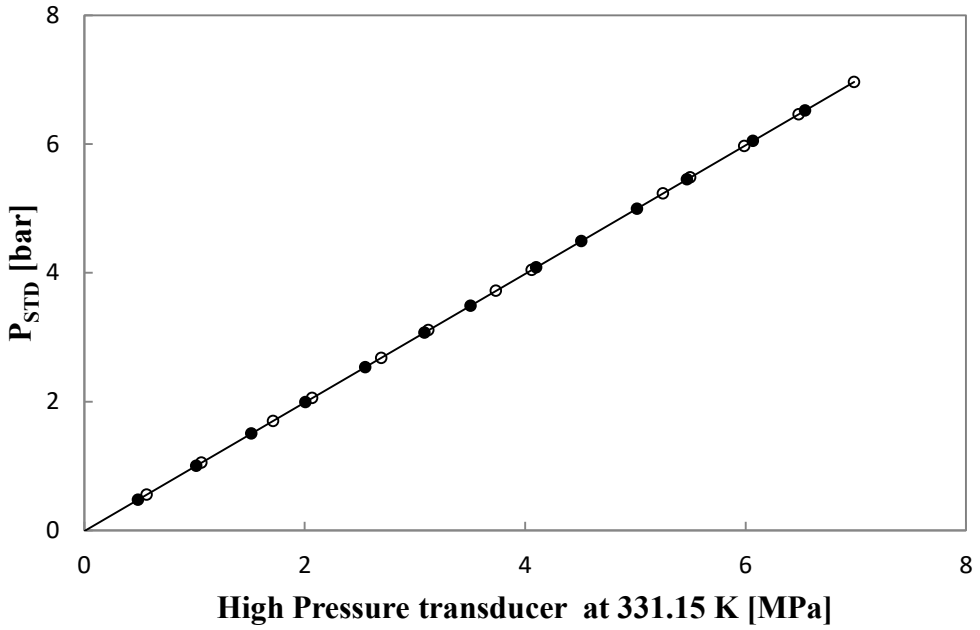

Figure 7- 1: High-pressure transducer calibration from 0 to 80 bar with a thermos-regulated bar at 313.15 K. Relationship between the standard transducer ($\boldsymbol{P_{STD}}$) and the measuring device is depicted as linear; ○-represents increasing pressure increments; ●-represents reductive steps in pressure.

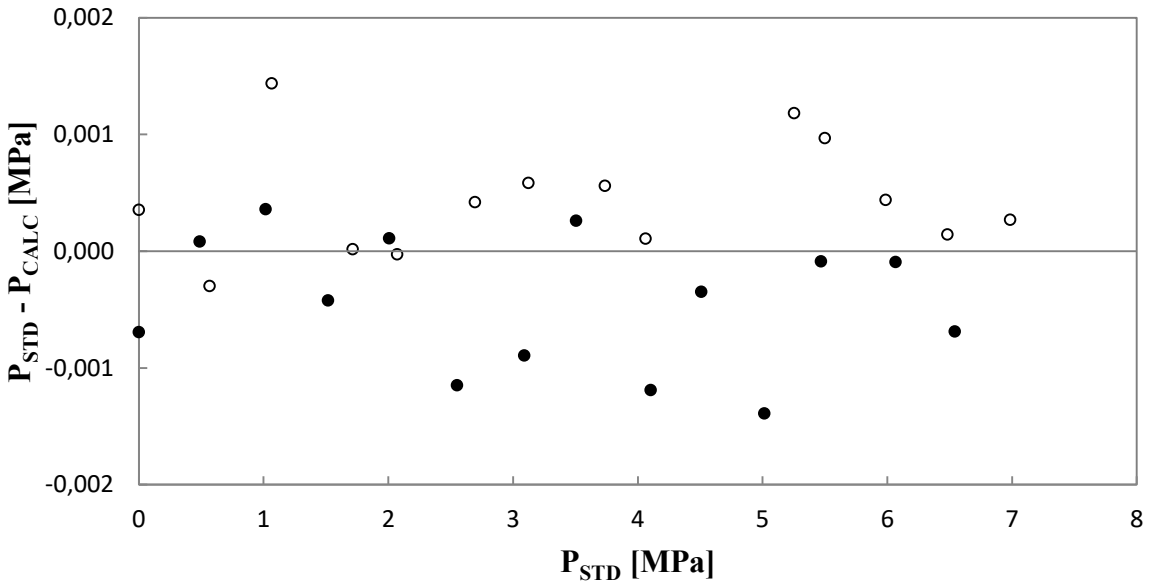

Figure 7- 2: Deviation of the reading from the standard pressure transmitter and readout from the pressure transducer reading the actual pressure using a first-order polynomial. ○-represents increasing pressure increments; ●-represents reductive steps in pressure.

Table 7- 1: Calibration polynomial for the high-pressure thermo-regulated transducer.

Pressure Range [MPa]	ΔP(max)[1] [MPa]	Correlation [bar]	R^2
0 - 70	0.014	$P_{CALC} = 0.9984P_{MEAS} + 0.1307$	0.999

[1] $\Delta P(max) = |P_{STD} - P_{CALC}|$, where $\Delta P(max)$ is the maximum absolute error brought about by the calibration correlation. P_{STD} and P_{CALC} are the pressure of the standard transducer and the pressure of the high pressure transducer via the correlation. P_{MEAS} is the pressure displayed by the high pressure transducer.

Temperature Calibration Results

As a result of the wide temperature range under which this study was conducted, the temperature calibration was split into two separate temperature regions: (i) 263 – 343 K and (ii) 323 – 428 K. Good results were obtained in the calibration of the Pt-100 probes. Figure 7-3 indicates the errors as a result of the calibration polynomial which was used to fit the experimentally determined temperature to the standard temperatures.

The regressing of the calibration data by way of the first-order polynomial gave a better fit of the measured data. Table 7-2 catalogues the ensuing calibration polynomials, maximum absolute errors and temperature ranges per probe at the specified temperature interval.

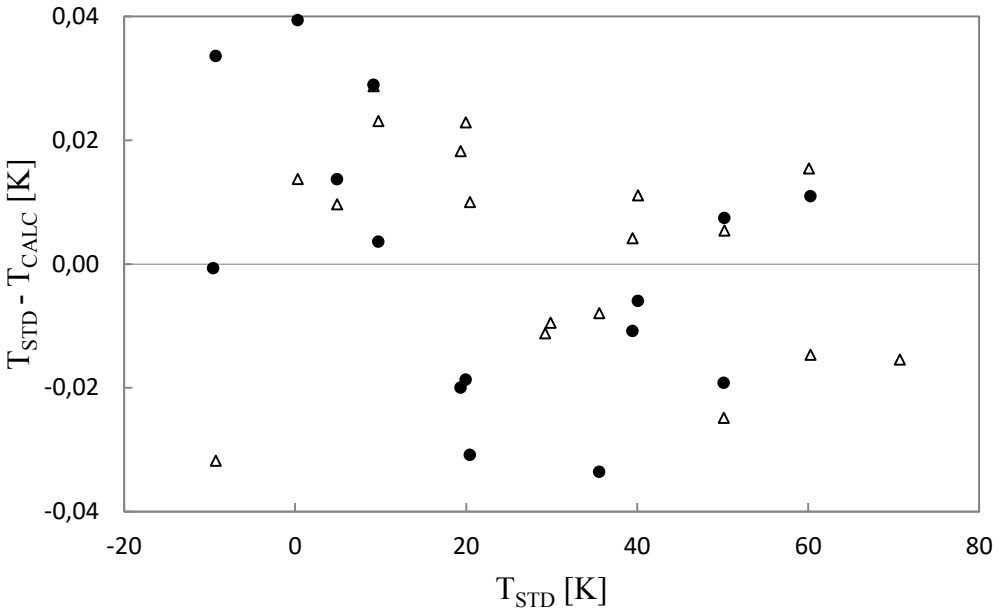

Figure 7- 3: Temperature calibration results for: ●, $\boldsymbol{T_{10}}$ and Δ, $\boldsymbol{T_{11}}$ in the range 263 K to 343 K. Deviations computed using a first-order polynomial. $\boldsymbol{T_{STD}}$ is the temperature logged by the temperature standard (actual temperature) whereas $\boldsymbol{T_{CALC}}$ is the calculated temperature of the Pt-100 using the calibration correlation.

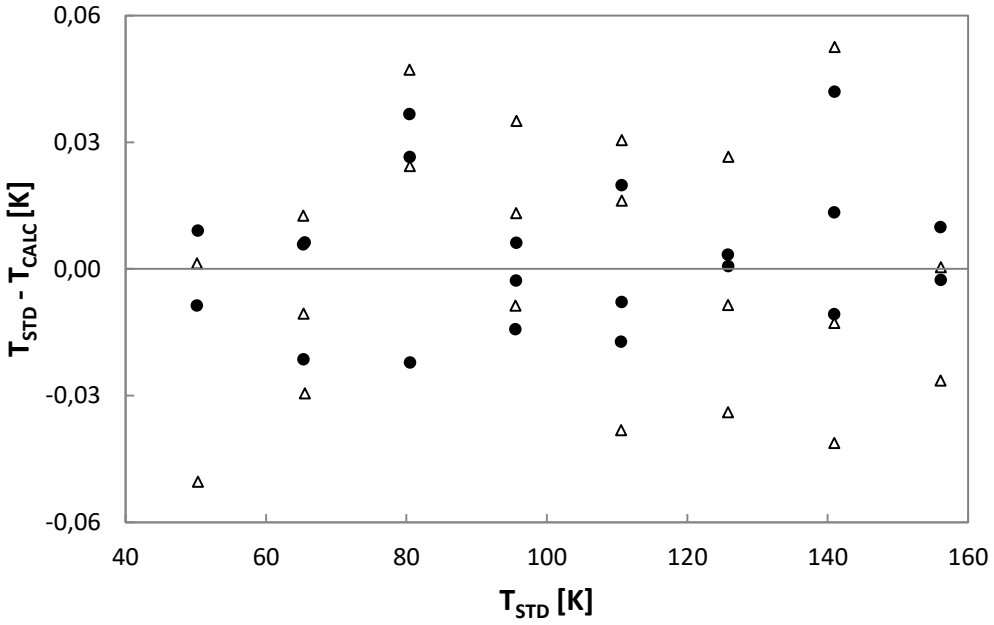

Figure 7- 4: Temperature calibration results for: ●, $\boldsymbol{T_{10}}$ and Δ, $\boldsymbol{T_{11}}$ in the range 323 K to 423 K. Deviations computed using a first-order polynomial. $\boldsymbol{T_{STD}}$ is the temperature logged by the temperature standard (actual temperature) whereas $\boldsymbol{T_{CALC}}$ is the calculated temperature of the Pt-100 using the calibration correlation.

Table 7- 2: Temperature calibration results for both Pt-100 probes.

Pt-100	T Range [K]	ΔT(max)[1] [K]	Correlation [K]	R^2
107	263 – 343	0.04	$T_{107\,CALC} = 1.003T_{MEAS} - 1.0701$	0.9999
107	323 - 423	0.04	$T_{110\,CALC} = 1.000T_{MEAS} - 1.672$	0.9999
110	263 – 343	0.03	$T_{107\,CALC} = 0.998T_{MEAS} - 1.553$	0.9999
110	323 - 423	0.06	$T_{110\,CALC} = 1.000T_{MEAS} - 1.845$	0.9999

[1] $\Delta T(max) = |T_{STD} - T_{CALC}|_{max}$=, where $\Delta T(max)$ is the maximum absolute error brought about by the calibration correlation. T_{STD} and T_{CALC} are the temperature of the standard probe and temperature of the Pt-100. T_{MEAS} denotes the temperature exhibited by the Pt-100.

7.2 Chemical Purities

Table 7-3 lists the chemical purities of the chemicals used in the measurement of the test system as well as phase equilibrium data of this study. The chemicals were generally of a high purity. The purity as stated by the supplier was checked using gas chromatography. The refractive

index for each individual liquid component was measured at 293.15 K and was compared to literature data as displayed in Table 7-4. Table 7-5 presents the measured component densities and compares the values with literature data. There is good agreement between the measured density of pentane and the literature value, whereas, the measured densities of n-hexane and n-heptane show slight differences from the literature data. Generally, the chemicals were of high purity. As such, the chemicals did not need further purification, with the exception of the degassing procedure that was performed to remove light volatile impurities.

Table 7- 3: Purities of the chemicals used.

Compound	CAS Number	Supplier	Purity [[a]vol. %, [b]mol. %]
R -1 216	116-15-4	Pelchem	99.9[a]
Ethane	74-84-0	Air products	99.9[a]
Ethylene	74-85-1	Air products	99.9[a]
n-Pentane	109-66-0	Sigma-Aldrich	>99.0[b]
n-Hexane	110-54-3	Sigma-Aldrich	>99.0[b]
n-Heptane	142-82-5	Sigma-Aldrich	>99.0[b]

Table 7- 4: Refractive indices of the chemicals used in this study.

Compound	Measured Refractive Index [20 °C]	Literature Refractive Index[1] [20 °C]
n-Pentane	1.37499	1.3749
n-Hexane	1.35754	1.3575
n-Heptane	1.38781	1.3876

[1]Engineering Toolbox. U(n) = 0.00005

Table 7- 5: Densities of chemicals used in this study.

Compound	Temperature [K]	Measured Density $[kg.m^3]$	Literature Density[1] $[kg.m^3]$
n-Pentane	292.75	626.52	626.52
n-Hexane	298.95	658.98	654.21
n-Heptane	302.15	675.94	676.13

[1]NIST ThermoData Engine of Aspen Plus® V8.0. U(ρ) = 0.004 $kg.m^3$

7.3 Test System Vapour-Liquid Equilibrium Measurement

The NIST TDE (National Institute of Standards and Technology ThermoData Engine) databank was used as a literature source in this work as it is established on a considerable array of experimentally determined data for each component. The NIST TDE databank was used principally for pure-component data in Aspen Plus® as it allows access to experimental data and permits performance of property evaluation. Property calculations for all experimental data within the NIST TDE for a pure component can be re-evaluated using user specified temperature increments.

A description of the procedure by which the experimental uncertainties were evaluated for the experimental measurement is examined in Appendix B. The combined uncertainties, taken over all data points for each binary isothermal VLE test system, are recorded in Table 7-6, whereas Table 7-7 lists the standard uncertainties, intrinsic to the calibration method, used to compute the combined expanded uncertainty for the phase compositions. The combined standard uncertainties for pressure and temperature are fairly low, whereas, the combined standard uncertainties for compositions for both systems are marginally high but tolerable.

Table 7- 6: Combined expanded uncertainty for mole composition, pressure and temperature for the isothermal binary VLE test systems, taken over all data points for each test system.

Component 1	Component 2	$U_c(T)^1$ [K]	$U_c(P)^1$ MPa	$U_c(x_1)^1$	$U_c(y_1)^1$
C_3F_6	C_2H_4	0.06	0.007	0.010	0.010
C_2H_6	C_6H_{14}	0.06	0.007	0.012	0.002

[1]Expanded uncertainties evaluated with a coverage factor of $k = 2$.

Table 7- 7: Standard uncertainties inherent to the calibration procedure of phase composition

Variable	Uncertainty*
Injected Volume[1] [gas]	2%
Temperature of injected gas	2 K
Pressure of injected gas	0.01 bar
Injected Volume[1] [liquid]	3%
Liquid Density Correlation	1%

*www.sge.com

Table 7- 8: Specifications of the gas chromatograph

Column	Porapak Q
Type	Packed
Material	Stainless Steel
Maximum Temperature [K]	523.15
Column length [m]	4
Inner diameter [mm]	3.2
Polarity	Polar

Table 7- 9: Gas chromatograph operating conditions for the VLE test systems.

System	$C_2H_4 + C_3F_6$	$C_2H_6 + C_6H_{14}$
Column	Porapak Q	Porapak Q
Colum temperature [K]	373.15	373.15
Detector temperature [K]	523.15	523.15
Detector current [mA]	60	60
Injector temperature [K]	473.15	473.15
Carrier gas velocity [$ml.min^{-1}$]	30	30
Column pressure (gauge) [kPa]	368.7	368.7

7.3.1 Vapour Pressure Measurement

The saturated vapour pressure data for ethylene and 1, 1, 2, 3, 3, 3-hexafluoro-1-propene components are presented in Figure 7-5 and Figure 7-6 respectively. It was of paramount importance that the components be thoroughly degassed to eliminate the volatile impurities. The linearity of the relationship $\ln P$ vs. $1/T$ is evidence of the absence of both the decomposition as well as polymerization of the components. Table 7-10 displays the average absolute deviations (AADs) and average relative deviations (AARDs) for the ensuing vapour pressures for each pure component. Generally, the measured vapour pressures are in agreement with the reference sources as shown by the AARDs which are well less than 1% besides those of the n-hexane measurements as shown by the circled values in the Table 7-10.The performance of the high-pressure transducer was adequate at high pressures, as shown by the ethylene and R-1216 vapour pressure results; as the AARDs remained well below 0.5%. The Bias and AARD remained well less than 1% excluding n-hexane which was below 2% all the same. It is observed that the deviation in the results of the vapour pressures is higher when a high-pressure transducer is used in the measurement of vapour pressures for components which are less volatile and have low vapour pressures. The vapour pressure results confirm that the temperature and pressure calibrations are of good quality.

Table 7- 10: Average absolute deviation (AAD), average relative deviation (AARD) and Bias for the experimental vapour pressures with the following databanks as reference sources, viz.: NIST TDE (NIST ThermoData Engine of Aspen Plus® V8.0). [Apparatus of (Chiyen, 2010)

Reference [MPa]	C_2H_4	C_3F_6	C_6H_{14}
AAD(P)[1] NIST TDE	0.005	0.004	0.003
PR-MC	0.0088	0.0016	0.0002
AARD(P)[2] NIST TDE	0.12 %	0.55 %	1.69 %
PR-MC	0.024 %	0.05 %	0.04 %
Bias(P)[3] NIST TDE	0.12 %	0.55 %	0.003
PR-MC	-0.0003 %	-0.0420 %	0.0051 %

[1] $AAD(P) = 1/N_p \sum|P_{EXP} - P_{LIT}|$, where P_{LIT} and P_{EXP} are the literature and experimental vapour pressure.

[2] $AAD(P) = 1/N_p \sum|P_{EXP} - P_{LIT}|/P_{EXP}$, where N_p is the total number of data points.

[3] $Bias(P) = 1/N_p \sum(P_{EXP} - P_{LIT})/P_{EXP}$

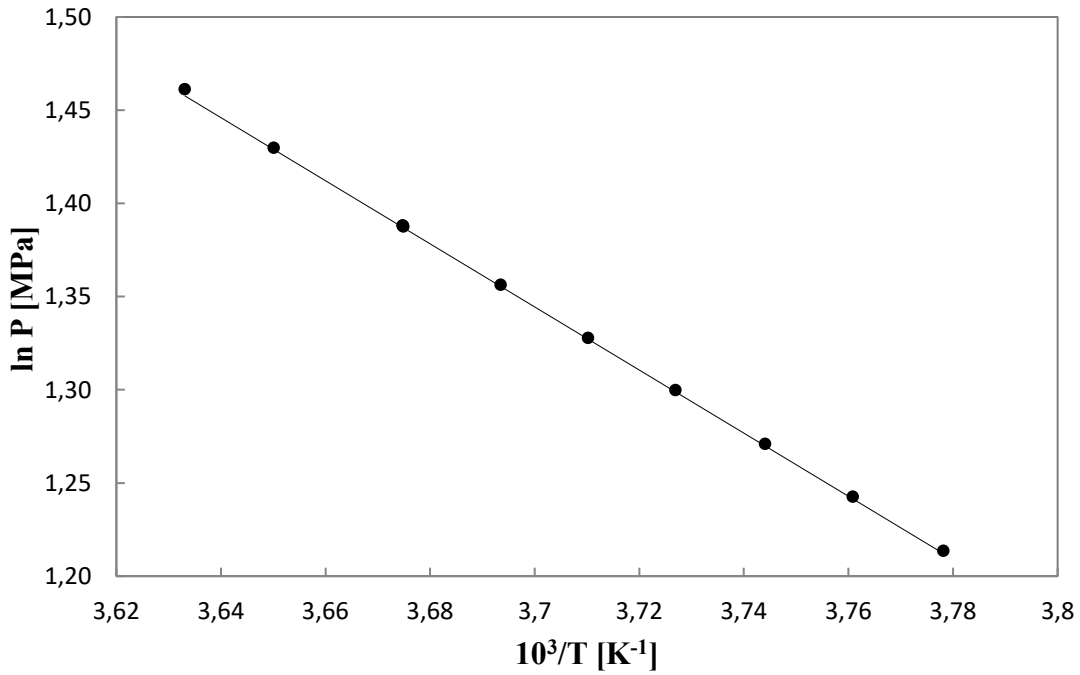

Figure 7- 5: Pure-component vapour pressure data for ethylene (●) in the range 264 to 275 K. NIST TDE data are characterised by the solid line.

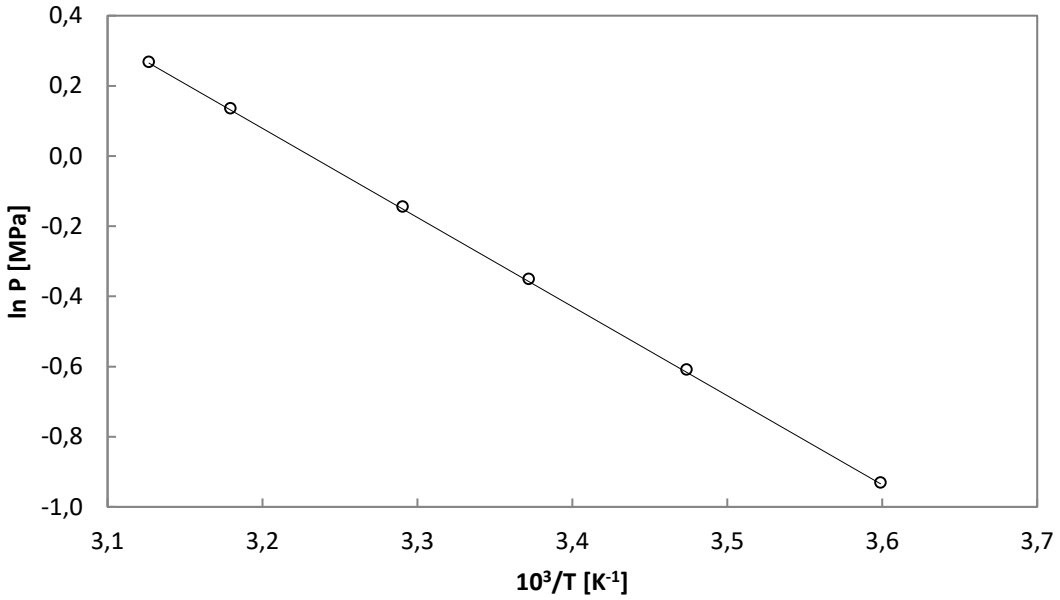

Figure 7- 6: Pure component vapour pressure data for 1, 1, 2, 3, 3, 3-Hexafluoro-1-propene (○) in the range 277 to 320 K. NIST TDE data are characterised by the solid line.

7.3.2 Phase Equilibria Measurement

Ethylene (1) + 1, 1, 2, 3, 3, 3-Hexafluoro-1-propene (2) Binary VLE Test System [Apparatus of (Chiyen, 2010)]

Isothermal binary VLE data for the ethylene (1) + 1, 1, 2, 3, 3, 3-hexafluoro-1-propene (2) test system was measured at 268.24 K. The experimental data were previously measured by Subramoney et al. (2013a) using a static analytic method based apparatus. Sampling was done using a movable ROLSI™ for repeatable phase sampling. The apparatus used in this work was based on the static analytic method and followed the same sampling method. The VLE data is presented in Figure 7-9 and also reported in Table 7-12. The GC calibration procedure implemented was the direct injection method which involved the use of a gas-tight syringe. Figure 7-8 shows the GC calibration results for ethylene and 1, 1, 2, 3, 3, 3-hexafluoro-1-propene; whereas Figure 7-9 displays the deviation in the number of moles using a polynomial fit. The maximum absolute deviation in the correlated number of moles is presented in Table 7-11. Figure 7-13 shows a comparison of the relative volatility for the ethylene + R-1216 system. The relative volatilities were computed from the phase composition data of the regressed data output of the entire phase envelope. The plot of the

relative volatility dependence on the composition is another indicator of the measure of agreement between the measured data and the calculated data. Table 7-12 shows the experimental and computed equilibrium phase compositions for the binary system. Table 7-13 displays a comparison between the experimental VLE and the data calculated from the model. The data were correlated with the PR-MC-WS-NRTL model which was also used by Subramoney et al. (2013a). The PR-MC-WS-NRTL model is a thermodynamic model based on the Peng-Robinson (PR) EoS containing the Mathis-Copeman (MC) α function, Wong Sandler (WS) mixing rule and the NRTL local composition model. The model is made up of interaction parameters which are adjustable to the data (κ_{12}, τ_{12} and τ_{21}). The data was regressed using the least squares method. Good agreement is observed between the experimental and correlated data. Figure 7-11 and Figure 7-11 display plots of the deviation of the vapour and liquid compositions for the ethylene (1) + R-1216 (2) system from the PR-MC-WS-NRTL model. As a result of the accuracy in the measurement of the saturated vapour pressure, the pressure and temperature calibrations were verified as accurate. The uncertainties in the temperature, pressure and phase composition for the two test systems are tabulated and discussed in §7.4.

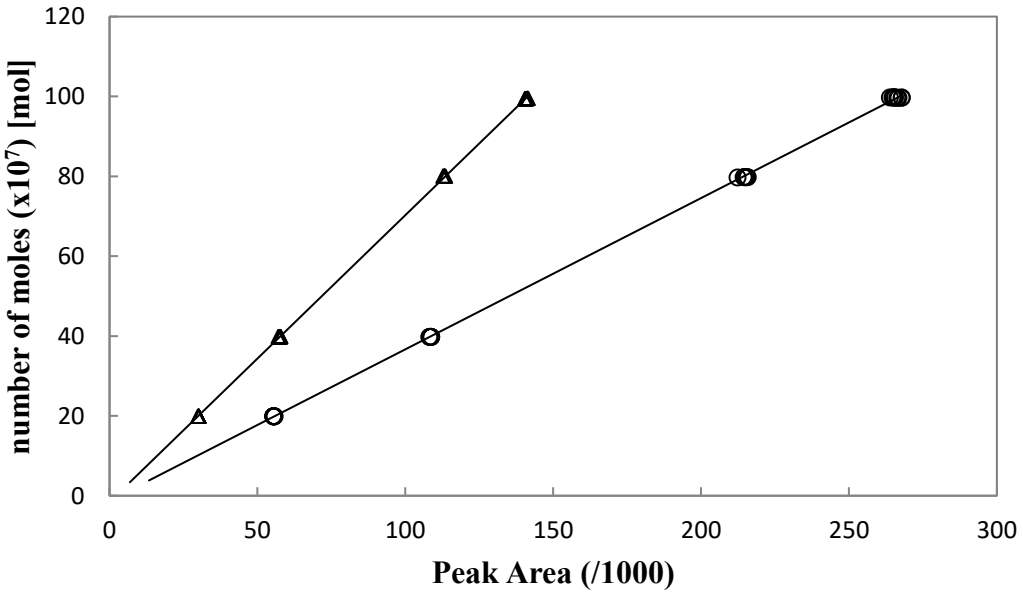

Figure 7- 7: Gas chromatograph detector calibration results via the direct injection method, utilising: Δ, 0 – 250 µl gas-tight syringe for ethylene and ○, 0 – 250 µl gas-tight syringe for 1, 1, 2, 3, 3, 3-Hexafluoro-1-propene.

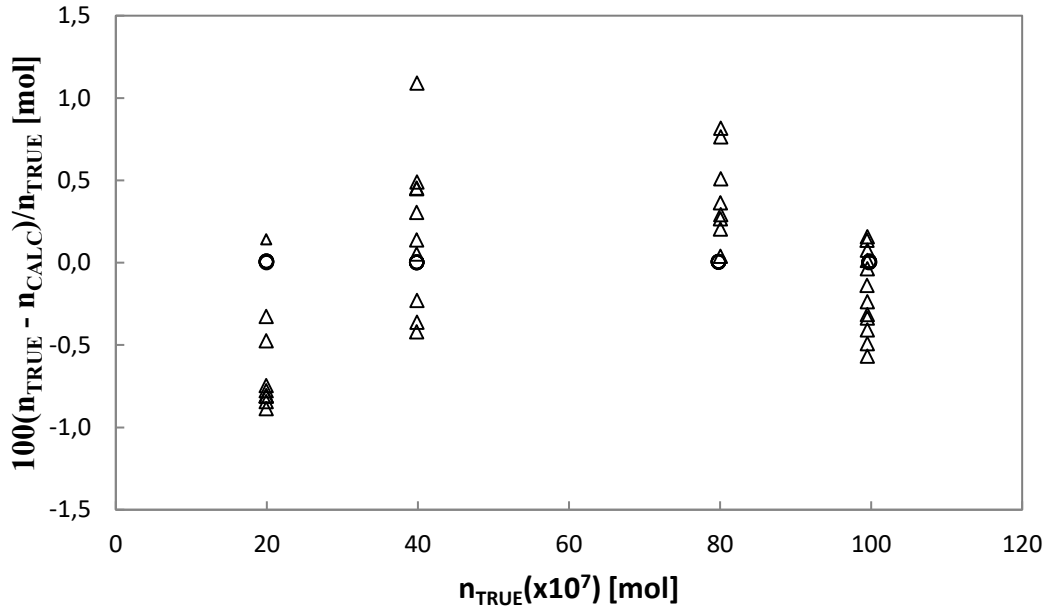

Figure 7- 8: Deviations in the number of moles by means of a first-order polynomial; $\boldsymbol{n_{CALC}}$ denotes the calculated number of moles via the correlation polynomial; and $\boldsymbol{n_{TRUE}}$ denotes the actual number of moles introduced into the gas chromatograph.

Table 7- 11: TCD calibration results for ethylene (C_2H_4) and 1, 1, 2, 3, 3, 3-Hexafluoro-1-propene (C_3F_6), displaying the maximum relative absolute errors with a first order polynomial

Chemical	**Volume (µl)**	**Δn/n(max)[1]**	**Correlation**	**R^2**
C_2H_4	0 - 250	1.09%	$\boldsymbol{n_{CALC} = 7.18 \times 10^{-11} A_i - 1.56 \times 10^{-7}}$	0.9999
C_3F_6	0 -250	1.03%	$\boldsymbol{n_{CALC} = 3.79 \times 10^{-11} A_i - 1.23 \times 10^{-7}}$	0.9999

Table 7- 12: Experimental VLE data for the ethylene (1) + 1, 1, 2, 3, 3, 3-hexafluoro-1-propene system at 268.24 K using the least squares regression method.

					PR-MC-WS-NRTL	
$P_{exp}(MPa)$	x_{1exp}	y_{1exp}	$P_{calc}\ (MPa)$	$P_{calc} - P_{exp}\ (MPa)$	y_{1calc}	$y_{1calc} - y_{1exp}$
T (K) = 268.24						
1.204	0.247	0.766	1.198	-0.0057	0.773	-0.007
1.367	0.303	0.805	1.378	-0.0115	0.805	0.000
1.519	0.346	0.821	1.513	-0.0061	0.824	-0.003
1.752	0.421	0.853	1.741	-0.0105	0.850	0.003
1.937	0.482	0.864	1.924	-0.0126	0.868	-0.004
2.235	0.588	0.890	2.240	0.0054	0.894	-0.004
2.449	0.659	0.910	2.454	0.0048	0.910	0.000
2.601	0.709	0.920	2.607	0.0055	0.920	0.000
3.081	0.857	0.955	3.088	0.0066	0.953	0.001
3.139	0.872	0.959	3.141	0.0019	0.957	0.002

[a] Expanded uncertainties ($k = 2$): $\bar{U}(T) = \pm 0.06\ K$, $\bar{U}(P) = \pm 0.007 MPa$, $\bar{U}(x) = \pm 0.010$, $\bar{U}(y) = \pm 0.010$.

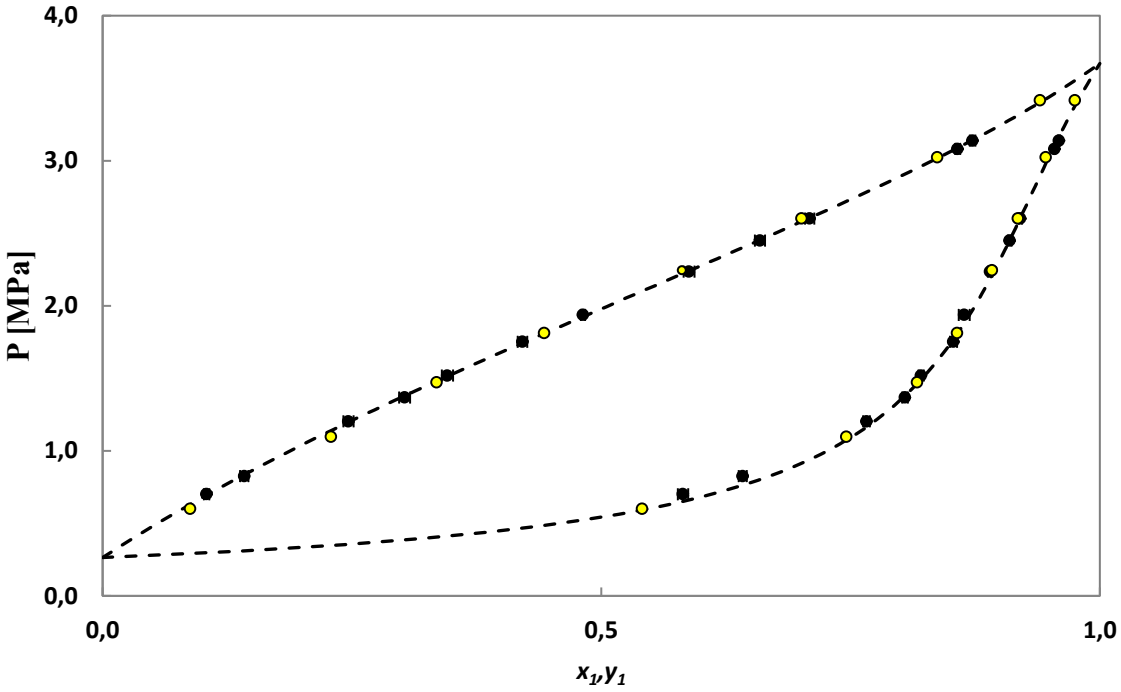

Figure 7- 9: Isothermal VLE data for the ethylene (1) + 1, 1, 2, 3, 3, 3-Hexafluoro-1-propene (2) binary test system (gas/gas): ●, experimental at 268.24 K; ○, literature data of Subramoney et al. (2013a); and – – –, PR-MC-WS-NRTL model. Error bars indicate the combined standard uncertainties in composition.

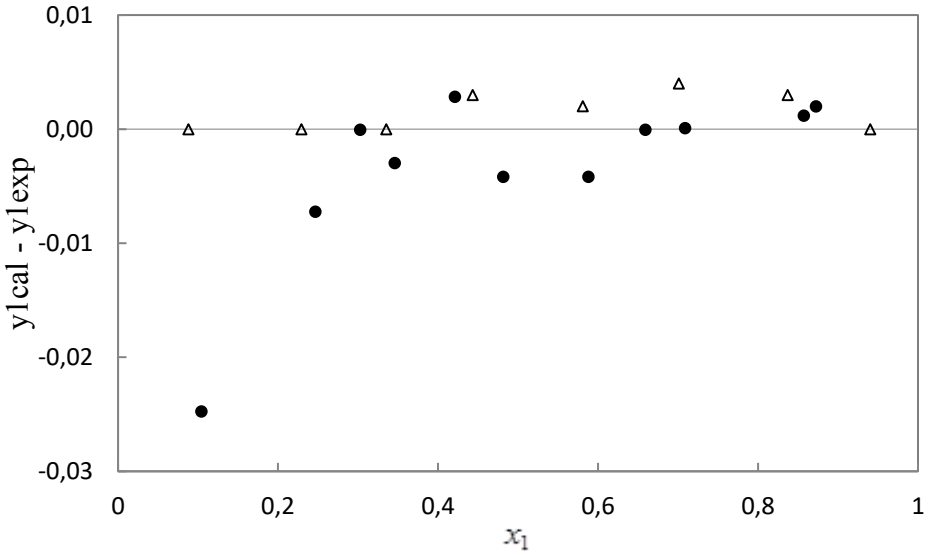

Figure 7- 10: Deviation of the vapour compositions for the ethylene (1) + 1, 1, 2, 3, 3, 3-Hexafluoro-1-propene (2) system regressed from the PR-MC-WS-NRTL model: ●, experimental at 268.24 K ; Δ, literature data of Subramoney et al. (2013a)

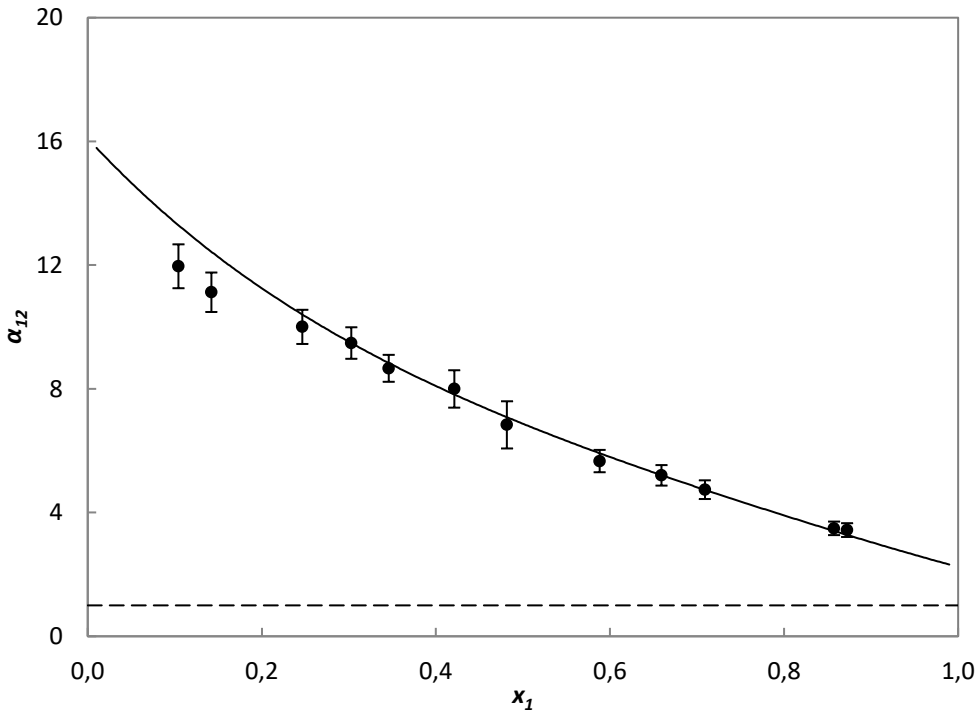

Figure 7- 11: Relationship between the relative volatility and composition for the ethylene (1) + 1, 1, 2, 3, 3, 3-Hexafluoro-1-propene (2) binary test system at 268.24 K (●). Line of invariable relative volatility α_{12} = 1 (– – –); PR-MC-WS-NRTL model (—). Error bars indicate the combined uncertainty for experimental results.

Table 7- 13: Comparison of the experimental VLE data to the regressed data using the PR-MC-WS-NRTL method in Aspen Plus® V8.0 using the least squares objective function.

$T[K]$	$P[MPa]$	$y_{C_2H_4}$	$\Delta P^1[MPa]$	$\Delta P/P^b\ [MPa]$	${\Delta y_{C_2H_4}}^a$	${\Delta y_{C_2H_4}/y_{C_2H_4}}^b$
268.25	1.204	0.766	-0.006	0.48%	-0.007	-0.95%
268.25	1.367	0.805	0.012	-0.84%	0.000	0.03%
268.22	1.519	0.821	-0.006	0.40%	-0.003	-0.35%
268.25	1.752	0.853	-0.010	0.60%	0.002	0.27%
268.24	1.937	0.864	-0.013	0.65%	-0.005	-0.52%
268.24	2.235	0.890	0.005	-0.24%	-0.005	-0.52%
268.24	2.449	0.910	0.005	-0.20%	0.000	-0.01%
268.25	2.601	0.920	0.006	-0.21%	-0.001	-0.07%
268.25	3.081	0.955	0.007	-0.22%	0.001	0.15%
268.24	3.139	0.959	0.002	-0.06%	0.002	0.17%

[a] $\Delta\bar{\theta} = \bar{\theta}_{EXP} - \bar{\theta}_{PR-MC-WS-NRTL}$, where $\bar{\theta}_{EXP}$ and $\bar{\theta}_{PR-MC-WS-NRTL}$ are the experimental and PR-MC-WS-NRTL values for either the pressure or the composition of the vapour phase .

[b] $\Delta\bar{\theta}/\bar{\theta} = (\bar{\theta}_{EXP} - \bar{\theta}_{PR-MC-WS-NRTL})/\bar{\theta}_{EXP}$

Ethane (1) + Hexane (2) Binary VLE Test System [Apparatus of Chiyen (2010)]

The second binary test system of ethane (1) + hexane (1) was for a gas/liquid system. The data were previously measured by Ohgaki et al. (1976). It is worth noting that the sampling method used in this work (use of the ROLSI™) is a significant improvement from the technique used by Ohgaki and Katayama (1975b). The sampler used by Ohgaki and Katayama (1975b) was a small steel tube which was approximately 0.15 cm^3 in volume and equipped with a ball valve on one side and a needle vale on the other, whereas the ROLSI™ allows withdrawal of very small repeatable volumes which are in the microliter ranges.

Table 7- 14: TCD calibration for C_2H_6 and n-hexane, displaying the maximum relative absolute errors with a first order polynomial

Chemical	Volume (µl)	Δn/n(max)[1]	Correlation	R^2
C_2H_6	0 - 250	1.28%	$n_{CALC} = 6.87 \times 10^{-11} A_i - 1.68 \times 10^{-7}$	0.9999
C_6H_{14}	0 – 0.5	1.20%	$n_{CALC} = 3.20 \times 10^{-11} A_i + 1.49 \times 10^{-7}$	0.9999

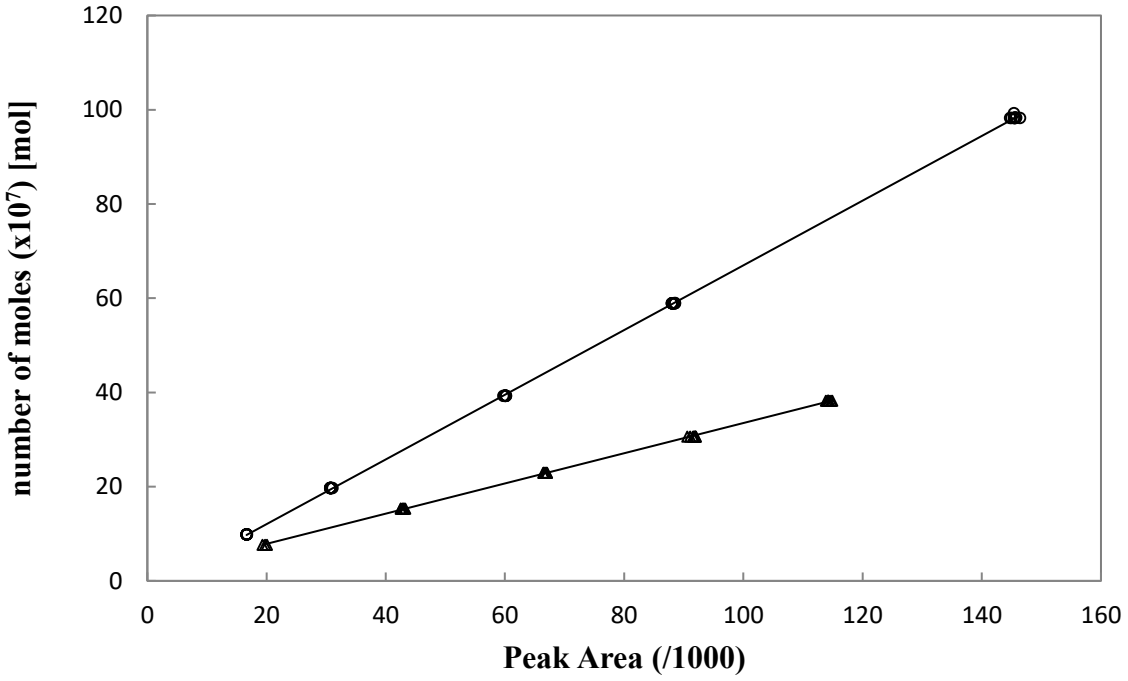

Figure 7- 12: Gas chromatograph detector calibration results with the direct injection method, using: ○, 0 – 250 µl gas-tight syringe for C_2H_6; Δ, 0 – 0.5 µl liquid syringe for n-hexane.

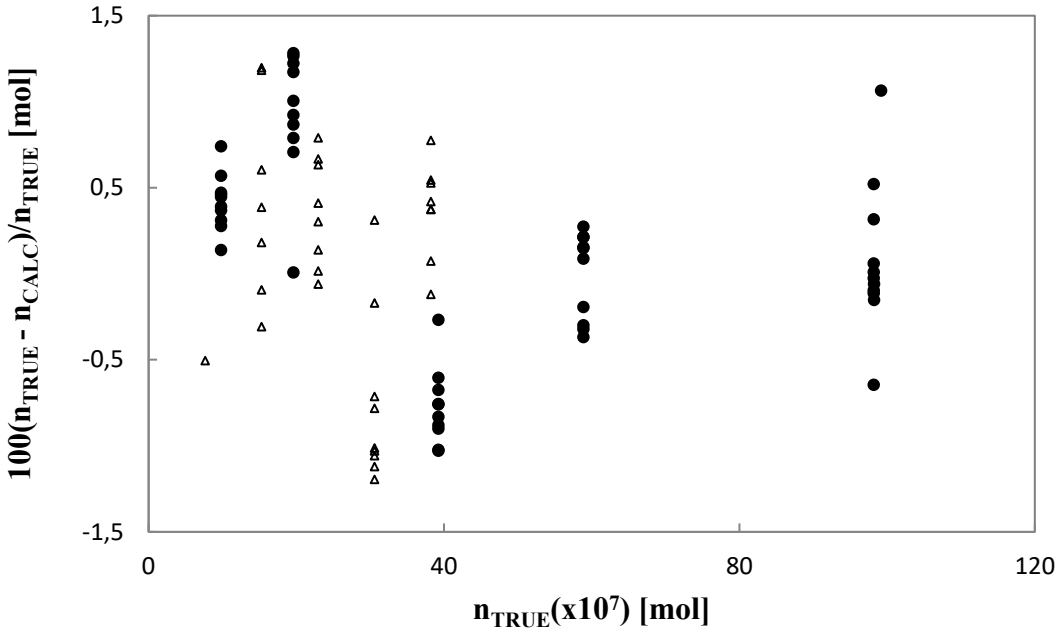

Figure 7- 13: Deviations in the number of moles by means of a first-order polynomial; $\boldsymbol{n_{CALC}}$ denotes the calculated number of moles via the correlation polynomial; and $\boldsymbol{n_{TRUE}}$ denotes the actual number of moles introduced into the gas chromatograph: ○, 0 – 250 µl gas-tight syringe for C_2H_6; Δ, 0 – 0.5 µl liquid syringe for n-hexane.

The gas chromatograph calibrations were performed using the direct injection method; the results are presented in Table 7-14 and Figure 7-13. The direct injection of hexane was performed via a 0.5 µL liquid syringe which is attached with a repeatability adapter, whereas direct injection of ethane was implemented via a gas tight 250 µL syringe. The maximum deviation in the correlated number of moles was 1.28% for ethane and 1.20% for n-hexane. The correlated number of moles for ethane exhibited comparatively high deviations. The uncertainty in the composition is tabulated in Table 7-5 where $U_c(x_1) = 0.012$ and $U_c(y_1) = 0.002$.

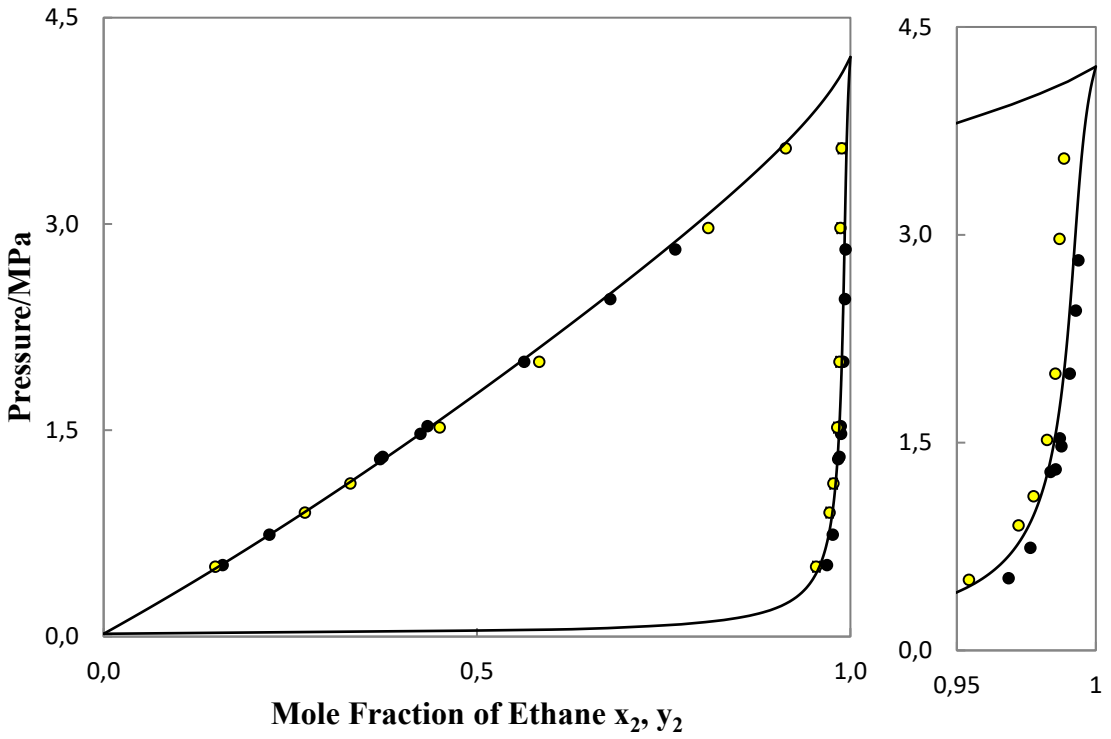

Figure 7- 14: Experimental VLE data and modelling results for the hexane (1) + ethane (2) test system: ●, experimental data at 298.15 K; ○, literature data of Ohgaki et al. (1976) at 298.15 K. Solid black line is representative of the PSRK model.

The experimental isothermal VLE data as well as the reference data are presented in Figure 7-14. The Predictive Soave-Redlich-Kwong (PSRK) method which is a group contribution method was employed for the prediction of the phase equilibrium behaviour for the binary mixture. As a consequence of the accuracy in the measurement of the isothermal VLE data, the pressure and temperature calibrations were then confirmed as accurate.

7.4 New Isothermal Measurements for Novel Systems

Throughout the measurement of the VLE data for this work the apparatus functioned well, although a few minor setbacks were encountered. The usage of the Viton® O-rings was sufficient for all binary systems as the equipment remained free of leaks even high pressures. The novel systems measured were HFP + pentane, HFP + hexane and HFP + heptane. The measurements were undertaken at high temperature and pressure. The novel binary systems are presented in the order in which they were measured.

The combined expanded uncertainties for pressure, temperature and phase composition for each system are recorded in Table 7-15. The uncertainties for each system are taken as an average over all data points of the isotherms. The combined expanded uncertainties for temperature and pressure are very small relative to the phase composition uncertainties. The high composition uncertainties are as a result of the uncertainty brought about by the direct injection technique.

Table 7- 15: Combined expanded uncertainties for pressure, temperature and phase composition for the novel binary VLE systems.

Component 1	Component 2	$U_c(T)^a[K]$	$U_c(P)^a[MPa]$	$U_c(x)^a$	$U_c(y)^a$
R-1216	n-pentane	0.06	0.007	0.010	0.011
R-1216	n-hexane	0.06	0.007	0.012	0.011
R-1216	n-heptane	0.06	0.007	0.011	0.010

[a] Combined expanded uncertainties calculated with a coverage factor of $k = 2$

7.4.1 Vapour Pressure Data

The saturated vapour pressure data for the n-pentane, n-hexane and 1, 1, 2, 3, 3, 3-hexafluoro-1-propene are presented in Figure 7-16 and in Tables 7-16 to 7-18. The pure components were thoroughly degassed to remove the volatile impurities. Although the stated manufacturer purity for the chemicals were all >99 %, a small percentage of other constituent chemicals can give an inaccurate representation of the pure component vapour pressure.

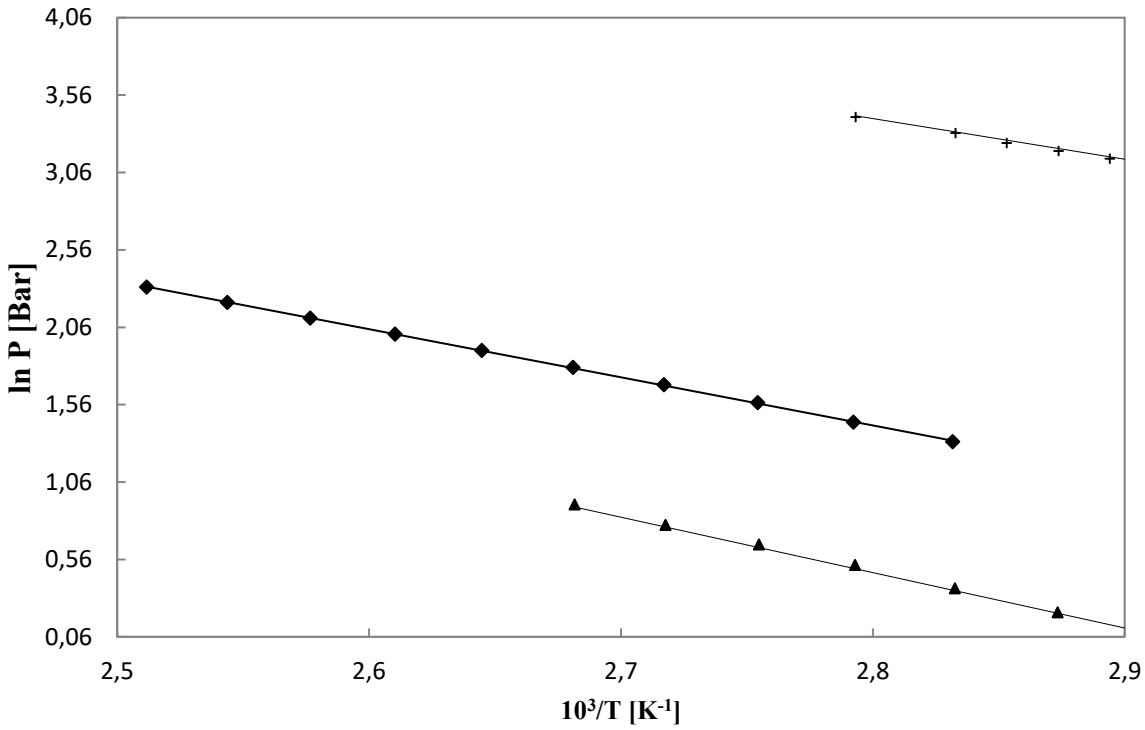

Figure 7- 15: Experimental saturated vapour pressure: n-pentane, ♦; n-hexane, ▲ and 1, 1, 2, 3, 3, 3-hexafluoro-1-propene, +. Reference date from NIST TDE is the solid black line.

The linearity in the relationships of lnP vs. $1/T$ indicates that neither decomposition nor polymerisation was observed. From Table 7-16 there appears to be a reasonable measure of difference between the experimentally determined vapour pressures at low pressures when compared to the reference databank evaluation. There is fairly good agreement between the experimental vapour pressures for n-hexane and R-1216 with the data from Coquelet et al. (2010) and the NIST TDE, as listed in Tables 7-16 to 7-19.

Table 7- 16: Comparison of the experimental saturated vapour pressure data for n-pentane to NIST.

T [K]	P [MPa]	Lit[a] P [MPa]	Lit[a] ΔP^{*} [Bar]	Lit[a] $\Delta P/P^{**}$
353.15	0.3748	0.3682	0.0066	1.77%
358.13	0.4247	0.4169	0.0079	1.85%
363.07	0.4824	0.4697	0.0127	2.63%
368.05	0.5411	0.5280	0.0131	2.41%
373.00	0.6045	0.5911	0.0134	2.22%
378.12	0.6749	0.6621	0.0129	1.90%
383.09	0.7505	0.7369	0.0136	1.81%
388.11	0.8334	0.8187	0.0147	1.76%
393.12	0.9216	0.9069	0.0147	1.60%
398.13	1.0170	1.0019	0.0150	1.48%
393.14	0.9222	0.9073	0.0149	1.62%

$^{*}\Delta P = P_{EXP} - P_{LIT}$, where P_{EXP} and P_{LIT} denote the experimental and literature vapour pressures respectively.

$^{**}\Delta P/P = (P_{EXP} - P_{LIT})/P_{EXP}$

[a] NIST ThermoData Engine of Aspen Plus® V8.0

Table 7- 17: Comparison of the experimental saturated vapour pressure data for n-hexane to NIST.

T [K]	P [MPa]	Lit[a] P [MPa]	Lit[a] ΔP[*] [MPa]	Lit[a] ΔP/P[**]
343.06	0.1071	0.1052	0.002	1.77%
348.03	0.1243	0.1225	0.002	1.46%
353.03	0.1454	0.1487	-0.003	-2.21%
358.04	0.1689	0.1640	0.005	2.88%
363.01	0.1928	0.1883	0.005	2.34%
367.95	0.2187	0.2151	0.004	1.63%
372.91	0.2496	0.2448	0.005	1.92%

[*] $\Delta P = P_{EXP} - P_{LIT}$, where P_{EXP} and P_{LIT} denote the experimental and literature vapour pressures respectively.

[**] $\Delta P/P = (P_{EXP} - P_{LIT})/P_{EXP}$

[a] NIST ThermoData Engine of Aspen Plus® V8.0

Table 7- 18: Comparison of the experimental saturated vapour pressure data for n-heptane to NIST

T [K]	P [MPa]	Lit[a] P [MPa]	Lit[a] ΔP[*] [MPa]	Lit[a] ΔP/P[**]
373.06	0.1333	0.1333	-0.0001	-0.09%
387.92	0.1891	0.1892	0.0011	0.06%
390.56	0.2021	0.2020	-0.0006	-0.03%
392.88	0.2125	0.2125	0.0002	0.01%
395.50	0.2266	0.2264	-0.0017	-0.08%
398.07	0.2381	0.2382	0.0014	0.06%
400.56	0.2527	0.2526	-0.0004	-0.01%
403.08	0.2668	0.2668	0.0001	0.05%

[*] $\Delta P = P_{EXP} - P_{LIT}$, where P_{EXP} and P_{LIT} denote the experimental and literature vapour pressures respectively.

[**] $\Delta P/P = (P_{EXP} - P_{LIT})/P_{EXP}$

[a] NIST ThermoData Engine of Aspen Plus® V8.0

Table 7- 19: Comparison of the experimental saturated vapour pressure data for 1, 1, 2, 3, 3, 3-hexafluoro-1-propene to NIST.

T [K]	P [MPa]	Lit[a] P [MPa]	Lit[a] ΔP[*] [MPa]	Lit[a] ΔP/P[**]
277.86	0.3942	0.3937	0.0005	0.13%
287.87	0.5441	0.5421	0.0020	0.37%
296.56	0.7043	0.7019	0.0024	0.34%
303.91	0.8660	0.8625	0.0035	0.40%
314.54	1.1459	1.1417	0.0042	0.37%
319.82	1.3073	1.3032	0.0041	0.31%

[*] $\Delta P = P_{EXP} - P_{LIT}$, where P_{EXP} and P_{LIT} denote the experimental and literature vapour pressures respectively.

[**] $\Delta P/P = (P_{EXP} - P_{LIT})/P_{EXP}$

[a] NIST ThermoData Engine of Aspen Plus® V8.0

7.4.2 Gas Chromatograph Calibration Results

Table 7-20 catalogues the operating conditions of the gas chromatograph for the three binary VLE systems. The direct injection method was used for calibrating the GC detector for all pure components. Direct handling of n-pentane was a challenge as a result of its low boiling point of 309.25 K. The boiling point of pentane is below the body temperature of the experimentalist [310.25 = 37 ºC]; hence n-pentane will evaporate as a result of the heat induced if the experimentalist is in contact with the arm of the injecting syringe. This will result in the injected volume being less than the one set. As such, the n-pentane vial was placed in an ice bath in a beaker so that the heat applied to the syringe within the short period that the experimentalist is in contact with it is not enough to cause vaporisation.

Figure 7-17 to Figure 7-22 and Table 7-21 present the results of the GC detector calibration. 1, 1, 2, 3, 3, 3-Hexafluoro-1-propene was calibrated using a gas-tight 0 – 250 µL syringe (furnished with a Hamilton® Chaney adapter). The GC TCD response was noted to be linear for the entire calibration range. The direct injection of the liquid components (n-pentane, n-hexane and n-heptane) was carried out using a 0 – 1.0 µL liquid syringe that is furnished with a *SGE* Repeating adapter.

Table 7- 20: Operating conditions of the gas chromatograph [SHIMADZU (TCD) (model GC-2014)].

System	$C_5H_{12} + C_3F_6$	$C_6H_{14} + C_3F_6$	$C_7H_{16} + C_3F_6$
Column	**Porapak Q**	**Porapak Q**	**Porapak Q**
Flow control mode	Flow	Flow	Flow
Colum temperature [K]	393	508	513
Detector temperature [K]	523	523	523
Detector current [mA]	70	60	60
Injector temperature [K]	423	473	473
Carrier gas velocity [ml.min^{-1}]	15	30	30
Column pressure (gauge) [kPa]	113	368.7	368.7

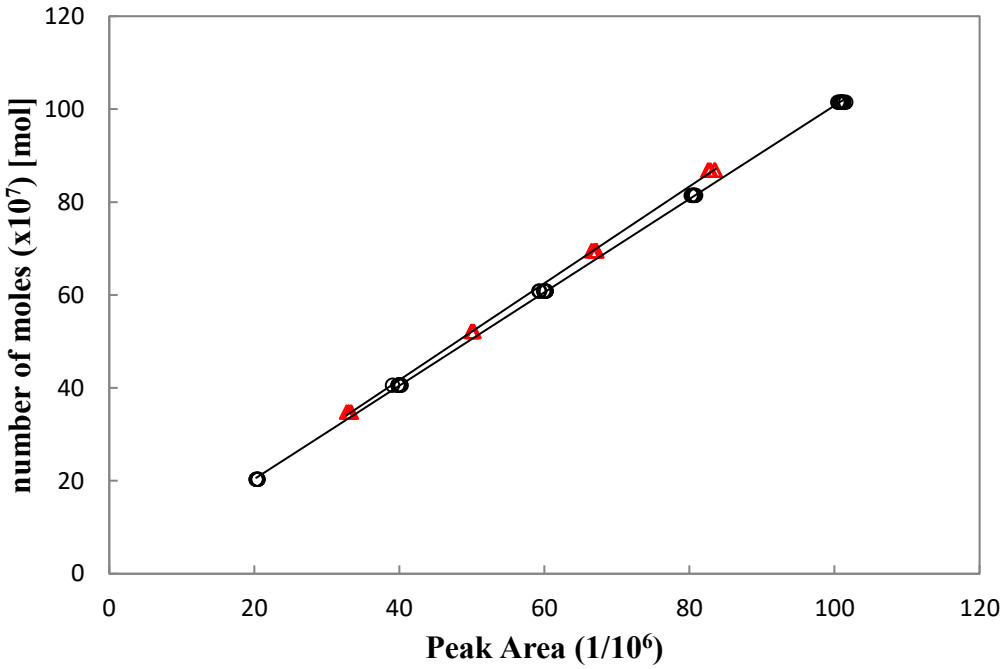

Figure 7-17: Gas chromatograph calibration results with the direct injection method, using: ○, 0 – 250 µl gas-tight syringe for 1, 1, 2, 3, 3, 3-hexafluoro-1-propene; Δ, 0 – 1 µl liquid syringe for n-pentane.

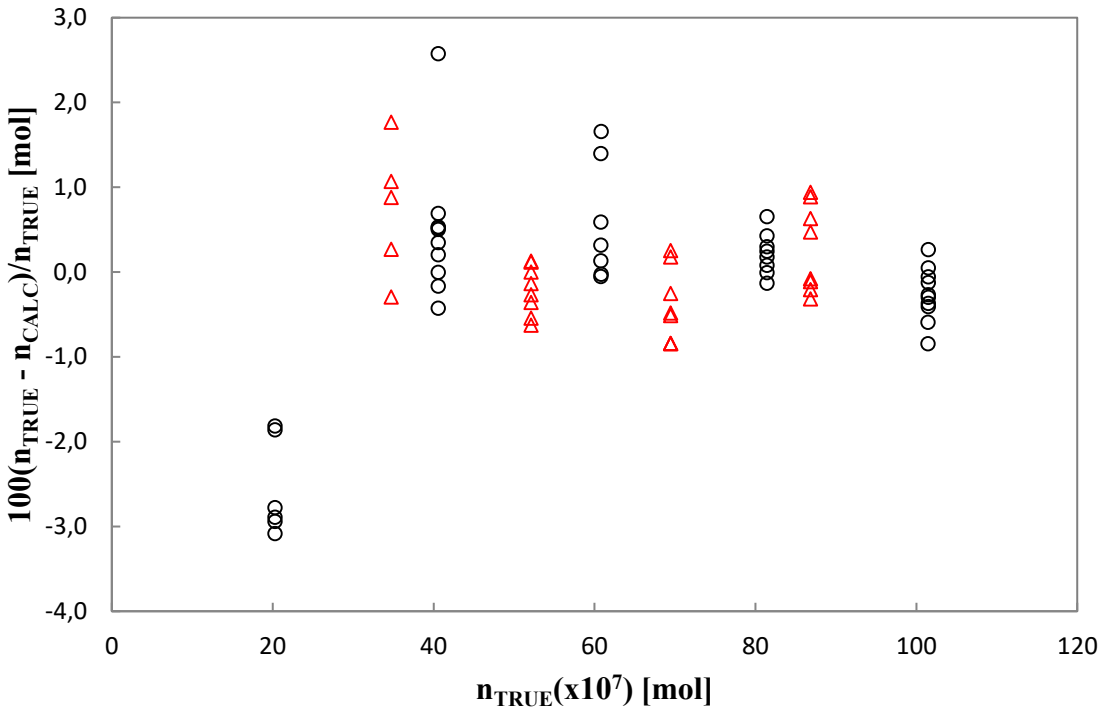

Figure 7- 18: Deviations in the number of moles by means of a first-order polynomial; $\boldsymbol{n_{CALC}}$ denotes the calculated number of moles via the correlation polynomial; and $\boldsymbol{n_{TRUE}}$ denotes the actual number of moles introduced into the gas chromatograph: ○, 0 – 250 µl gas-tight syringe for 1, 1, 2, 3, 3, 3-hexafluoro-1-propene; Δ, 0 – 1 µl liquid syringe for n-pentane.

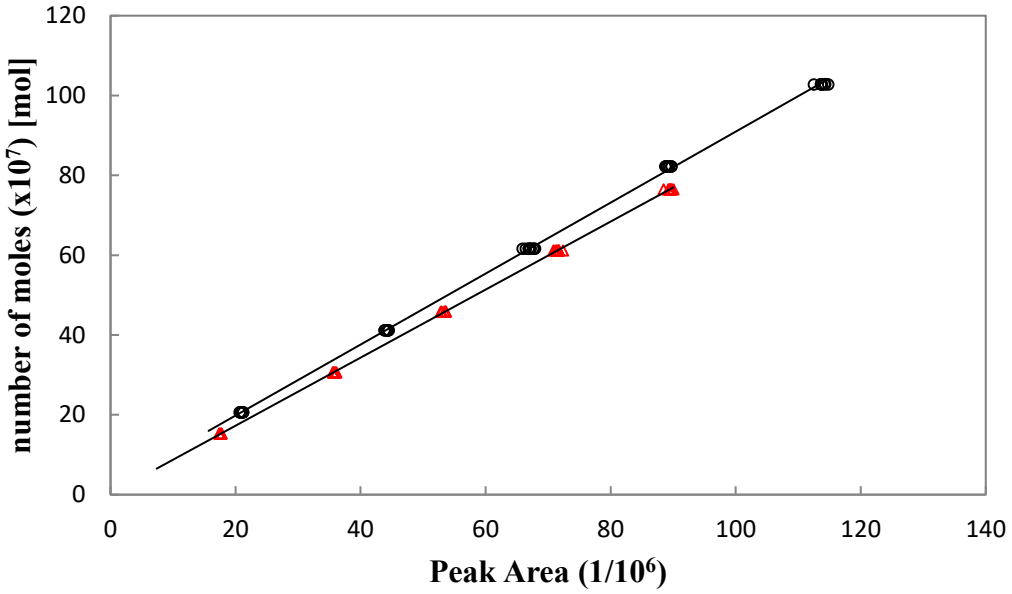

Figure 7- 19: Gas chromatograph calibration results with the direct injection method, using: ○, 0 – 250 µl gas-tight syringe for 1, 1, 2, 3, 3, 3-hexafluoro-1-propene; Δ, 0 – 1 µl liquid syringe for n-hexane.

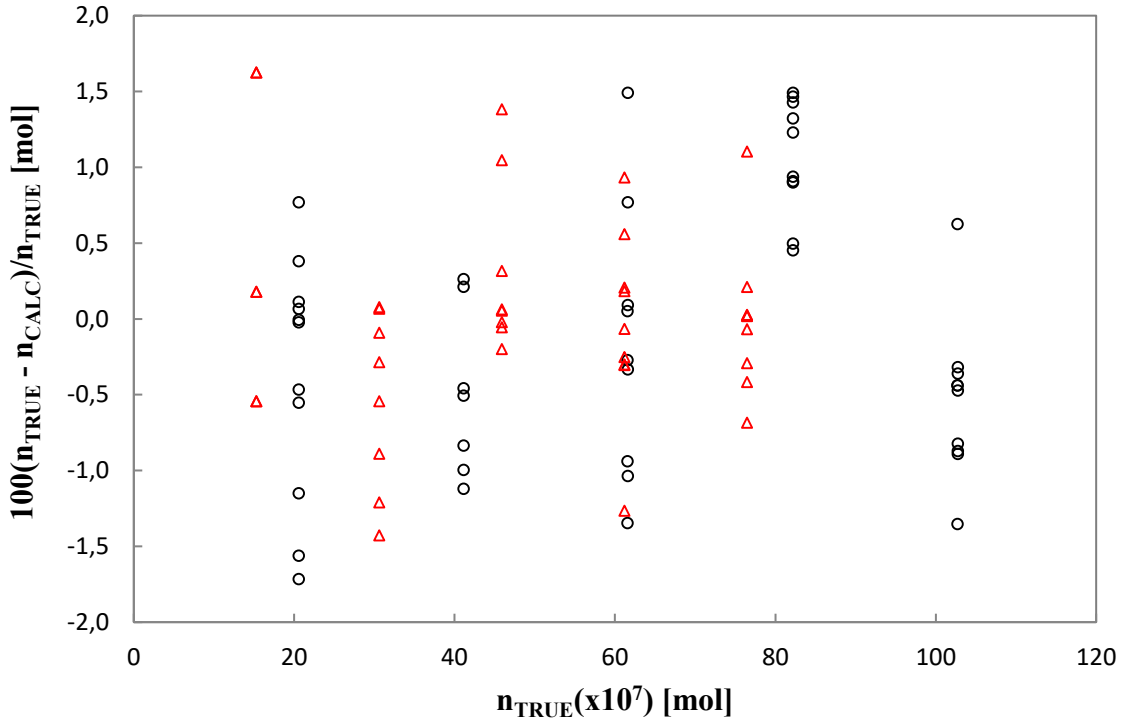

Figure 7- 20: Deviations in the number of moles by means of a first-order polynomial; $\boldsymbol{n_{CALC}}$ denotes the calculated number of moles via the correlation polynomial; and $\boldsymbol{n_{TRUE}}$ denotes the actual number of moles introduced into the gas chromatograph: ○, 0 – 250 µl gas-tight syringe for 1, 1, 2, 3, 3, 3-hexafluoro-1-propene; Δ, 0 – 1 µl liquid syringe for n-hexane.

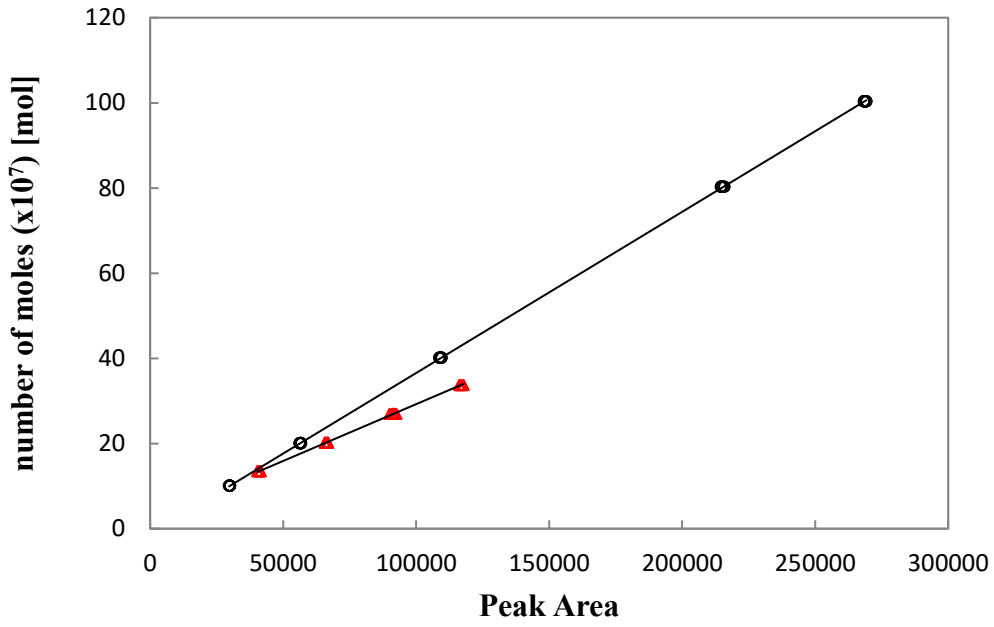

Figure 7- 21: Gas chromatograph calibration results with the direct injection method, using: ○, 0 – 250 µl gas-tight syringe for 1, 1, 2, 3, 3, 3-hexafluoro-1-propene; Δ, 0 – 1 µl liquid syringe for n-heptane.

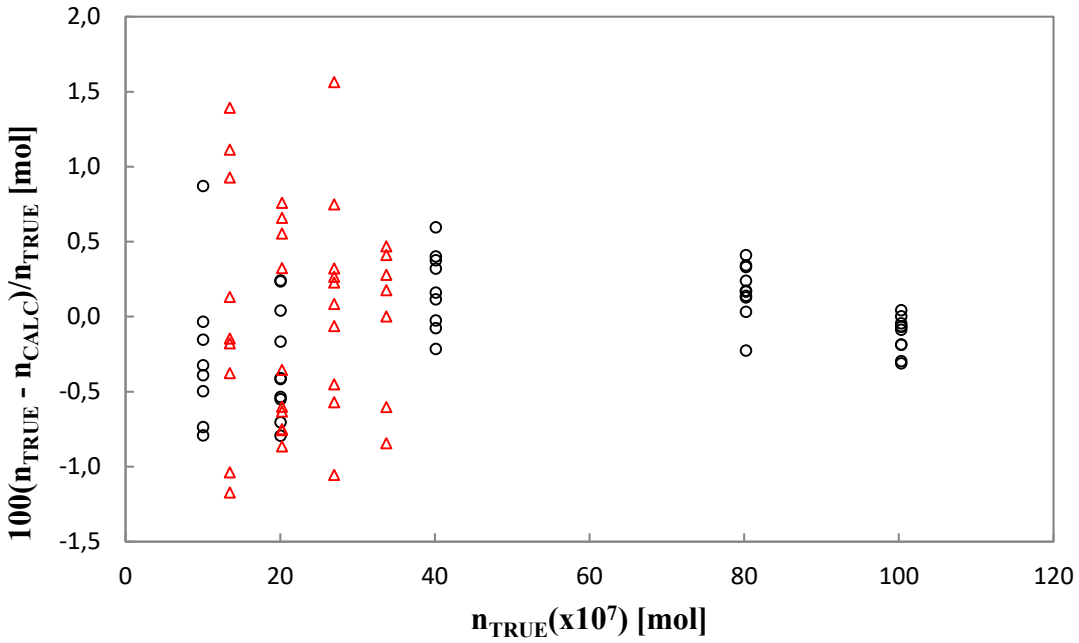

Figure 7- 22: Deviations in the number of moles by means of a first-order polynomial; $\boldsymbol{n_{CALC}}$ denotes the calculated number of moles via the correlation polynomial; and $\boldsymbol{n_{TRUE}}$ denotes the actual number of moles introduced into the gas chromatograph: ○, 0 – 250 µl gas-tight syringe for 1, 1, 2, 3, 3, 3-hexafluoro-1-propene; Δ, 0 – 1 µl liquid syringe for n-heptane.

Table 7- 21: Thermal Conductivity Detector (TCD) calibration correlations attained from the direct injection method employed in composition analysis of the binary systems.

Chemical	Δn/n(max)[a]	Volume (µL)	Correlation	R^2
C_5H_{12}	1.77%	0 to 1	$n_{CALC} = 1.04 \times 10^{-13} A_i + 3.07 \times 10^{-9}$	0.9998
C_3F_6	2.89%	0 to 250	$n_{CALC} = 1.00 \times 10^{-13} A_i + 2.88 \times 10^{-8}$	0.9996
C_6H_{14}	1.62%	0 to 1	$n_{CALC} = 8.52 \times 10^{-14} A_i + 2.31 \times 10^{-8}$	0.9998
C_3F_6	1.72%	0 to 250	$n_{CALC} = 8.89 \times 10^{-14} A_i + 2.05 \times 10^{-7}$	1.0000
C_7H_{16}	1.56%	0 to 1	$n_{CALC} = 2.67 \times 10^{-11} A_i + 2.54 \times 10^{-7}$	1.0000
C_3F_6	0.87%	0 to 250	$n_{CALC} = 3.785 \times 10^{-11} A_i - 1.30 \times 10^{-7}$	0.9996

7.4.3 Thermodynamic Modelling and Data Regression

As a result of the costly and challenging nature of undertaking HPVLE measurements, it is vital that experimental VLE data be correctly modelled and interpreted. The approaches and techniques adopted in this work for the modelling and interpretation of the measured novel HPVLE binary systems are discussed in § 4.3. This section presents and discusses the results of the regression and modelling.

The modelling of the experimentally determined HPVLE data for the systems R-1216 + pentane, R-1216 + hexane, R-1216 + heptane and for pure component vapour pressures, were carried out on the software package Aspen Plus®. The data was regressed and modelled using the direct method, which featured a single EoS model, mixing rules and an activity coefficient model. For the pure component vapour pressures data; an equation of state model (EoS) model was utilised.

Ramjugernath (2000) and Mühlbauer and Raal (1995) attest to the preference of the direct method of data reduction for HPVLE data by a vast majority. The direct method uses a single equation of state to describe both the liquid and vapour phases. The equation of state model used in this work was the Peng-Robinson EoS (Peng and Robinson, 1976).

The Mathias-Copeman alpha function was employed in conjunction with the Peng-Robinson equation of state. The Mathias-Copeman alpha function provided a more accurate fit of the pure component vapour pressures by improving the fit of the data. This was of paramount

importance since according to Mathias and Copeman (1983) the inaccurate representation of the pure component vapour pressure can artificially misrepresent the excess Helmholtz free energy and obstruct the mixture effects analysis. The Wong-Sandler mixing rules were incorporated to extend the use of the equation of state to mixtures.

The NRTL (Renon and Prausnitz, 1968) local composition activity coefficient model was utilised in collaboration with the Wong-Sandler mixing rules. A comprehensive description of the activity coefficient model, mixing rules and the EoS model is presented in §4.3 together with the equations used for regressing and modelling the data.

The data regression procedure entailed fitting parameters for each model using the least squares method objective function to regress the experimental data. As a result of the EoS and mixing rules utilised, three parameters were fitted for the model sets. For the NRTL G^E model, two adjustable binary interaction parameters were used, $\tau_{1,2}$ and $\tau_{2,1}$ whereas the non-randomness factor $(\alpha_{1,2})$ was set to 0.3. This is as a result of the weak temperature dependence of the non-randomness factor. A value of 0.3 is recommended for non-polar substances, non-polar with polar associated liquid, small differences from ideality. A total of three parameter were fitted for the model set using the PR EoS and the WS mixing rules; viz. the mixing rule interaction parameter $(\kappa_{1,2})$ and the NRTL binary interaction parameters ($\tau_{1,2}$ and $\tau_{2,1}$). It must be taken into consideration that a minimum of three isotherms were measured for each system, making it possible to compare the temperature dependency of the binary interaction parameters for each of the three model combinations. As such, much can be discussed about the binary interaction parameters.

To measure the degree of how well the thermodynamic model correlate the data, the Bias and the absolute average relative deviation (AARD) values for fitting of the experimental VLE data to the thermodynamic model (PR-MC-WS-NRTL) were computed using the equations listed in §7.4.

The regressed fitting parameters were then used to model each system on Aspen Plus® to determine the entire phase envelope. A comparison was then drawn between the experimental data measured in this work to the data correlated using the direct method.

Experimental VLE data correlation for each novel binary system is presented in the following manner:

1. The experimental VLE data for the binary systems are tabulated for all the systems at the temperatures at which the study was undertaken. The table also reports the differences between the experimental and regressed (PR-MC-WS-NRTL) phase compositions.

2. The phase envelopes for the calculated and experimental data are plotted.

3. The composition dependence of the relative volatility (experimental) is graphically compared to the calculated data (PR-MC-WS-NRTL).

4. The errors (δx, δy, and δP), AADs, Bias and AARDs in the phase compositions, using the PR-MC-WS-NRTL thermodynamic model, are tabulated; permitting the immediate demonstration of the model performance. As a measure of the quality of the model fit, the AAD should be less than 0.01 for the vapour compositions. The deviations in the phase composition for each isotherm were computed with one set of adjustable parameters. The parameters are spread between the mixing (α, $\tau_{1,2}$, $\tau_{2,1}$) and the combining rules $(\kappa_{1,2})$. It is acknowledged that independently regressing each isothermal *P-x-y* dataset would possibly give an improved model fit, but then extrapolation of the *P-x-y* data over a range of temperatures is essential for simulation (Nelson, 2012). The regressed NRTL parameters can take one of two forms; that is, scalar ($\tau_{ij} = a_{ij}$ and $\tau_{ji} = a_{ji}$) or temperature dependent ($\tau_{ij} = a_{ij} + b_{ij}/T$ and $\tau_{ji} = a_{ji} + b_{ji}/T$) if valid temperature-dependence is implementable into the NRTL parameters.

7.4.3.1 Vapour Pressure

Table 7-22 lists the deviations in the experimental saturated vapour pressure data modelled with the PR EoS with the MC alpha function. The saturated vapour pressure measurement was undertaken from a temperature just below the lowest vapour-liquid equilibrium isotherm to a temperature above the highest vapour-liquid equilibrium isotherm but at the same time below

the pure component critical temperature. The fitted parameters for the Mathias-Copeman alpha function are reported in Table 7-23. In general, the Peng-Robinson EoS and the Mathias-Copeman expression offers an improved fit of the pure component saturated vapour data ($0.03\% \leq AARD_p \leq 0.06\%$).

Table 7- 22: Absolute average relative deviation (AARD) and average absolute deviation (AAD) values for the fitting of the experimental saturated vapour pressure to the PRMC model.

Component	AAD(P)[a] [MPa]	AAD(T) [K]	AARD(P)[b] [MPa]	AARD(T) [K]
n-pentane	0.0014	0.057	0.02%	0.06%
n-hexane	0.0005	0.102	0.04%	0.12%
n-heptane	0.0007	0.075	0.03%	0.06%
R-1216	0.0132	0.110	0.05%	0.14%

[a] $AAD\ (\bar{\theta}) = 1/N_p \sum_1^{N_p} \left|\bar{\theta}_{exp} - \bar{\theta}_{calc}\right|$, where $\bar{\theta}_{calc}$ and $\bar{\theta}_{exp}$ are the modelled and experimental data of *T* or *P* and N_p is the number of data points.

[b] $AARD\ (\bar{\theta}) = 1/N_p \sum_1^{N_p} \left(\left|\bar{\theta}_{exp} - \bar{\theta}_{calc}\right|\right)/\bar{\theta}_{exp}$, where N_p is the total number of data points.

Table 7- 23: Regressed Mathias-Copeman parameters

Component	Temperature range [K]	$C_{1,i}$	$C_{2,i}$	$C_{3,i}$
n-pentane	353 - 393	0.803	-1.567	7.434
n-hexane	343 – 372	0.915	-1.767	6.389
n-heptane	373 - 403	0.786	0.687	-5.372
R-1216	343 - 363	1.07119	-4.2204	-0.32058

7.4.3.2 Vapour-Liquid Equilibrium Data

Hexafluoropropylene R-1216 (1) + pentane (2) binary system

The experimental VLE data for the 1, 1, 2, 3, 3, 3-hexafluoro-1-propene (1) + pentane (2) binary system are reported in Table 7-24 for one isotherm below the critical temperature of 1,

1, 2, 3, 3, 3-hexafluoro-1-propene (352.99 K), and two isotherms above this temperature (373.01 and 393.09 K).

The experimental binary mixture data were used in fitting the interaction parameters for the PR-MC-WS-NRTL model. The parameters were fitted for the two regions below and above the critical temperature of 1, 1, 2, 3, 3, 3-hexafluoro-1-propene and are detailed in Table 7-23. For parameters regressed for individual isotherms, it is observed that there is a discontinuity of the regressed model parameters at the critical temperature of R-1216 (358.9 K). The parameters change in magnitude in the transition from the 352.99 K isotherm to the 373.01 K isotherm as shown in Table 7-25. Parallel observations have hitherto been detailed (Valtz et al., 2003, Valtz et al., 2004, Ramjugernath et al., 2009) and is perceived to be a consequence of the variance in absorption of a subcritical gas along with a supercritical gas inside a liquid (Valtz et al., 2003, Subramoney et al., 2012). This is even apparent from the *P-x-y* plots in that the phase envelopes of the isotherms which are above the critical temperature of R-1216 do not reach a component composition of 1.

Figure 7-25 shows the temperature dependence of the fitted binary interaction parameters. It is apparent from the figure that the parameters do not exhibit a linear trend. The measured VLE data as well as its depiction by way of the PR-MC-WS-NRTL model are plotted in Figure 7-23. The differences between the measured and computed (PR-MC-WS-NRTL) vapour composition are detailed in Table 7-24. Furthermore, the statistical analysis (AAD, AARD and Bias) of the data fit is reported in Table 7-25 and Table 7-26. The deviations in the vapour compositions and pressure between the experimental and modelled data for the R-1216 + n-pentane binary system are presented in Table 7-25 and Table 7-26 respectively. The AARDs in pressure consistently remain below 1 percent for all isotherms. The AARDs for in the pressures for the first two isotherms (352.99 K and 373.01 K) are just above 0.5 percent whereas the 393.09 K isotherm has an AARD of 0.98%. Generally, the experimental (*P-x-y*) is satisfactorily correlated by the regression model implemented.

The relative volatility $(\alpha_{ij})$was computed from the experimental data and was compared to values computed using the PR-MC-WS-NRTL model. The dependence of relative volatility on the composition is plotted in Figure 7-27. A good agreement was observed between the experimental and computed values for the entire range of all investigated isotherms.

Table 7- 24: Experimental VLE data for the 1, 1, 2, 3, 3, 3-hexafluoro-1-propene (1) + pentane (2) binary system.

			PR-MC-WS-NRTL		
$P_{exp}(MPa)$	x_{1exp}	y_{1exp}	$(P_{exp} - P_{cal})MPa$	y_{1calc}	$y_{1exp} - y_{1calc}$
T (K) = 352.99					
0.844	0.096	0.537	-0.012	0.532	0.005
1.068	0.166	0.641	0.011	0.643	0.020
1.368	0.275	0.718	0.003	0.722	0.009
1.691	0.434	0.773	0.004	0.779	0.000
1.800	0.482	0.786	-0.019	0.789	-0.005
1.903	0.553	0.802	0.002	0.806	-0.002
2.041	0.634	0.821	0.004	0.822	-0.010
2.160	0.702	0.838	0.007	0.839	-0.010
T (K) = 373.01					
1.116	0.087	0.438	0.013	0.441	0.005
1.834	0.252	0.636	0.007	0.639	0.014
1.990	0.298	0.660	0.002	0.664	0.011
2.221	0.375	0.689	-0.005	0.693	-0.009
2.350	0.433	0.705	0.018	0.710	-0.013
2.513	0.485	0.716	-0.017	0.722	-0.010
T (K) = 393.09					
1.515	0.081	0.348	-0.023	0.347	-0.001
1.855	0.145	0.468	0.030	0.460	-0.008
2.236	0.211	0.514	0.000	0.525	0.011
2.686	0.308	0.583	-0.018	0.575	-0.008
2.924	0.367	0.607	-0.031	0.597	-0.010

[a] Expanded uncertainties ($k = 2$): $\overline{U}(T) = \pm 0.06\ K$, $\overline{U}(P) = \pm 0.007 MPa$, $\overline{U}(x) = \pm 0.010$, $\overline{U}(y) = \pm 0.011$.

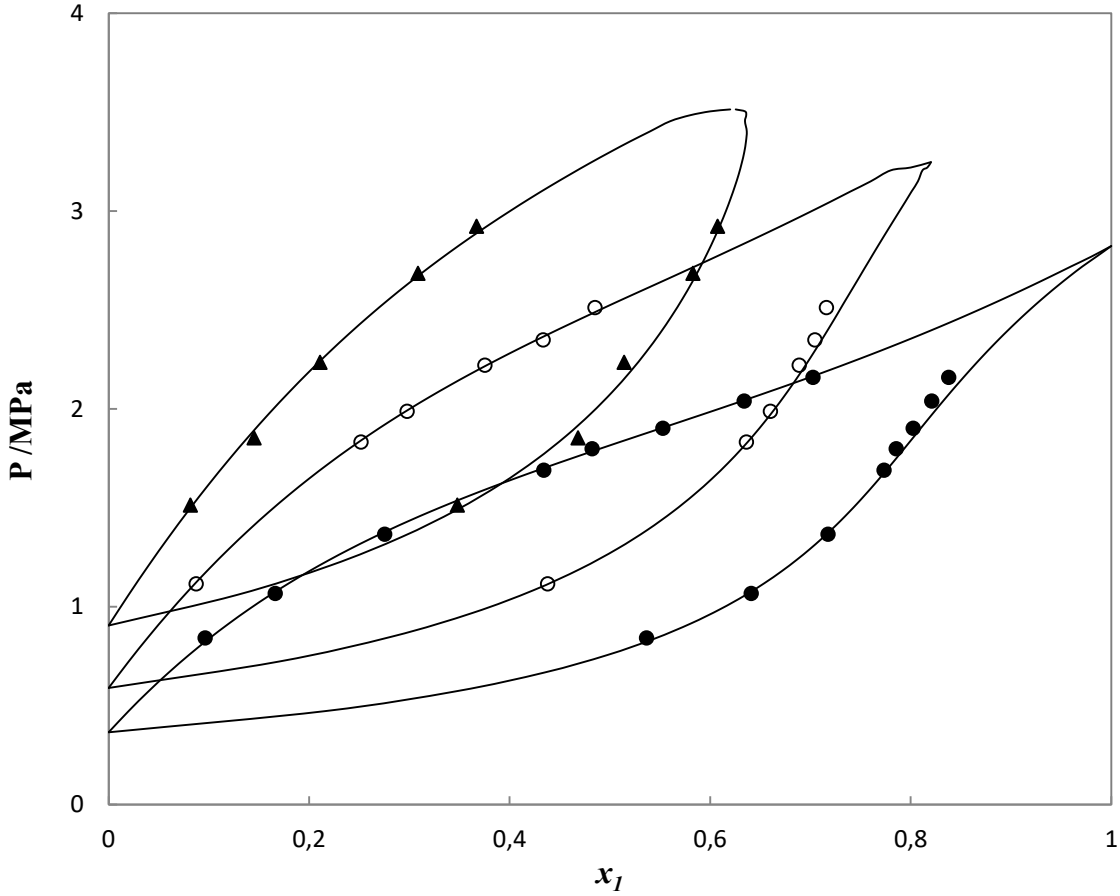

Figure 7- 23: Experimental VLE data and modelling results for the 1, 1, 2, 3, 3, 3-hexafluoro-1-propene (1) + pentane (2) binary system at temperatures: 352.99 K (●), 373.01 K (○) and 393.09 K (▲). Modelled data (*P-x-y*) using the PR-MC-WS-NRTL model represented by the solid black line.

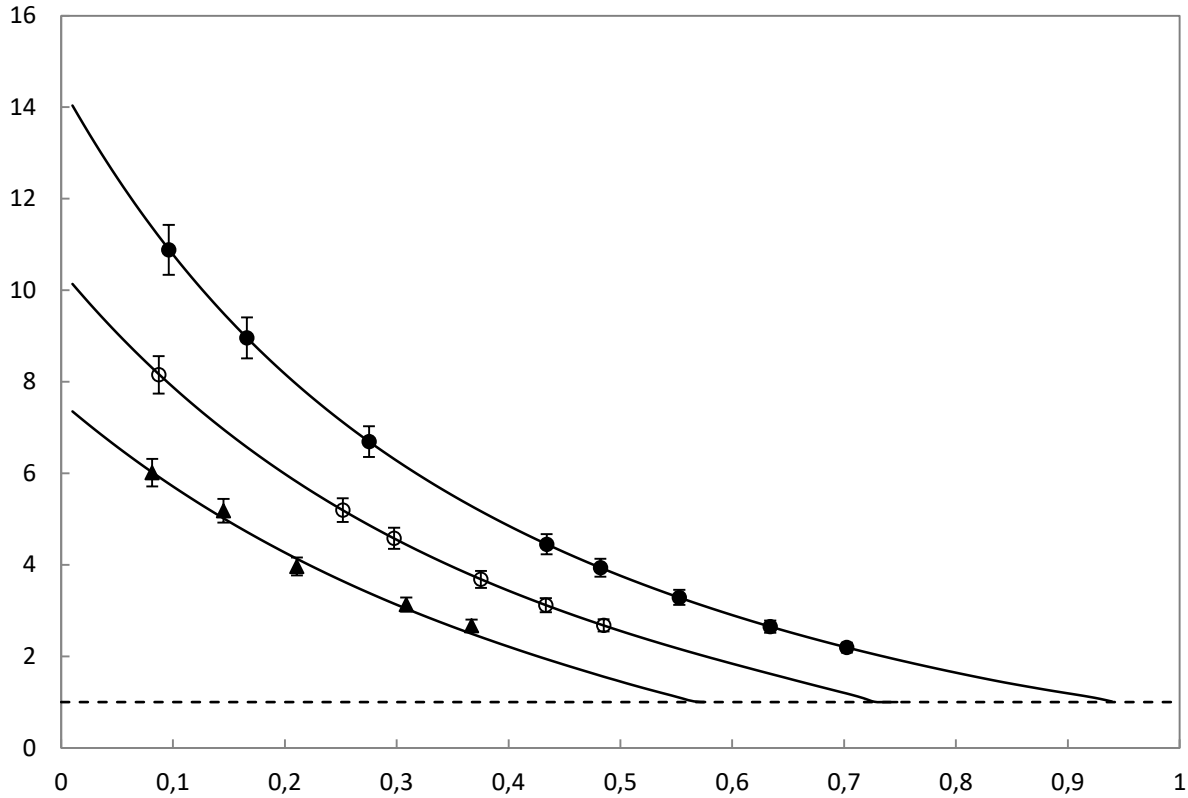

Figure 7- 24: Dependence of relative volatility on the composition for the 1, 1, 2, 3, 3, 3-hexafluoro-1-propene (1) + pentane (2) binary system at 352.99 K (●), 373.01 K (×), and 393.09 K (▲). PR-MC-WS-NRTL model (—), line of invariable relative volatility α = 1 (……). Error bands are indicative of the expanded uncertainties in relative volatility.

Table 7- 25: Regressed model parameters and statistical analysis of the data fit for the 1,1,2,3,3,3-hexafluoro-1-propene (1) + pentane (2) binary system.

Model parameters [a]				Statistical analysis		
Temperature/K	τ_{12}/Jmol^{-1}	τ_{21}/Jmol^{-1}	κ_{12}	AAD (y_i)[b]	AARD (y_i)/%[c]	Bias (y_i)/%[d]
Parameters regressed for individual isotherms						
352.99	757	3120	0.239	0.007	1.04	1.04
373.01	3333	1420	0.174	0.007	1.19	0.73
393.09	3118	1386	0.215	0.008	1.53	1.39
Parameters regressed for all subcritical isotherms						
352.99	757	3120	0.239	0.007	1.04	1.04
Parameters regressed for all supercritical isotherms						
373.01 - 393.09	4444	818	0.181	0.007	1.07	0.37

[a] Data modelled via the PR-MC-WS-NRTL model with $\alpha_{1,2}$ set = 0.3

[b] $AAD\ (\bar{\theta}) = 1/N_p \sum_1^{N_p} \left|\bar{\theta}_{exp} - \bar{\theta}_{calc}\right|$

[c] $AARD\ (\bar{\theta}) = 1/N_p \sum_1^{N_p} \left(\left|\bar{\theta}_{exp} - \bar{\theta}_{calc}\right|\right)/\bar{\theta}_{exp}$

[d] $Bias\ (\bar{\theta}) = 1/N_p \sum_1^{N_p} \left(\bar{\theta}_{exp} - \bar{\theta}_{calc}\right)/\bar{\theta}_{exp}$

Table 7- 26: Statistical analysis of the data fit for the 1,1,2,3,3,3-hexafluoro-1-propene (1) + pentane (2) binary system.

Temperature [K]	Statistical analysis		
	AAD(P)[a] [bar]	AARD(P)[b] [bar]	Bias(P)[c]
352.99	0.078	0.58%	-0.06%
373.01	0.103	0.55%	0.26%
393.09	0.206	0.98%	-0.33%

[a] Data modelled via the PR-MC-WS-NRTL.

[b] $AAD\ (\bar{\theta}) = 1/N_p \sum_1^{N_p} \left|\bar{\theta}_{exp} - \bar{\theta}_{calc}\right|$

[c] $AARD\ (\bar{\theta}) = 1/N_p \sum_1^{N_p} \left(\left|\bar{\theta}_{exp} - \bar{\theta}_{calc}\right|\right)/\bar{\theta}_{exp}$

[d] $Bias\ (\bar{\theta}) = 1/N_p \sum_1^{N_p} \left(\bar{\theta}_{exp} - \bar{\theta}_{calc}\right)/\bar{\theta}_{exp}$

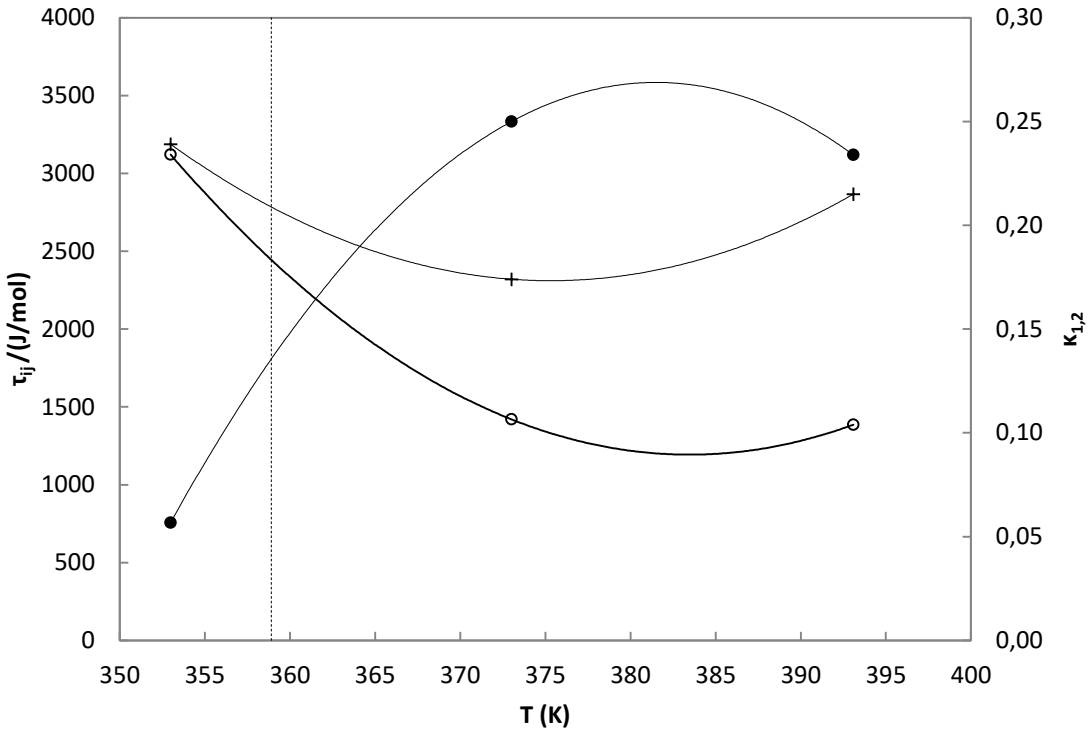

Figure 7- 25: Variation of the binary interaction parameters with temperature for the R-1216 (1) + n-pentane (2) binary system: NRTL activity coefficient model, $\boldsymbol{\tau_{12}}$(●) and $\boldsymbol{\tau_{21}}$(○); Wong-Sandler mixing rule, $\boldsymbol{\kappa_{12}}$(+) and⋯⋯, R-1216 critical temperature. The solid lines represent a second-order polynomial.

Hexafluoropropylene R-1216 (1) + n-Hexane (2) binary system

The experimental VLE data for the binary system R-1216 (1) + n-hexane (2) are reported in Table 7-27 for two isotherms below the critical temperature of 1, 1, 2, 3, 3, 3-hexafluoro-1-propene [(343.48 and 353.34) K] and two isotherms above this temperature [(362.44 and 372.98) K]. There was much difficulty in measuring the R-1216 + n-hexane system as the equilibrium cell was not holding pressure at pressures above 25 bar as the O-rings seemed to be worn away yet Viton® is stated to be compatible with the chemicals used hence the data was eventually measured on the apparatus of Narasigadu et al. (2013). Although R-1216 and n-hexane are said to be compatible with Viton® O-rings, there was much difficulty with sealing at high temperature and pressure. This necessitated the use of another cell to continue with measurements. The differences between the measured and the calculated VLE data differed significantly at low pressures with the use of the two different apparatus. Table 7-29 reports

the bias and AARD on the vapour and liquid phase compositions. Generally, the VLE data correlated over all the fitting methods undertaken had $AAD_{x_1,y_1} < 2\%$ in all occurrences. The poorest data fitting was for the vapour phase composition of the 353.34 K isotherm ($AARD_{y_1} = 1.49\%$). The binary interaction parameters are regressed for separate isotherms. However, further measurement need to be conducted for the 372.98 K isotherm to complete the phase envelope and improve the quality of the fit especially in the locality of the equimolar region. For parameters regressed for separate isotherms, there appears to be a discontinuity in the correlated model parameters at the critical temperature of R-1216 (358.9 K), as the parameters change magnitude significantly. Figure 7-28 shows a plot of the interaction parameter plots for the PR-MC-WS-NRTL model for the system R-1216 (1) + n-hexane (2) as a function of temperature to show the discontinuity. It is apparent from the figure that the parameters do not exhibit a linear trend. The magnitude of the difference between the experimental and computed (PR-MC-WS-NRTL) vapour and liquid phase compositions is reported in Table 7-27.

An accurate representation of the relative volatility (α_{ij}) of binary mixtures is vital for the purposes of process design. Relative volatilities were computed from the experimental data and were compared to values computed using the PR-MC-WS-NRTL model. The dependence of relative volatility on the composition is plotted in Figure 7-27. A good agreement was observed between the experimental and computed values for the entire range of all investigated isotherm

Table 7- 27: Experimental VLE data for the 1,1,2,3,3,3-hexafluoro-1-propene (1) + n-hexane (2) binary system using the least squares regression.

			PR-MC-WS-NRTL		
$P_{exp}(MPa)$	x_{1exp}	y_{1exp}	$(P_{exp} - P_{cal})MPa$	y_{1calc}	$y_{1cal} - y_{1exp}$
T (K) = 343.48					
0.723	0.144	0.853	0.015	0.854	0.001
0.860	0.184	0.866	-0.021	0.873	0.007
1.271	0.390	0.915	0.011	0.923	0.008
1.398	0.482	0.925	0.019	0.934	0.009
1.429	0.514	0.924	0.028	0.936	0.012
1.568	0.621	0.932	-0.020	0.943	0.011
1.762	0.768	0.949	-0.151	0.949	0.000
T (K) = 353.34					
0.593	0.084	0.754	0.002	0.755	0.002
0.816	0.137	0.829	0.005	0.824	-0.004
0.970	0.174	0.842	-0.009	0.851	0.009
1.365	0.302	0.879	0.004	0.899	0.019
1.783	0.560	0.907	0.062	0.930	0.023
1.935	0.651	0.919	-0.036	0.934	0.015
2.123	0.770	0.936	-0.170	0.938	0.002
T (K) = 362.44					
0.668	0.084	0.709	0.002	0.718	0.009
1.530	0.289	0.860	-0.007	0.879	0.019
2.049	0.544	0.895	0.070	0.900	0.005
2.244	0.650	0.913	-0.020	0.924	0.010

Table 7-27
Continuing

2.477	0.759	0.921	-0.200	0.928	0.007
T (K) = 372.98					
1.834	0.292	0.809	-0.003	0.824	0.015
1.967	0.338	0.826	0.011	0.837	0.011
2.288	0.457	0.846	0.060	0.854	0.008
2.558	0.569	0.863	0.037	0.865	0.005
2.780	0.661	0.873	-0.081	0.878	0.005
2.961	0.733	0.882	0.020	0.887	0.005

[a] Expanded uncertainties ($k = 2$): $\overline{U}(T) = \pm 0.06\ K$, $\overline{U}(P) = \pm 0.007 MPa$, $\overline{U}(x) = \pm 0.012$, $\overline{U}(y) = \pm 0.011$.

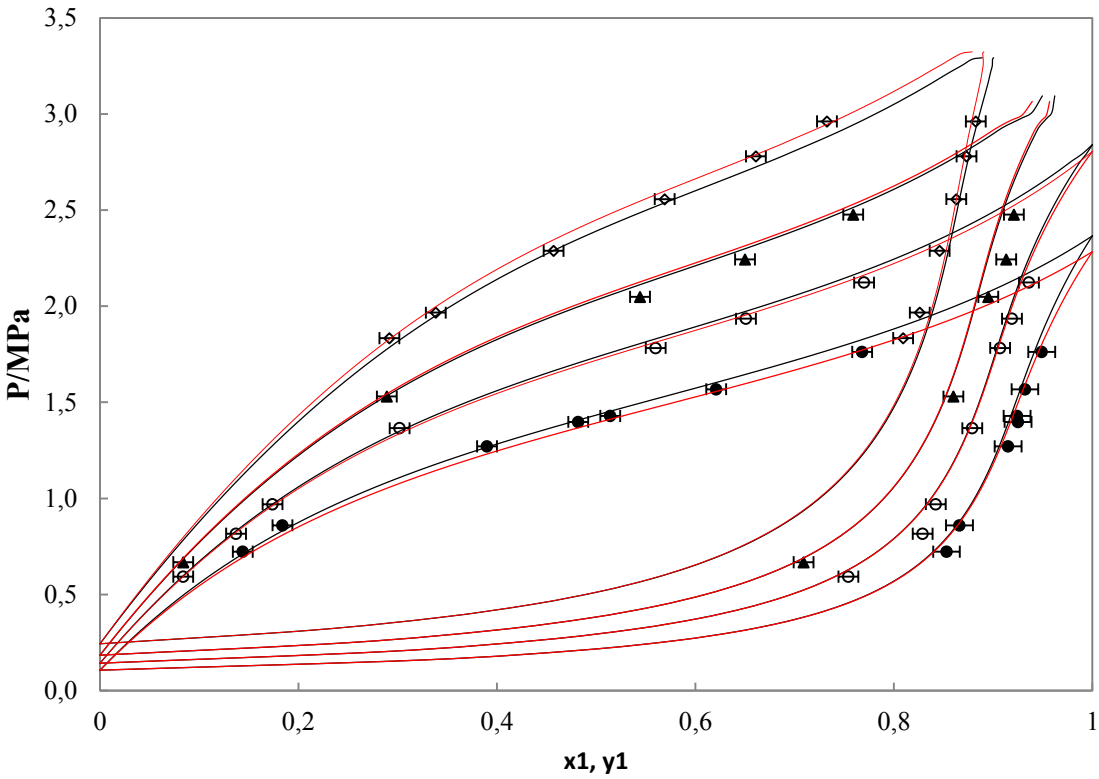

Figure 7- 26: Experimental VLE data and modelling results for the 1, 1, 2, 3, 3, 3-hexafluoro-1-propene (1) + n-hexane (2) binary system at 343.48 K (●), 353.34 K (○), 362.44 K (▲) and 372.98 K (◊) using the PR-MC-WS-NRTL model (—), and PR-MC EoS (—).

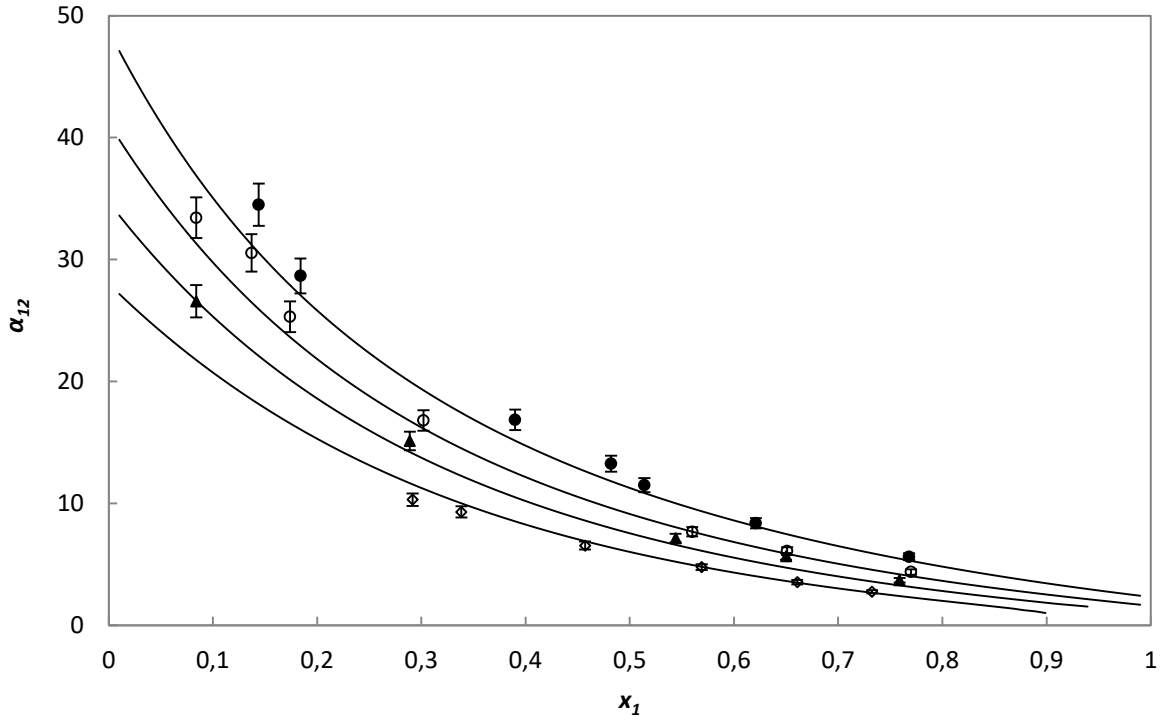

Figure 7-27: Dependence of relative volatility on the composition for the 1, 1, 2, 3, 3, 3-hexafluoro-1-propene (1) + n-hexane (2) binary system at 343.48 K (●), 353.34 K (○), 362.44 K (▲) and 372.98 K (◊) and PR-MC-WS-NRTL model (—).

Table 7- 28: Regressed model parameters and statistical analysis of the data fit for the 1,1,2,3,3,3-hexafluoro-1-propene (1) + n-hexane (2) binary system.

Model parameters [a]			
Temperature/K	τ_{12}/Jmol^{-1}	τ_{21}/Jmol^{-1}	κ_{12}
Parameters regressed for individual isotherms			
343.48	2013	2444	0.202
353.34	3654	1494	0.191
362.44	3552	1256	0.225
372.98	29597	9287	0.377

[a] Data modelled via the PR-MC-WS-NRTL model (with $\alpha_{1,2}$ set = 0.3).

Table 7- 29: Statistical analysis of the data fit for the 1,1,2,3,3,3-hexafluoro-1-propene (1) + n-hexane (2) binary system.

Statistical analysis			
T/K	AAD_{y_1} (%)[a]	$AARD_{y_1}$ (%)[b]	$Bias_{y_1}$ (%)[c]
Parameters regressed for individual isotherms			
343.48	0.007	0.833	-0.784
353.34	0.011	1.229	-0.831
362.44	0.014	1.641	-0.571
372.98	0.009	1.124	0.800

[a] Data modelled via the PR-MC-WS-NRTL model

[b] $AAD\ (\bar{\theta}) = 1/N_p \sum_1^{N_p} \left|\bar{\theta}_{exp} - \bar{\theta}_{calc}\right|$

[c] $AARD\ (\bar{\theta}) = 1/N_p \sum_1^{N_p} \left(\left|\bar{\theta}_{exp} - \bar{\theta}_{calc}\right|\right)/\bar{\theta}_{exp}$

[d] $Bias\ (\bar{\theta}) = 1/N_p \sum_1^{N_p} \left(\bar{\theta}_{exp} - \bar{\theta}_{calc}\right)/\bar{\theta}_{exp}$

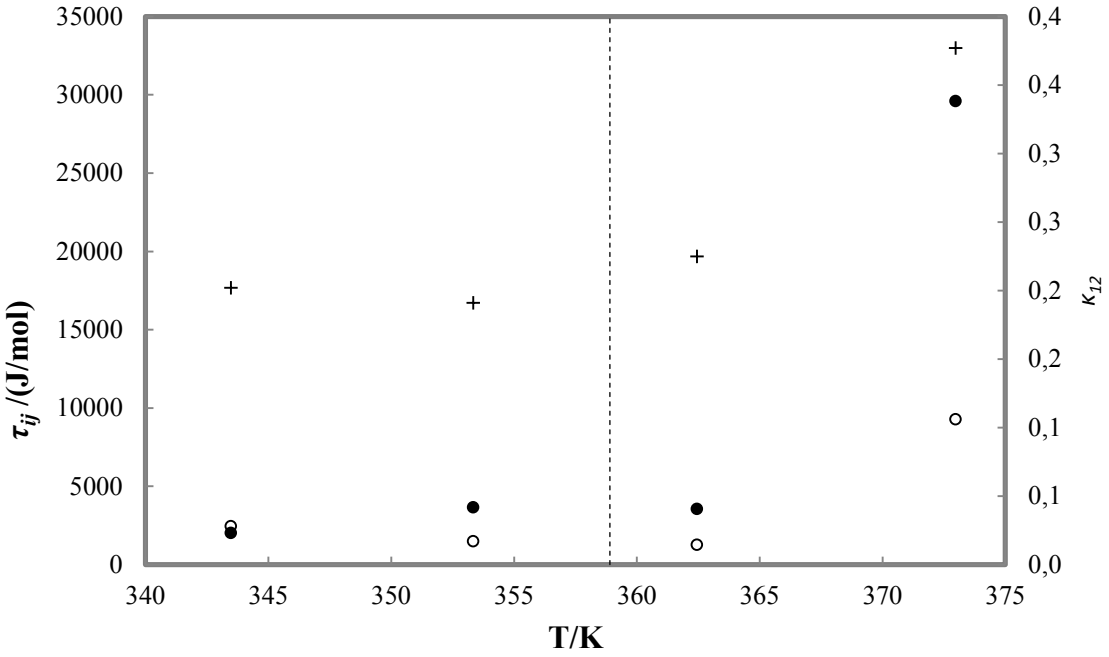

Figure 7-28: Interaction parameter plots for the PR-MC-WS-NRTL model for the system R-1216 (1) + n-hexane (2). Primary axis: ●, $\boldsymbol{\tau_{12}}$; ○, $\boldsymbol{\tau_{21}}$; Secondary axis: +, $\boldsymbol{\kappa_{12}}$. ⋯⋯, R-1216 critical temperature.

Hexafluoropropylene R-1216 (1) + n-Heptane (2) binary system

The experimental VLE data for the 1, 1, 2, 3, 3, 3-hexafluoro-1-propene (1) + n-heptane (2) binary system are reported in Table 7-30 for three isotherms above the critical temperature of 1, 1, 2, 3, 3, 3-hexafluoro-1-propene (373.25, 398.39 and 423.60) K. The experimental VLE binary mixture data were used in fitting the interaction parameters for the PR-MC-NRTL (κ_{12}, τ_{12} and τ_{21}) model. Initially, the standard Peng-Robinson (PR) equation of state was used to correlate the data to examine if a simple model would not give a better fit. The fitted Mathias-Copeman for the Peng Robinson alpha function was incorporated into the PR EoS. The parameters were fitted for the three isotherms and are reported in Table 7-31. The experimental VLE data as well as its representation by way of the PR-MC-WS-NRTL model are plotted in Figure 7-29. The deviations between the measured and computed (PR-MC-WS-NRTL) vapour composition are reported in Table 7-30.

Furthermore, the statistical analysis (AAD, AARD and Bias) of the data fit is reported in Table 7-31. The poorest fit for the experimental VLE data was observed for the vapour composition of the 398.39 K isotherm ($\text{AARD}_{y_1} = 1.98\ \%$). Similarly, for parameters regressed for individual isotherms, it is observed that there is a discontinuity of the regressed model parameters observed between the 398.39 K and 423.60 K isotherms as signalled by change in sign or magnitude as shown in Table 7-31. From the plot of the variation of binary interaction parameters in Figure 7-31 is observed that the values of τ_{12} steadily increase before a sharp decline to a negative value of -997 J/mol for the 423.60 K isotherm, whereas the values for the τ_{21} parameter have a decline in the range from the 373.25 K isotherm to the 398.39 K isotherm and the plot which is fitted by a second order polynomial then sharply increases. No linearity was observed from the fitting of the parameters.

It is interesting that small changes in the carbon alkane chain length considerably alter the phase behaviour as well as the ensuing model parameters. It was observed from previous studies the R-170 + R-1216 binary system displayed neither azeotropic behaviour nor liquid-liquid immiscibility for the investigated temperature range (Subramoney et al., 2012). However, the propane + R-1216 system displays a pressure-maximum azeotrope over the range of the investigated temperatures (312 – 343) K (Subramoney et al., 2015). In the transition

from C_3 to C_4 of the alkane chain length, the n-butane + R-1216 system exhibits near-azeotropic behaviour at elevated 1, 1, 2, 3, 3, 3-hexafluoro-1-propene concentrations.

The relative volatility was computed from the experimental data and was compared to values computed using the PR-MC-WS-NRTL model. The dependence of relative volatility on the composition is plotted in Figure 7-30. The trends observed across the homologous series of the alkane + R-1216 binary systems are explained below.

Table 7- 30: Experimental VLE data for the 1,1,2,3,3,3-hexafluoro-1-propene (1) + n-heptane (2) binary system.

			PR-MC-WS-NRTL		
$P_{exp}(MPa)$	x_{1exp}	y_{1exp}	$(P_{exp} - P_{cal})MPa$	y_{1calc}	$y_{1cal} - y_{1exp}$
T (K) = 373.25					
0.928	0.127	0.887	0.019	0.876	0.011
1.036	0.144	0.894	0.003	0.889	0.005
1.280	0.189	0.914	-0.016	0.907	0.007
1.446	0.223	0.922	-0.030	0.912	0.010
1.701	0.296	0.928	-0.002	0.925	0.003
1.919	0.367	0.934	0.011	0.933	0.001
2.043	0.406	0.936	0.000	0.934	0.002
2.154	0.450	0.939	0.006	0.929	0.010
2.339	0.531	0.942	0.018	0.931	0.011
2.679	0.700	0.943	0.050	0.935	0.007
T (K) = 398.39					
0.966	0.092	0.785	0.016	0.766	0.019
1.362	0.144	0.838	-0.009	0.819	0.019
1.616	0.183	0.857	-0.012	0.846	0.011
1.813	0.214	0.868	-0.022	0.859	0.009
2.149	0.283	0.876	0.017	0.865	0.011
2.475	0.347	0.881	0.003	0.872	0.009
2.641	0.382	0.881	-0.005	0.875	0.006
2.803	0.424	0.887	0.012	0.879	0.008
3.067	0.493	0.888	0.023	0.883	0.004
T (K) = 423.60					
1.299	0.094	0.682	0.002	0.665	0.017
2.002	0.180	0.766	-0.008	0.754	0.011
2.286	0.222	0.777	0.011	0.777	0.000
2.533	0.255	0.789	-0.007	0.790	0.001
2.819	0.300	0.801	0.004	0.803	-0.002

[a] Expanded uncertainties ($k = 2$): $\bar{U}(T) = \pm 0.06\ K$, $\bar{U}(P) = \pm 0.007 MPa$, $\bar{U}(x) = \pm 0.012$, $\bar{U}(y) = \pm 0.011$.

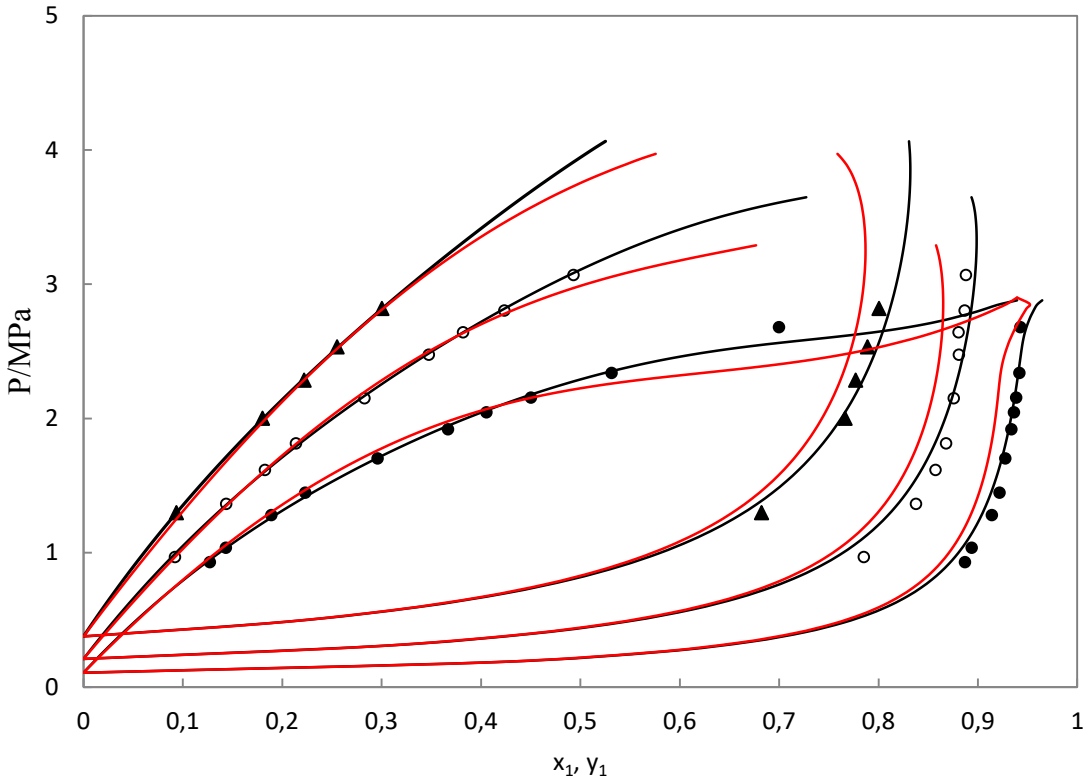

Figure 7-29: Experimental VLE data and modelling results for the 1, 1, 2, 3, 3, 3-hexafluoro-1-propene (1) + n-heptane (2) binary system at temperature: 373.25 K (●), 398.39 K (×) and 423.60 (▲). PR-MC-WS-NRTL model (—) and PR-MC EoS (—).

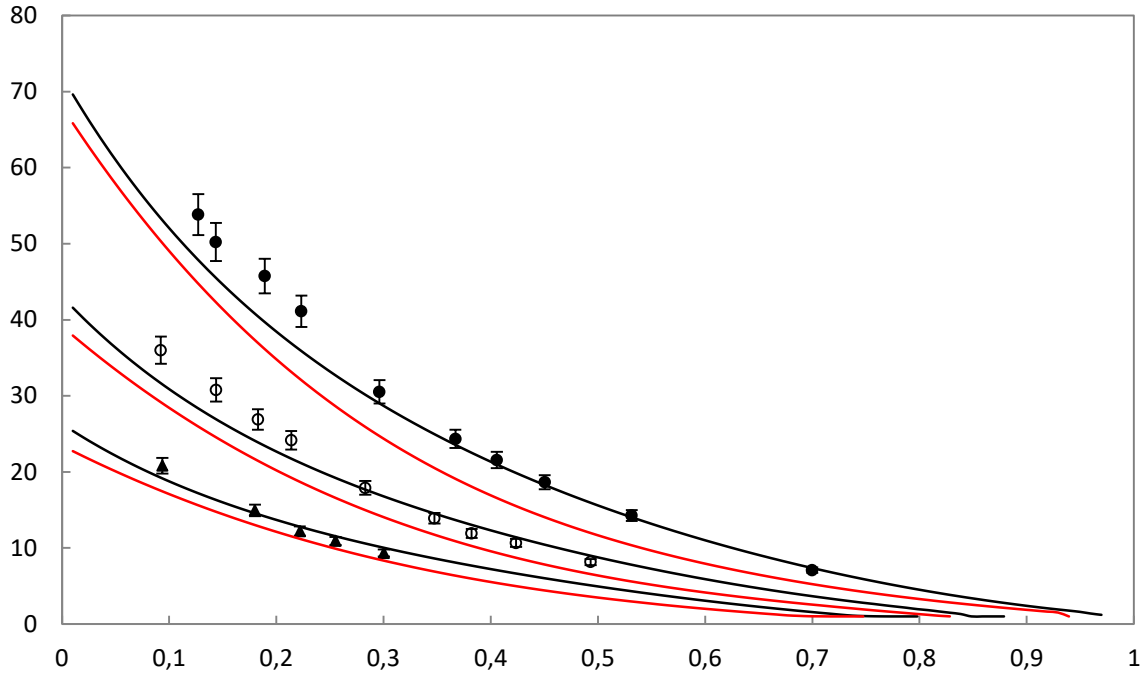

Figure 7- 30: Dependence of relative volatility on the composition for the 1, 1, 2, 3, 3, 3-hexafluoro-1-propene (1) + n-heptane (2) binary system at temperatures: 373.25 K (●), 398.39K (▲), 3423.60 K (◊). PR-MC-WS-NRTL model (—) and PR-MC EoS (—).

Table 7- 31: Regressed model parameters and statistical analysis of the data fit for the 1,1,2,3,3,3-hexafluoro-1-propene (1) + n-heptane (2) binary system.

Model parameters [a]						
Temperature/K	τ_{12}/Jmol^{-1}	τ_{21}/Jmol^{-1}	κ_{12}	AAD_{y_1} (%)	$AARD_{y_1}$ (%)[b]	$Bias_{y_1}$ (%)[c]
Parameters regressed for individual isotherms						
373.25	695	3187	0.015	0.514	1.739	-0.565
398.39	1039	2685	0.040	0.016	1.984	-0.515
423.60	-977	4637	0.004	0.007	1.042	0.071

[a] Data modelled via the PR-MC-WS-NRTL model

[b] $AAD\ (\bar{\theta}) = 1/N_p \sum_1^{N_p} \left|\bar{\theta}_{exp} - \bar{\theta}_{calc}\right|$

[c] $AARD\ (\bar{\theta}) = 1/N_p \sum_1^{N_p} \left(\left|\bar{\theta}_{exp} - \bar{\theta}_{calc}\right|\right)/\bar{\theta}_{exp}$

[d] $Bias\ (\bar{\theta}) = 1/N_p \sum_1^{N_p} \left(\bar{\theta}_{exp} - \bar{\theta}_{calc}\right)/\bar{\theta}_{exp}$

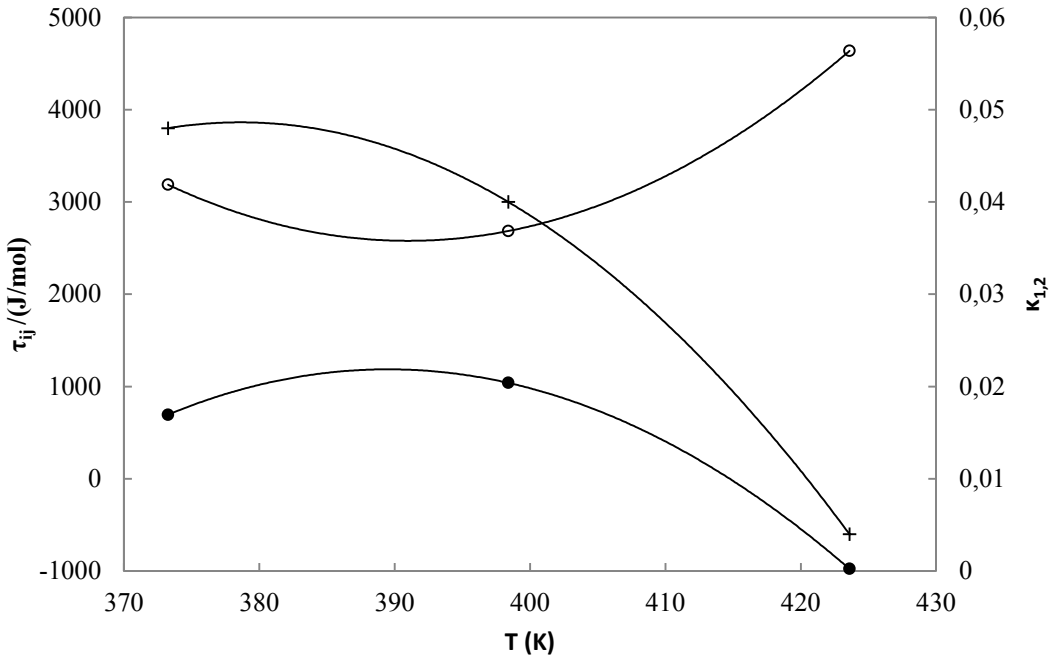

Figure 7-31: Variation of the binary interaction parameters for the R-1216 (1) + n-heptane (2) binary system: NRTL activity coefficient model, $\boldsymbol{\tau_{1,2}}$(●) and $\boldsymbol{\tau_{2,1}}$(○); Wong-Sandler mixing rule, $\boldsymbol{\kappa_{1,2}}$(+). The solid lines represent a second-order polynomial.

Analysis of the trends observed

Binary VLE data for the [ethane, propane, butane] + R-1216 binary systems are available in literature. This work added to the binary mixtures of the alkane homologous series with R-1216, that is, [n-pentane, n-hexane, and n-heptane] + R-1216. An analysis of the liquid and vapour phase composition deviations as the alkane chain length increases shows that the solubility of R-1216 in the vapour phase decreases, except for high pressures where the R-1216 concentration is high.

Plots of the dependence fitted binary interaction parameters (κ_{ij}) upon the temperature for the systems [ethane, propane, butane] + R-1216exhibit a non-linear relationship. The same was observed in this work. For the ethane (R-170) + R-1216 binary system, for parameters regressed for separate isotherms, a discontinuity of the fitted model parameters was observed at the critical temperature of ethane (305 K) as the parameters changed either the magnitude or sign (Tshibangu et al., 2013) . The same behaviour was observed for the R-1216 + n-hexane binary system where a discontinuity was observed at the critical temperature of R-1216. This is alluded to the difference in absorption of a gas that is at a supercritical temperature and a gas

that is at a subcritical temperature in a liquid. For process simulators, it is recommended to use the model fitted parameters obtained at temperatures above and below the critical temperature. For the [propane, butane] + R1216 binary systems, the data was measured at subcritical temperatures for both components and the data also exhibited a non-linear relationship between the temperature and the fitted binary interaction parameters.

The data measured contributes to the literature and adds to the array of data for binary mixtures R-1216 and hydrocarbons. Pure component vapour pressure and binary VLE data cannot be predicted using the group contribution based methods (PSRK/UNIFAC) on ASPEN since the UNIFAC model for liquid phase activity coefficient for R-1216 is missing. The UNIFAC group counts (UFGRP for standard UNIFAC and PSRK) for only 40 components have been updated within the Aspen PURE24 databank to include newly defined groups. As such, experimental data can now be used for developing models for the predictions especially for R-1216 since this is currently not possible

8

CHAPTER EIGHT

8. CONCLUSIONS

This work was initiated as a continuation of the research on the measurement and correlation of phase equilibrium data of binary mixtures of R-1216 and alkanes. Previously, phase equilibrium data for mixtures involving 1, 1, 2, 3, 3, 3-hexafluoro-1-propene with (ethane (R-170)/ propane/ n-butane have been measured. This study involved a measurement of the high pressure phase equilibrium data of binary mixtures of R-1216 with (n-pentane/ n-hexane/ n-heptane).

Two apparatuses were made use of in the project. The first being the apparatus design of (Chiyen, 2010) on which modifications undertaken on it are outlines in § 5.1. Secondly, the same apparatus to that of Narasigadu (2011) was used to measure the isothermal *P-x-y* VLE data. The low volume equilibrium cell 18 cm^3 and the movable Rapid-Online Sampler – Injector (ROLSI™) for repeatable phase sampling highly befits the high pressure phase equilibrium measurement together with improved sealing of the equilibrium cell.

The pure component saturated vapour pressures for n-pentane, n-hexane, n-heptane and 1, 1, 2, 3, 3, 3-hexafluoro-1-propene were also measured. The measured pure component vapour pressure data vapour pressure data were compared with literature values and there was a good agreement observed. The saturated vapour pressure measurement was undertaken from a temperature just below the lowest vapour-liquid equilibrium isotherm to a temperature above the highest vapour-liquid equilibrium isotherm but at the same time below the pure component critical temperature. The fitted parameters for the Mathias-Copeman for the Peng-Robinson

alpha function were incorporated into the PR EoS. Generally, the Peng-Robinson EoS and the Mathias-Copeman expression offered a good fit of the pure component saturated vapour data $\left(0.03\ \% \leq AARD_p \leq 0.06\ \%\right)$. As a result of the low deviations, the measured vapour pressure data was regarded as being in good agreement with the literature data.

Two high pressure isothermal binary test systems were measured, that is, the ethylene + R-1216 (gas/gas) and ethane + n-hexane (gas/liquid) binary systems. The measurement of the test systems was used to evaluate the performance of the experimental apparatus operating at high pressure and to enable the experimentalist to gain experience in the procedures in conducting measurements. The ethylene + R-1216 system exhibited good agreement with literature data. For second test system (ethane + n-hexane); a marginal difference between the measured data and the literature was observed. The observed difference was alluded to the n-hexane GC calibration coupled with the improved apparatus design in comparison to that used of Ohgaki et al. (1976).

The direct injection method was used for GC detector calibrations undertaken throughout the project and proved sufficient as the difference between the actual number of moles introduced and the correlated number of moles was almost always consistently below 1 percent for liquid component and 2 percent for gases.

The measured isothermal VLE data were correlated using a thermodynamic model comprising the Peng-Robinson equation of state with the Mathias-Copeman alpha function, non-random two-liquid (NRTL) local composition model, and the Wong-Sandler mixing rule. The parameters were regressed for two cases, viz. for each individual isotherm, for isotherms below and above the critical point of 1, 1, 2, 3, 3, 3-hexafluoro-1-propene. There was good agreement between the experimental and correlated data as the model results showed an absolute average deviation in the mole compositions of < 2% in all occurrences. The VLE data was further examined by reviewing the relative volatility; such a plot magnifies quality of the fit and increase the possibility of recognising inaccurate data points. The plots of relative volatility against phase compositions and they show that there is a large difference of between the vapour pressure of the R-1216 at low concentrations in the liquid mixture and the vapour pressure of the less volatile alkanes of the mixture. A relationship of the variation between binary

interaction parameters with temperature was plotted to display whether the parameters exhibited linearity.

9

CHAPTER NINE

9. RECOMMENDATIONS

To further improve the quality of the data churned out by the experimental apparatus, the following recommendations must be taken into consideration:

1. The mixing in the equipment cell design of Narasigadu (2011) needs to be improved to ensure the quick attainment of equilibrium. The current design which comprises an externally stirred rotating magnet can be replaced within an internal stirrer that has blades that make contact with the equilibrium mixture and whose speed can be adjusted according to need. This modification will ensure equilibrium is attained in a shorter period and improved mixture homogeneity.
2. The equilibrium cell of Chiyen (2010) to be modified and adapted to that of Narasigadu (2011) and Nelson (2012) by using the sapphire cell in place of the stainless steel cell. The current design has many fittings and sealing O-rings which are prone to leaks. The low volume of the sapphire cells is economic in the volume of chemicals used.
3. An auxiliary stirring equipment to be incorporated for agitating the bath fluid when undertaking measurements as temperature gradients are most common at high temperatures.
4. A stepper motor be introduced in controlling the movement of the ROLSI™ instead of manual operation of the differential screw.

REFERENCES

Aravindan, V. & Vickraman, P. 2007. Polyvinylidenefluoride–hexafluoropropylene based nanocomposite polymer electrolytes (NCPE) complexed with LiPF 3 (CF 3 CF 2) 3. *European Polymer Journal,* 43**,** 5121-5127.

Aspentech. 2010. *Aspen Physical Property System - Physical Property Models* [Online]. Available: http://www.chemeng.lth.se/ket050/Arkiv/AspenPhysPropModelsV7_2-Ref.pdf [Accessed 2015].

Baba-Ahmed, A., Guilbot, P. & Richon, D. 1999. New equipment using a static analytic method for the study of vapour–liquid equilibria at temperatures down to 77 K. *Fluid phase equilibria,* 166**,** 225-236.

Bengesai, P. 2016. *High Pressure Vapour-Liquid Equilibrium Measurements For R116 and Ethane with Perfluorohexane and Perfluorooctane.* Master of Science in Engineering University of KwaZulu-Natal.

Besserer, G. & Robinson, D. 1971. A high pressure autocollimating refractometer for determining coexisting liquid and vapor phase densities. *The Canadian Journal of Chemical Engineering,* 49**,** 651-656.

Blanc, C. J. & Setier, J. C. B. 1988. Vapor-liquid equilibria for the ethane-propane system at low temperature. *Journal of Chemical and Engineering Data,* 33**,** 111-115.

Britt, H. & Luecke, R. 1973. The estimation of parameters in nonlinear, implicit models. *Technometrics,* 15**,** 233-247.

Chiyen, K. J. 2010. *Modification and commissioning of a static high pressure apparatus and phase equilibria measurements for fluorinated hydrocarbons.* Master of Science in Engineering, University of Kwazulu Natal.

Christov, M. & Dohrn, R. 2002. High-pressure fluid phase equilibria: experimental methods and systems investigated (1994–1999). *Fluid Phase Equilibria,* 202**,** 153-218.

Coquelet, C., Ramjugernath, D., Madani, H., Valtz, A., Naidoo, P. & Meniai, A. H. 2010. Experimental measurement of vapor pressures and densities of pure hexafluoropropylene. *Journal of Chemical & Engineering Data,* 55**,** 2093-2099.

Coquelet, C., Valtz, A., Naidoo, P., Ramjugernath, D. & Richon, D. 2009. Isothermal Vapor− Liquid Equilibrium Data for the Hexafluoropropylene (R1216)+ Propylene System at Temperatures from (263.17 to 353.14) K. *Journal of Chemical & Engineering Data,* 55**,** 1636-1639.

Deiters, U. & Schneider, G. 1986. High pressure phase equilibria: experimental methods. *Fluid Phase Equilibria,* 29**,** 145-160.

Dohrn, R. & Brunner, G. 1995. High-pressure fluid-phase equilibria: experimental methods and systems investigated (1988–1993). *Fluid Phase Equilibria,* 106**,** 213-282.

Dohrn, R., Fonseca, J. M. & Peper, S. 2012. Experimental methods for phase equilibria at high pressures. *Annual review of chemical and biomolecular engineering,* 3**,** 343-367.

Dohrn, R., Peper, S. & Fonseca, J. 2010. High-pressure fluid-phase equilibria: experimental methods and systems investigated (2000–2004). *Fluid Phase Equilibria,* 288**,** 1-54.

Figuiere, P., Hom, J., Laugier, S., Renon, H., Richon, D. & Szwarc, H. 1980. Vapor-liquid equilibria up to 40,000 KPa and 400° C: A new static method. *AIChE Journal,* 26**,** 872-875.

Fonseca, J., Dohrn, R. & Peper, S. 2011. High-pressure fluid-phase equilibria: experimental methods and systems investigated (2005–2008). *Fluid Phase Equilibria,* 300**,** 1-69.

Francisco, J. S. & Maricq, M. M. 1996. Making Sure That Hydrofluorocarbons Are "Ozone Friendly". *Accounts of chemical research,* 29**,** 391-397.

Fredenslund, A., Mollerup, J. & Christiansen, L. 1973. An apparatus for accurate determinations of vapour-liquid equilibrium properties and gas PVT properties. *Cryogenics,* 13**,** 414-419.

Freitag, N. P. & Robinson, D. B. 1986. Equilibrium phase properties of the hydrogen—methane—carbon dioxide, hydrogen—carbon dioxide—n-pentane and hydrogen—n-pentane systems. *Fluid phase equilibria,* 31**,** 183-201.

Grob, S. & Hasse, H. 2005. Thermodynamics of phase and chemical equilibrium in a strongly nonideal esterification system. *Journal of Chemical & Engineering Data,* 50**,** 92-101.

Guilbot, P., Valtz, A., Legendre, H. & Richon, D. 2000. Rapid on-line sampler-injector: a reliable tool for HT-HP sampling and on-line GC analysis. *Analusis,* 28**,** 426-431.

Guillevic, J. L., Richon, D. & Renon, H. 1983. Vapor-liquid equilibrium measurements up to 558 K and 7 MPa: a new apparatus. *Industrial & engineering chemistry fundamentals,* 22**,** 495-499.

Han, S., Lin, H. & Chao, K. 1988. Vapor-liquid equilibrium of molecular fluid mixtures by equation of state. *Chemical engineering science,* 43**,** 2327-2367.

Henley, E. J., Seader, J. D. & Roper, D. K. 2011. *Separation process principles*, Wiley New York.

Huang, Z., Zhang, Y., Zhao, C., Qin, J., Li, H., Xue, M. & Liu, Y. 2006. Direct gas-phase epoxidation of hexafluoropropylene with molecular oxygen using Ag catalyst. *Applied Catalysis A: General,* 303**,** 18-22.

Ikeda, M., Miura, M. & Aoshima, A. 1990. Process for the production of hexafluoropropylene oxide. Google Patents.

Inomata, H., Kondo, T., Hirohama, S., Arai, K., Suzuki, Y. & Konno, M. 1989. Vapour—liquid equilibria for binary mixtures of carbon dioxide and fatty acid methyl esters. *Fluid phase equilibria,* 46**,** 41-52.

Kalra, H., Kubota, H., Robinson, D. B. & Ng, H.-J. 1978. Equilibrium phase properties of the carbon dioxide-n-heptane system. *Journal of Chemical and Engineering Data,* 23**,** 317-321.

Kaminishi, G. I., Takano, S., Yokoyama, C., Takahashi, S. & Takeuchi, K. 1989. Concentration of triethylene glycol, diethylene glycol and ethylene glycol in supercritical carbon dioxide up to 16 MPa at 313. 15 and 333. 15K. *Fluid Phase Equilibria,* 52**,** 365-372.

Kissun, S. 2001. *A Static Equilibrium Cell for Low Temperature Vapour-Liquid Equilibrium Measurements* Master of Science in Engineeering (Chemical Engineering) MSc Eng Dissertation, University of Natal.

Klink, A., Cheh, H. & Amick, E. 1975. The vapor-liquid equilibrium of the hydrogen—n-butane system at elevated pressures. *AIChE Journal,* 21**,** 1142-1148.

Konrad, R., Swaid, I. & Schneider, G. 1983. High-pressure phase studies on fluid mixtures of low-volatile organic substances with supercritical carbon dioxide. *Fluid Phase Equilibria,* 10**,** 307-314.

Krespan, C. G. 1986. Fluoroalkyl azide chemistry. *The Journal of Organic Chemistry,* 51**,** 332-337.

Legret, D., Richon, D. & Renon, H. 1980. Static still for measuring vapor-liquid equilibria up to 50 bar. *Industrial & Engineering Chemistry Fundamentals,* 19**,** 122-126.

Luyben, W. L. 2013. *Distillation design and control using Aspen simulation*, John Wiley & Sons.

Malanowski, S. 1982. Experimental methods for vapour-liquid equilibria. Part I. Circulation methods. *Fluid Phase Equilibria,* 8**,** 197-219.

Marrero-Morejón, J. & Pardillo-Fontdevila, E. 1999. Estimation of pure compound properties using group-interaction contributions. *AIChE journal,* 45**,** 615-621.

Mathias, P. M. & Copeman, T. W. 1983. Extension of the Peng-Robinson equation of state to complex mixtures: evaluation of the various forms of the local composition concept. *Fluid Phase Equilibria,* 13**,** 91-108.

Molina, M. J. & Rowland, F. S. 1974. Stratospheric sink for chlorofluoromethanes: chlorine atom-catalysed destruction of ozone. *Nature,* 249**,** 810-812.

Mühlbauer, A. 1990. *Measurement and Thermodynamic Interpretation of High Pressure Vapour-Liquid Equilibrium Data* PhD, University of Natal.

Muhlbauer, A. & Raal, J. 1991. Measurement and thermodynamic interpretation of high-pressure vapour—liquid equilibria in the toluene ▪ CO< sub> 2</sub> system. *Fluid phase equilibria,* 64**,** 213-236.

Mühlbauer, A. & Raal, J. 1995. Computation and thermodynamic interpretation of high-pressure vapour--liquid equilibrium--a review. *The Chemical Engineering Journal and The Biochemical Engineering Journal,* 60**,** 1-29.

Naidoo, P. 2004. *High-Pressure Vapour-Liquid Equilibrium Studies* PhD, University of Kwazulu Natal.

Naidoo, P., Ramjugernath, D. & Raal, J. D. 2008. A new high-pressure vapour–liquid equilibrium apparatus. *Fluid Phase Equilibria,* 269**,** 104-112.

Narasigadu, C. 2011. *Design of a static micro-cell for phase equilibrium measurements: measurements and modelling.* Paris, ENMP.

Narasigadu, C., Naidoo, P., Coquelet, C., Richon, D. & Ramjugernath, D. 2013. A novel static analytical apparatus for phase equilibrium measurements. *Fluid Phase Equilibria,* 338**,** 188-196.

Nelson, W. M. 2012. *Separation of Trichlorosilane: Measurement, Modelling and Simulation.* PhD, University of KwaZulu Natal.

Nelson, W. M., Naidoo, P. & Ramjugernath, D. 2015a. Phase equilibrium data for potentially hazardous binary mixtures involving dichlorosilane, trichlorosilane and silicon-tetrachloride. *The Journal of Chemical Thermodynamics,* 91**,** 420-426.

Nelson, W. M., Williams-Wynn, M., Subramoney, S. C. & Ramjugernath, D. 2015b. Isothermal Vapor–Liquid Equilibrium Data for the Binary System 1, 1, 2, 3, 3, 3-Hexafluoro-1-propene (R1216)+ 2, 2, 3-Trifluoro-3-(trifluoromethyl) oxirane from (268.13 to 308.19) K. *Journal of Chemical & Engineering Data,* 60**,** 568-573.

Ohgaki, K. & Katayama, T. 1975a. Isothermal vapor-liquid equilibria for systems ethyl ether-carbon dioxide and methyl acetate-carbon dioxide at high pressures. *Journal of Chemical and Engineering Data,* 20**,** 264-267.

Ohgaki, K. & Katayama, T. 1975b. Isothermal vapor-liquid equilibriums for systems ethyl ether-carbon dioxide and methyl acetate-carbon dioxide at high pressures. *Journal of Chemical and Engineering Data,* 20**,** 264-267.

Ohgaki, K., Sano, F. & Katayama, T. 1976. Isothermal vapor-liquid equilibrium data for binary systems containing ethane at high pressures. *Journal of Chemical and Engineering Data,* 21**,** 55-58.

Orbey, H. & Sandler, S. I. 1998. *Modeling vapor-liquid equilibria: cubic equations of state and their mixing rules*, Cambridge University Press.

Peng, D.-Y. & Robinson, D. B. 1976. A new two-constant equation of state. *Industrial & Engineering Chemistry Fundamentals,* 15**,** 59-64.

Poling, B., Prausnitz, J. & O'connell, J. The properties of gases and liquids, 2001. *Chapters,* 2**,** 4.

Prausnitz, J. M., Lichtenthaler, R. N. & De Azevedo, E. G. 1998. *Molecular thermodynamics of fluid-phase equilibria*, Pearson Education.

Privat, R., Gani, R. & Jaubert, J.-N. 2010. Are safe results obtained when the PC-SAFT equation of state is applied to ordinary pure chemicals? *Fluid Phase Equilibria,* 295**,** 76-92.

Raal, J. & Mühlbauer, A. 1994a. The Measurement of High Pressure Vapour-Liquid-Equilibria: Part I: Dynamic Methods. *Developments in Chemical Engineering and Mineral Processing,* 2**,** 69-87.

Raal, J. & Mühlbauer, A. 1994b. The Measurement of High Pressure Vapour-Liquid-Equilibria: Part II: Static Methods. *Developments in Chemical Engineering and Mineral Processing,* 2**,** 88-104.

Raal, J. D., Jeffery, G. & Tonkin, T. G. 1980. Chemical Engineering Research Group Report: 331, CSIR, Pretoria.

Raal, J. D. & Mühlbauer, A. L. 1998. *Phase Equilibria: Measurement & Computation*, CRC Press.

Ramjugernath, D. 2000. High Pressure Phase Equilibrium Studies. *PhD Dissertation*.

Ramjugernath, D., Valtz, A., Coquelet, C. & Richon, D. 2009. Isothermal Vapor− Liquid Equilibrium Data for the Hexafluoroethane (R116)+ Propane System at Temperatures from (263 to 323) K. *Journal of Chemical & Engineering Data,* 54**,** 1292-1296.

Renon, H. & Prausnitz, J. M. 1968. Local compositions in thermodynamic excess functions for liquid mixtures. *AIChE journal,* 14**,** 135-144.

Richon, D. New Measurements for Phase Equilibria and PVT Determinations in a Large Range of Pressures (0 to 100 Mpa) and Temperatures (0 to 770 K). Proceedings of the South African Chemical Engineering Congress, 2003. 3-5.

Rigas, T., Mason, D. & Thodos, G. 1958. Vapor-Liquid Equilibria. Microsampling Technique Applied to a New Variable-Volume Cell. *Industrial & Engineering Chemistry,* 50**,** 1297-1300.

Rivollet, F., Chapoy, A., Coquelet, C. & Richon, D. 2004. Vapor–liquid equilibrium data for the carbon dioxide (CO2) + difluoromethane (R32) system at temperatures from 283.12 to 343.25 K and pressures up to 7.46 MPa. *Fluid Phase Equilibria,* 218**,** 95-101.

Rogers, B. & Prausnitz, J. 1970. Sample-Extrusion Apparatus for High-Pressure Vapor-Liquid Equilibria Compositions and Densities at Pressures up to the Critical. *Industrial & Engineering Chemistry Fundamentals,* 9**,** 174-177.

Schotte, W. 1980. Collection of phase equilibrium data for separation technology. *Industrial & Engineering Chemistry Process Design and Development,* 19**,** 432-439.

Schwartzentruber, J., Renon, H. & Watanasiri, S. 1990. K-values for non-ideal systems: an easier way. *Chemical Engineering,* 97**,** 118.

Smith, J. M., Van Ness, H. C. & Abbott, M. M. 2005. *Introduction to chemical engineering thermodynamics*, Boston: McGraw-Hill; 7th ed.

Soo, C.-B. 2011. *Experimental thermodynamic measurements of biofuel-related associating compounds and modeling using the PC-SAFT equation of state.* École Nationale Supérieure des Mines de Paris.

Spuhl, O. & Arlt, W. 2004. COSMO-RS Predictions in Chemical Engineering A Study of the Applicability to Binary VLE. *Industrial & engineering chemistry research,* 43**,** 852-861.

Stolarska, M., Niedzicki, L., Borkowska, R., Zalewska, A. & Wieczorek, W. 2007. Structure, transport properties and interfacial stability of PVdF/HFP electrolytes containing modified inorganic filler. *Electrochimica Acta,* 53**,** 1512-1517.

Street, W. & Sonntag, R. 1964. GJ Wylen van. *Liquid—vapour equilibrium in system normal hydrogen-helium, J Chem. Phys,* 40**,** 1390.

Subramoney, S. C., Courtial, X., Naidoo, P., Coquelet, C., Richon, D. & Ramjugernath, D. 2013a. Isothermal vapor–liquid equilibrium data for the ethylene+ 1, 1, 2, 3, 3, 3-

hexafluoro-1-propene binary system between 258 and 308K at pressures up to 4.56 MPa. *Fluid Phase Equilibria,* 353**,** 7-14.

Subramoney, S. C., Nelson, W. M., Naidoo, P., Coquelet, C., Richon, D. & Ramjugernath, D. 2015. Phase equilibrium data for mixtures involving 1, 1, 2, 3, 3, 3-hexafluoro-1-propene with either propane or n-butane between 312 and 343K. *Fluid Phase Equilibria*.

Subramoney, S. C., Valtz, A., Coquelet, C., Richon, D., Naidoo, P. & Ramjugernath, D. 2012. Vapor–Liquid Equilibrium Measurements and Modeling for the Ethane (R-170)+ 1, 1, 2, 3, 3, 3-Hexafluoro-1-propene (R-1216) Binary System. *Journal of Chemical & Engineering Data,* 57**,** 2947-2955.

Subramoney, S. C., Valtz, A., Coquelet, C., Richon, D., Naidoo, P. & Ramjugernath, D. 2013b. Experimental vapour–liquid equilibrium data and modeling for binary mixtures of 1-butene with 1, 1, 2, 3, 3, 3-hexafluoro-1-propene, 2, 2, 3-trifluoro-3-(trifluoromethyl) oxirane, or difluoromethane. *The Journal of Chemical Thermodynamics,* 61**,** 18-26.

Swaid, I. 1984. Ph.D. thesis Doctoral Dissertation, University of Bochum.

Swanepoel, E. 2009. *Nesca launches fluorochemical expansion initiative* [Online]. South Africa ENGINEERING NEWS Available: http://www.engineeringnews.co.za/article/necsa-launches-fluorochemical-expansion-initiative-2009-03-24 [Accessed 11 February 2014].

Taylor, B. N., Mohr, P. J. & Douma, M. 2007. The NIST Reference on constants, units, and uncertainty. *available online from:. physics. nist. gov/cuu/index*.

Tshibangu, M. M., Courtial, X., Coquelet, C., Naidoo, P. & Ramjugernath, D. 2013. Isothermal Vapor–Liquid Equilibrium Data and Modeling for the Ethane (R170)+ Perfluoropropane (R218) System at Temperatures from (264 to 308) K. *Journal of Chemical & Engineering Data,* 58**,** 1316-1320.

Valtz, A., Coquelet, C., Baba-Ahmed, A. & Richon, D. 2003. Vapor–liquid equilibrium data for the CO 2+ 1, 1, 1, 2, 3, 3, 3,-heptafluoropropane (R227ea) system at temperatures from 276.01 to 367.30 K and pressures up to 7.4 MPa. *Fluid phase equilibria,* 207**,** 53-67.

Valtz, A., Coquelet, C. & Richon, D. 2004. Vapor–liquid equilibrium data for the sulfur dioxide (SO 2)+ 1, 1, 1, 2, 3, 3, 3-heptafluoropropane (R227ea) system at temperatures from 288.07 to 403.19 K and pressures up to 5.38 MPa: Representation of the critical point and azeotrope temperature dependence. *Fluid phase equilibria,* 220**,** 75-82.

Valtz, A., Gicquel, L., Coquelet, C. & Richon, D. 2005. Vapour–liquid equilibrium data for the 1,1,1,2 tetrafluoroethane (R134a) + dimethyl ether (DME) system at temperatures from 293.18 to 358.15 K and pressures up to about 3 MPa. *Fluid Phase Equilibria,* 230**,** 184-191.

Velders, G. J., Andersen, S. O., Daniel, J. S., Fahey, D. W. & Mcfarland, M. 2007. The importance of the Montreal Protocol in protecting climate. *Proceedings of the National Academy of Sciences,* 104**,** 4814-4819.

Wagner, Z. & Wichterle, I. 1987. High-pressure vapour—liquid equilibrium in systems containing carbon dioxide, 1-hexene, and n-hexane. *Fluid Phase Equilibria,* 33**,** 109-123.

Walas, S. M. 2013. *Phase equilibria in chemical engineering*, Butterworth-Heinemann.

Weir, R. D. & De Loos, T. W. 2005. *Measurement of the thermodynamic properties of multiple phases*, Gulf Professional Publishing.

Westhaus, I. U. & Sass, R. 2004. From raw physical data to reliable thermodynamic model parameters through DECHEMA Data Preparation Package. *Fluid Phase Equilibria,* 222–223**,** 49-54.

Wong, D. S., Orbey, H. & Sandler, S. I. 1992. Equation of state mixing rule for nonideal mixtures using available activity coefficient model parameters and that allows extrapolation over large ranges of temperature and pressure. *Industrial & engineering chemistry research,* 31**,** 2033-2039.

Wong, D. S. H. & Sandler, S. I. 1992. A theoretically correct mixing rule for cubic equations of state. *AIChE Journal,* 38**,** 671-680.

Yonker, C., Wright, B., Udseth, H. & Smith, R. 1984. New methods for characterization of supercritical fluid solutions. *Berichte der Bunsengesellschaft für physikalische Chemie,* 88**,** 908-911.

APPENDIX A

A. THERMODYNAMIC FUNDAMENTALS

A.1 Criterion for Equilibrium

For a heterogeneous, closed system composed of π phases and *k* components in equilibrium, the following equations describe the fundamental criterion for phase equilibrium (Prausnitz et al., 1998):

$$T^{(1)} = T^{(2)} = \cdots\cdots\cdots = T^{(\pi\pi)}$$
$$P^{(1)} = P^{(2)} = \cdots\cdots\cdots = P^{(\pi)}$$
$$\mu_1^{(1)} = \mu_1^{(2)} = \cdots\cdots\cdots = \mu_1^{(\pi)}$$
$$\mu_2^{(1)} = \mu_2^{(2)} = \cdots\cdots\cdots = \mu_2^{(\pi)}$$
$$\vdots \quad \vdots \qquad\qquad \vdots$$
$$\mu_k^{(1)} = \mu_k^{(2)} = \cdots\cdots\cdots = \mu_k^{(\pi)}$$

According to Raal and Mühlbauer (1998); the criterion for equilibrium can thus be stated as: *"The temperature and pressure for each phase must be identical, as must the chemical potential* (μ)*of each component i in each of the phases."*

$$\mu_i^{\alpha} = \mu_i^{\beta} = \cdots\cdots\cdots = \mu_i^{\pi} \qquad\qquad i = 1, 2, \ldots\ldots, k$$

A.2 Gibbs Duhem Equation

The mathematical determination of partial properties can be carried out from knowledge of solution-property data. Also, the definition of partial molar property suggests though not directly expressed that solution properties can also be calculated from partial properties. Functions such as pressure, temperature, and the number of moles of the individual species that make up the phase are used to express a thermodynamic property *M* of a homogenous phase (Smith et al., 2005). Therefore, for a thermodynamic property *M*:

$$nM = \mathcal{M}(T, P, n_1, n_2, \ldots\ldots, n_i, \ldots\ldots) \qquad \text{(A-2)}$$

The total differential of *nM* is (Smith et al., 2005):

$$d(dM) = \left[\frac{\partial(nM)}{\partial P}\right]_{T,n} dP + \left[\frac{\partial(nM)}{\partial T}\right]_{P,n} dT + \sum_i \left[\frac{\partial(nM)}{\partial n_i}\right]_{P,T,n_j} \quad \text{(A-3)}$$

The subscript n_j indicates that all mole numbers are kept constant with the exception of n_i and subscript *n* that all mole numbers are kept constant.

Eq. (A-4) expresses the partial molar property $\overline{M_i}$ of species *i* in solution:

$$\overline{M_i} = \left[\frac{\partial(nM)}{\partial n_i}\right]_{P,T,n_j} \quad \text{(A-4)}$$

The partial molar property characterises the change of total property nM due to addition at constant temperature and pressure of a differential quantity of species i to a finite amount of solution. The symbol $\overline{M}_i$ may be representative partial molar entropy$\bar{S}_i$, the partial molar enthalpy $\overline{H}_i$, the partial molar Gibbs energy $\bar{G}_i$, and the partial molar internal energy $\overline{U}_i$ are examples of such a property.

Substituting Eq. (A-4) into Eq. (A-3) and expressing the terms by means of the following identities,

$$n_i = x_i n \quad \text{(A-5)}$$

$$dn_i = x_i dn + n dx_i \quad \text{(A-6)}$$

$$d(nM) \equiv n dM + M dn \quad \text{(A-7)}$$

Equation (A-3) becomes (Smith et al., 2005):

$$n dM + M dn = n\left(\frac{\partial M}{\partial P}\right)_{T,x} dP + n\left(\frac{\partial M}{\partial T}\right)_{P,x} dT + \sum_i \overline{M}_i \,(x_i dn + n dx_i) \quad \text{(A-8)}$$

The equation is factorised to separate terms containing n from those containing dn to give:

$$\left[dM - \left(\frac{\partial M}{\partial P}\right)_{T,x} dP - \left(\frac{\partial M}{\partial T}\right)_{P,x} dT - \sum_i \overline{M}_i dx_i\right] n + \left[M - \sum_i x_i \overline{M}_i\right] dn = 0 \quad \text{(A-9)}$$

The left side of the equation can only be zero by means of each term in the brackets being zero. Consequently,

$$dM = \left(\frac{\partial M}{\partial P}\right)_{T,x} dP + \left(\frac{\partial M}{\partial T}\right)_{P,x} dT + \sum_i \overline{M}_i \, dx_i \quad \text{(A-10)}$$

And

$$M = \sum_i \bar{M}_i \, dx_i \tag{A-11}$$

Multiplying Eq. (A-11) by n gives the alternate expression:

$$nM = \sum_i n_i \bar{M}_i \tag{A-12}$$

Equations (A-11) and (A-12) are identified as *summability relations.*
Differentiating Eq. (A-11) gives the general expression for dM:

$$dM = \sum_i x_i d\bar{M}_i + \sum_i \bar{M}_i dx_i \tag{A-13}$$

Substituting Eq. (A-13) into Eq. (A-9) gives the Gibbs-Duhem Equation:

$$0 = \left(\frac{\partial M}{\partial P}\right)_{T,x} dP + \left(\frac{\partial M}{\partial T}\right)_{P,x} dT - \sum_i x_i d\bar{M}_i \tag{A-14}$$

It is a necessity that the Gibbs-Duhem equation be satisfied for all changes in temperature, pressure, and the partial molar property brought about by changes of state in a homogenous phase.

For the peculiar case of changes at constant temperature and pressure, the Gibbs-Duhem equation reduces to:

$$\sum_i x_i d\bar{M}_i = 0 \tag{A-15}$$

A.3 The Chemical Potential

For a closed homogenous system, the internal energy is considered to be a function exclusively of volume and entropy; that is,

$$U = U(S, V) \tag{A-16}$$

The laws of thermodynamics that apply for a closed system can be extrapolated to be relevant to an open system.
For an open system, considering U as the expression

$$U = U(S, V, n_1, n_2, \cdots \cdots, n_k) \tag{A-17}$$

where *k* denotes the number of components. The derivative of the internal is then expressed as

$$dU = \left(\frac{\partial U}{\partial S}\right)_{V,n_j} dS + \left(\frac{\partial U}{\partial V}\right)_{S,n_j} dV + \sum_i \left(\frac{\partial U}{\partial n_i}\right)_{S,V,n_j} dn_i \tag{A-18}$$

Further, introducing the function μ_i, this is an intensive property which depends on pressure, composition and temperature. The *chemical potential*, μ_i, is defined as

$$\mu_i = \left(\frac{\partial U}{\partial n_i}\right)_{S,V,n_j} \tag{A-19}$$

The total differential is then rewritten as

$$dU = TdS - PdV + \sum_i \mu_i dn_i \tag{A-20}$$

By making use of the defining equations for the *Helmholtz energy* (*A*), *Gibbs energy* (*G*) and the *enthalpy* (*H*); we may replace *dU* in Eq. (A-20 in each instance and reach the subsequent additional three principal equations for an open system;

$$dH = TdS + VdP + \sum_i \mu_i dn_i \tag{A-21}$$

$$dA = -SdT - PdV + \sum_i \mu_i dn_i \tag{A-22}$$

$$dG = -SdT + VdP + \sum_i \mu_i dn_i \tag{A-23}$$

It then follows that

$$\mu_i \equiv \left(\frac{\partial U}{\partial n_i}\right)_{S,V,n_j} = \left(\frac{\partial H}{\partial n_i}\right)_{S,P,n_j} = \left(\frac{\partial A}{\partial n_i}\right)_{T,V,n_j} = \left(\frac{\partial G}{\partial n_i}\right)_{T,P,n_j} \tag{A-24}$$

A.4 Partial Molar Property

The *partial molar property* of entity i is described as the molar derivative of property *M*. It represents the variation in the total property *nM* as a result of addition at constant temperature and pressure of a differential quantity of entity i to a determinate quantity of solution. Thus,

$$\left[\frac{\partial(nM)}{\partial n_i}\right]_{P,T,n_j} \tag{A-25}$$

A.5 Fugacity and the Fugacity Coefficient

As a result of the abstractness of the concept of chemical potential μ, it is not easy to relate it to measurable quantities. Notwithstanding the fact that the mathematical description of chemical potential can be specified clearly, its physical implication is not easy to comprehend fully. However, this can be simplified by expressing the chemical potential in terms of an auxiliary function whose parameters are measurable quantities and that could be more simply associated with physical reality. For this reason, the concept of fugacity is instituted. Physically, fugacity is a more meaningful quantity which is largely employed phase equilibria solutions and has units of pressure. While fugacity is still an abstract concept itself, it is with ease related to measurable quantities such as temperature, pressure and volume.
So as to relate fugacity to chemical, a point of departure is the definition of chemical potential:

$$\mu_i = \left(\frac{\partial nU}{\partial n_i}\right)_{S,V,n_j} \equiv \left(\frac{\partial(nG)}{\partial n_i}\right)_{T,P,n_j} \equiv \overline{G}_i \tag{A-26}$$

From the succeeding identity we see that $(\partial nG/\partial n_i)_{T,P,n_i}$ is a partial molar quantity as it possesses the defining conditions to be satisfied of constant temperature, pressure and number of moles of species n_j, i.e., $\mu_i \equiv \overline{G}_i$. Chemical potential happens to be an intensive variable, that is, its value is independent of the quantity of material present. It is then considered to be a function of entropy *S*, volume *V*, and the mole numbers $n_1, n_2, \cdots\cdots, n_k$, that is,

$$\mu = U(S, V, n_1, n_2, \cdots\cdots, n_k) \tag{A-27}$$

Considering a pure substance *i*, the following differential equation relates the chemical potential to temperature and pressure:

$$d\mu_i = -S_i dT + V_i dP \tag{A-28}$$

In Eq. (A-28) S_i denotes the molar entropy whereas V_i denotes the molar volume. Taking the integral and solving for μ_i at some pressure P and temperature T, we have:

$$\mu_i(T,P) = \mu_i(T^r,P^r) - \int_{T^r}^{T} S_i dT + \int_{P^r}^{P} V_i dP \tag{A-29}$$

where the subscript r denotes a particular arbitrary reference state.
For a pure ideal gas, the chemical potential (G. N. Lewis) from Eq. (2-19) is:

$$\left(\frac{\partial \mu_i}{\partial P}\right)_T = V_i \tag{A-30}$$

Substituting the ideal gas equation,

$$V_i = \frac{RT}{P} \tag{A-31}$$

and integrating at constant temperature,

$$\mu_i - \mu_i^0 = RTln\frac{P}{P^0} \tag{A-32}$$

Equation (A-32) illustrates that for an ideal gas, the change in chemical potential, in going from pressure P^0 to pressure P at constant temperature, is equivalent to the product of RT and the natural logarithm of the pressure ratio P/P^0. Therefore, the isothermal alteration in the abstract thermodynamic quantity μ is a straightforward logarithmic function of a quantity having a physical bearing, pressure.

$$\mu_i - \mu_i^0 = RTln\frac{f}{f^0} \tag{A-33}$$

From Eq. (A-33) it is apparent that the thermodynamic quantity *f* is a "corrected pressure", and these corrections are as a consequence of the non-idealities that could be explained by molecular considerations.
The fugacity concept has its origins in Eq. (A-34) below, which holds exclusively for pure species *i* in the ideal gas condition.

$$G_i^{ig} = \Gamma_i(T) + RTlnP \tag{A-34}$$

For a real fluid, Smith et al. (2005) derived the analogous equation:

$$G_i = \Gamma_i(T) + RTlnf_i \tag{A-35}$$

Using Eq. (A-35), it can be shown that extending to phases $\alpha, \beta, \ldots\ldots, \pi$, a new form of the fundamental phase equilibrium equation is given (Prausnitz et al., 1998, Smith et al., 2005):

$$\hat{f}_i^{\alpha} = \hat{f}_i^{\beta} = \cdots = \hat{f}_i^{\pi} \qquad (i = 1,2,\cdots N) \tag{A-36}$$

For the particular instance of multicomponent vapour-liquid equilibrium, Eq. (A-36) becomes:

$$\hat{f}_i^{v} = \hat{f}_i^{l} \qquad (i = 1,2,\cdots N) \tag{A-37}$$

A.6 The Concept of Fugacity Coefficient

The fugacity coefficient is given by the dimensionless coefficient(f/P), that is,

$$\phi = \left(\frac{f}{P}\right) \tag{A-38}$$

For a component in *i* solution,

$$\hat{\phi}_i = \frac{\hat{f}_i}{y_i P} \tag{A-39}$$

In Eq. (A-39) the mole fraction of component *i* in a gaseous solution was employed here, as the fugacity confident $\hat{\phi}_i$ finds greatest service in analysing a multicomponent gas phase (Raal and Mühlbauer, 1998).

A.7 The Concept of Activity Coefficient

In phase equilibrium studies it is most appropriate to describe liquid phase behaviour as well as non-ideality in relation to an *activity coefficient* (γ). A suitable definition is

$$\gamma_i = \frac{\hat{f}_i}{x_i f_i^o} \tag{A-40}$$

where x_i is the mole fraction and f_i^o is the fugacity of pure species *i* at some particular standard state. The relationship between the fugacity and the fugacity coefficient is represented in Eq. (A-41):

$$\hat{\phi}_i = \frac{\hat{f}_i}{y_i P} \tag{A-41}$$

An appropriate measure of the propensity of a given chemical species to partition itself preferentially between the vapour and liquid phases is the equilibrium ratio K_i expressed as:

$$K_i = \frac{y_i}{x_i} \tag{A-42}$$

This dimensionless quantity is commonly termed a *K-value*. It functions as a measure of the propensity of a constituent species to favour the vapour-phase. In Eq. (A-42) the vapour and liquid mole fractions of a species *i* are denoted by y_i and x_i respectively. When the equilibrium ratio K_i is more than unity, it depicts that component *i* displays a higher concentration in the vapour-phase, when less, concentrates more in the liquid-phase. The equilibrium ratio provides for computational convenience, permitting elimination of either y_i or x_i.

APPENDIX B

TABULATED EXPERIMENTAL DATA
B.1 VAPOUR PRESSURE DATA

Table B- 1: Experimental [a] and regressed pure component vapour pressures for n-pentane

$T_{exp}[K]$	$P_{exp}[MPa]$	*PR-MC*		
		$P_{calc}[MPa]$	$P_{exp} - P_{calc}[MPa]$	$10^2\left(P_{exp} - P_{calc}\right)/P_{exp}$
353.15	3.750	3.751	0.001	0.024
358.13	4.250	4.251	0.001	0.031
363.07	4.820	4.817	-0.003	-0.054
368.05	5.410	5.408	-0.002	-0.035
373.00	6.050	6.048	-0.002	-0.027
378.12	6.750	6.752	0.002	0.024
383.09	7.500	7.503	0.003	0.034
388.11	8.330	8.331	0.001	0.013
393.12	9.220	9.220	0.000	-0.003
398.13	10.170	10.169	-0.001	-0.006
				$AARD_p = 0.06\ \%$

[a] Expanded uncertainties ($k = 2$): $\overline{U}(T) = \pm 0.06\ K$, $\overline{U}(P) = \pm 0.007\ MPa$.

Table B- 2: Experimental [a] and regressed pure component vapour pressures for n-hexane

$T_{exp}[K]$	$P_{exp}[MPa]$	*PR-MC*		
		$P_{calc}[MPa]$	$P_{exp} - P_{calc}[MPa]$	$10^2\left(P_{exp} - P_{calc}\right)/P_{exp}$
343.06	0.107	0.107	0.0001	-0.017
348.03	0.124	0.124	0.0002	0.061
353.03	0.145	0.145	0.0004	0.004
358.04	0.169	0.169	0.0000	-0.086
363.01	0.193	0.193	-0.0002	-0.024
367.95	0.219	0.219	-0.0004	0.054
372.91	0.250	0.250	-0.0004	0.010
				$AARD_p = 0.04\ \%$

[a] Expanded uncertainties($k = 2$): $\overline{U}(T) = \pm 0.06\ K$, $\overline{U}(P) = \pm 0.007\ MPa$.

Table B- 3: Experimental [a] and regressed pure component vapour pressures for n-heptane

$T_{exp}[K]$	$P_{exp}[MPa]$	*PR-MC*		
		$P_{calc}[MPa]$	$P_{exp} - P_{calc}[MPa]$	$10^2\left(P_{exp} - P_{calc}\right)/P_{exp}$
373.06	0.133	0.133	0.0000	-0.009
387.92	0.189	0.189	-0.0001	0.058
390.57	0.202	0.202	0.0001	-0.033
392.89	0.213	0.213	0.0000	0.010
395.50	0.227	0.226	0.0002	-0.077
398.07	0.238	0.238	-0.0001	0.060
400.56	0.253	0.253	0.0000	-0.015
403.08	0.267	0.267	0.0000	0.005
				$AARD_p = 0.03\ \%$

[a] Expanded uncertainties ($k = 2$): $\overline{U}(T) = \pm 0.06\ K$, $\overline{U}(P) = \pm 0.007\ MPa$.

Table B- 4: Experimental [a] and regressed pure component vapour pressures for 1, 1, 2, 3, 3, 3-hexafluoro-1-propene

$T_{exp}[K]$	$P_{exp}[MPa]$	*PR-MC*		
		$P_{calc}[MPa]$	$P_{exp} - P_{calc}[MPa]$	$10^2\left(P_{exp} - P_{calc}\right)/P_{exp}$
343.11	2.214	2.213	0.000	0.02
348.12	2.466	2.467	-0.001	-0.03
353.00	2.749	2.749	-0.001	-0.02
358.02	3.051	3.054	-0.003	-0.09
362.98	3.371	3.374	-0.003	-0.09
				$AARD_p = 0.05\ \%$

[a] Expanded uncertainties ($k = 2$): $\bar{U}(T) = \pm 0.06\ K$, $\bar{U}(P) = \pm 0.007\ MPa$.

APPENDIX C

Evaluation of Experimental Uncertainty

Uncertainties in temperature, pressure and the equilibrium phase compositions for each binary system were evaluated and reported. The method of the evaluation of the uncertainty followed the guidelines outlined by the National Institute of Science and Technology (NIST) (Taylor et al., 2007). A comprehensive outline on the evaluation of uncertainty for vapour-liquid equilibrium measurement is accessible in literature (Soo, 2011). Usually two scenarios arise in the evaluation of $u_i(\bar{\theta})$, that is, either Type A or Type B evaluation.

Type A: Uncertainties which are estimated using statistical methods. A common feature of uncertainty adhering to a Type A distribution is the large tendency to lie about the mean. Is essence Type A uncertainty may be estimated from:

$$u_i(\bar{\theta}) = \frac{\sigma}{\sqrt{N_{rp}}} \qquad \text{(C-1)}$$

In Eq. (7 - 1) σ denotes the standard deviation and N_{rp} denotes the total number of repeated data points.

Type B: Uncertainties which are estimated using other methods. This is applicable for variables that have an equal probability of residing anywhere within the distribution. Distributions of this nature are called rectangular, and are estimated as follows:

$$u_i(\theta) = \frac{b}{\sqrt{3}} \qquad \text{(C-2)}$$

where b takes a value of the upper half the width of the interval. In this study all measured variables computed from polynomials make use of Type B evaluations.

Temperature and Pressure

Taking into consideration all non-negligible sources of uncertainty existent in temperature measurements, the combined standard uncertainty for temperature is given by:

$$u_c(T) = \pm\sqrt{u_{calib}(T)^2 + u_{rep}(T)^2} \qquad \text{(C-3)}$$

In Eq. (7 - 3) $u_{rep}(T)$ denotes the standard uncertainty as a result of repeatability, and $u_{calib}(T)$ denotes the standard uncertainty brought about by the temperature calibration:

$$u_{calib}(T) = \pm\sqrt{u_{std}(T)^2 + u_{corr}(T)^2} \qquad \text{(C-4)}$$

where $u_{corr}(T)$ denotes the standard uncertainty as a result of the temperature calibration correlation and $u_{std}(T)$ denotes the standard uncertainty inherent in the standard temperature probe.

Likewise, the combined standard uncertainty for pressure is given by:

$$u_c(P) = \pm\sqrt{u_{corr}(P)^2 + u_{std}(P)^2 + u_{atm}(P)^2 + u_{rep}(P)^2} \qquad \text{(C-5)}$$

where $u_{corr}(P)$ denotes the standard uncertainty as a result of the computation of the pressure calibration correlation, $u_{std}(P)$ is the standard uncertainty inherent in the pressure transducer, $u_{atm}(P)$ denotes the standard uncertainty inherent in the barometer and $u_{rep}(P)$ is the standard uncertainty as a result of the repeatability in the measurement of pressure. The computed standard uncertainties are finally multiplied by a coverage factor of 2 to attain the combined standard uncertainty.

Phase composition

The non-negligible sources of uncertainty in the estimation of the number of moles are the accuracy in GC detector calibration and the standard deviation in taking an average of the repeated samples. The combined standard uncertainty is divided into the standard uncertainty as a result of sample repeatability $u_{rep}(x_i)$ (Type A), and the standard uncertainty arising from the calibration technique $u_{calib}(x_i)$:

$$u_c(x_i) = \pm\sqrt{u_{rep}(x_i)^2 + u_{calib}(x_i)^2} \qquad \text{(C-6)}$$

In the direct injection technique for the TCD calibration, phase compositions are estimated from correlations that relate the number of moles and the detector response area. For gaseous components, the ideal gas law is made use of in estimating the experimental uncertainty. As a result the uncertainties in the pressure, volume and temperature of the injected gas need to be accounted for. The standard uncertainty as a result of the TCD calibration method is evaluated as follows:

$$u_{calib}(x_i) = \sqrt{\left[\left(\frac{\partial x_i}{\partial n_i}\right)_{n_j} u(n_i)\right]^2 + \left[\left(\frac{\partial x_i}{\partial n_j}\right)_{n_i} u(n_j)\right]^2} \qquad \text{(C-7)}$$

The standard uncertainty in the number of moles $u(n_i)$ is dependent on the standard uncertainty as a result of the correlation $u_{corr}(n_i)$ and the standard uncertainty emanating from making use of the ideal gas law $u_{ig}(n_i)$:

$$u(n_i) = \pm\sqrt{u_{corr}(n_i)^2 + u_{ig}(n_i)^2} \quad \text{(C-8)}$$

The standard uncertainty arising from using the ideal gas law is expressed as follows:

$$u_{ig}(n_i) = \sqrt{\left[\left(\frac{\partial n_i}{\partial P}\right)_{V,T} u(P)\right]^2 + \left[\left(\frac{\partial n_i}{\partial V}\right)_{P,T} u(V)\right]^2 + \left[\left(\frac{\partial n_i}{\partial T}\right)_{P,V} u(T)\right]^2} \quad \text{(C-9)}$$

by taking the derivative and re-substituting the ideal gas law relationship ($n_i = PV/RT$) where necessary:

$$u_{ig}(n_i) = n_i\sqrt{\left[\frac{u(P)}{P}\right]^2 + \left[\frac{u(V)}{V}\right]^2 + \left[\frac{u(T)}{T}\right]^2} \quad \text{(C-10)}$$

Where $u(P)$, $u(V)$ and $u(T)$ are the standard uncertainties for the pressure, volume and temperature respectively. The standard uncertainty introduced by the temperature $u(T)$ is set to 2 K. This permits an offset of 2 degrees, as a result of the probable cooling effect brought about by gas expansion or heat introduced by the contact the hand makes with the syringe. $u(P)$ is set to 0.01 bar to permit a small positive pressure to be existent in the syringe. For $u(V)$ a 2% is allowed for error in the volume of the gas injected, emanating from manufacturing errors.

The uncertainty due to the calibration polynomial is expressed as:

$$u_{corr}(n_i) = \frac{n_i\left(\left|\frac{N_{i,TRUE} - N_{i,CALC}}{N_{i,TRUE}}\right|\right)}{\sqrt{3}} \quad \text{(C-11)}$$

For a gas/liquid system, the evaluation of the combined standard uncertainty follows the same method for a gas/gas system.

Reporting Uncertainty

The indicated NIST procedure concerning reporting uncertainty is that *U* must be reported together with the coverage factor used to attain it, or report u_c. The expanded uncertainty is expressed as:

$$U(\theta) = ku_c(\theta) \quad \text{(C-12)}$$